

NAVAL POSTGRADUATE SCHOOL MONTEREY, CALIFORNIA



THESIS

SEARCH RADAR TRACK-BEFORE-DETECT USING THE HOUGH TRANSFORM

by

Moshe Elazar

March 1995

Thesis Advisor:

D. Curtis Schleher

Approved for public release; distribution is unlimited

DTIC QUALITY INSPECTED 6

~~19960508~~ 183

REPORT DOCUMENTATION PAGE			Form Approved OMB No. 0704-0188	
Public reporting burden for this collection of information is estimated to average 1 hour per response, including the time for reviewing instruction, searching existing data sources, gathering and maintaining the data needed, and completing and reviewing the collection of information. Send comments regarding this burden estimate or any other aspect of this collection of information, including suggestions for reducing this burden, to Washington Headquarters Services, Directorate for Information Operations and Reports, 1215 Jefferson Davis Highway, Suite 1204, Arlington, VA 22202-4302, and to the Office of Management and Budget, Paperwork Reduction Project (0704-0188) Washington DC 20503.				
1. AGENCY USE ONLY (Leave blank)	2. REPORT DATE March 1995	3. REPORT TYPE AND DATES COVERED Master's Thesis		
4. TITLE AND SUBTITLE SEARCH RADAR TRACK-BEFORE-DETECT USING THE HOUGH TRANSFORM		5. FUNDING NUMBERS		
6. AUTHOR(S) Moshe, Elazar				
7. PERFORMING ORGANIZATION NAME(S) AND ADDRESS(ES) Naval Postgraduate School Monterey CA 93943-5000		8. PERFORMING ORGANIZATION REPORT NUMBER		
9. SPONSORING/MONITORING AGENCY NAME(S) AND ADDRESS(ES)		10. SPONSORING/MONITORING AGENCY REPORT NUMBER		
11. SUPPLEMENTARY NOTES The views expressed in this thesis are those of the author and do not reflect the official policy or position of the Department of Defense or the U.S. Government.				
12a. DISTRIBUTION/AVAILABILITY STATEMENT Approved for public release; distribution is unlimited.			12b. DISTRIBUTION CODE	
13. ABSTRACT (maximum 200 words) Detection of small targets in the presence of noise and sea clutter interference presents a formidable task in a radar system design. Conventional radar detection schemes such as spectral discrimination and noncoherent integration, have been employed with limited success. This thesis investigates an improved target detection scheme suggested by Carlson, Evans and Wilson [Ref 1], applicable to search radars, using the Hough transform image processing technique. The system concept involves a track-before-detect processing method which allows previous data to help in target detection. The technique provides many advantages compared to traditional techniques. The improved detectability results from better use of old energy and which is equivalent to using a three-dimensional filter matched to the target trajectories in addition to the conventional target parameters. The questions answered by this thesis concern the effectiveness of the Hough transform in achieving improved radar target detection and system detection performance, (i.e., probability of detection and false alarm rate as a function of signal to noise ratio) for small, slow targets. System design concepts are considered and a full environment simulation including sea clutter and noise is implemented to determine the algorithm efficiency and performance in various scenarios.				
14. SUBJECT TERMS Radar Detection, Track-Before-Detect, Hough Transform, K-Distribution Clutter.			15. NUMBER OF PAGES 139	
			16. PRICE CODE	
17. SECURITY CLASSIFICATION OF REPORT Unclassified	18. SECURITY CLASSIFICATION OF THIS PAGE Unclassified	19. SECURITY CLASSIFICATION OF ABSTRACT Unclassified	20. LIMITATION OF ABSTRACT UL	

NSN 7540-01-280-5500

Standard Form 298 (Rev. 2-89)
Prescribed by ANSI Std. Z39-18 298-102

DTIC QUALITY INSPECTED 3

i
Revised Copy

Approved for public release; distribution is unlimited

**SEARCH RADAR TRACK-BEFORE-DETECT USING THE
HOUGH TRANSFORM**

Moshe, Elazar

Lieutenant Commander, Israeli Navy

B.S.E.E., Tel Aviv University, 1987

M.B.A., Tel Aviv University, 1993

Submitted in partial fulfillment
of the requirements for the degree of

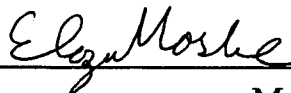
MASTER OF SCIENCE IN ELECTRICAL ENGINEERING

from the

NAVAL POSTGRADUATE SCHOOL

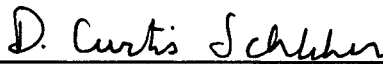
March 1995

Author:




Moshe Elazar

Approved by:



D. Curtis Schleher, Thesis Advisor



Robert G. Hutchins, Second Reader



Michael A. Morgan., Chairman
Department of Electrical and Computer Engineering

ABSTRACT

Detection of small targets in the presence of noise and sea clutter interference presents a formidable task in a radar system design. Conventional radar detection schemes such as spectral discrimination and noncoherent integration, have been employed with limited success. This thesis investigates an improved target detection scheme suggested by Carlson, Evans and Wilson [Ref 1], applicable to search radars, using the Hough transform image processing technique. The system concept involves a track-before-detect processing method which allows previous data to help in target detection. The technique provides many advantages compared to traditional techniques. The improved detectability results from better use of old energy and which is equivalent to using a three-dimensional filter matched to the target trajectories in addition to the conventional target parameters. The questions answered by this thesis concern the effectiveness of the Hough transform in achieving improved radar target detection and system detection performance, (i.e., probability of detection and false alarm rate as a function of signal to noise ratio) for small, slow targets. System design concepts are considered and a full environment simulation including sea clutter and noise is implemented to determine the algorithm efficiency and performance in various scenarios.

TABLE OF CONTENTS

I.	INTRODUCTION	1
A.	BACKGROUND.	1
B.	OBJECTIVE.	2
C.	THESIS OUTLINE.	3
II.	TRACK-BEFORE-DETECT-PROCESSING	5
A.	TRACK-BEFORE-DETECT BASIS.	5
B.	THE HOUGH TRANSFORM	7
C.	USE OF THE HOUGH TRANSFORM IN SEARCH RADAR ...	10
III.	RADAR DETECTION THEORY	15
A.	OPTIMUM DETECTION PROCESS.	15
1.	Detection Performance of an Optimum Detection Process. ...	16
2.	Albersheim's Detection Equation	17
3.	Collapsing Loss	17
B.	DOUBLE THRESHOLD PROCESS DETECTION PERFORMANCE	19
1.	Probability of Detection for Nonfluctuating Target	20
2.	Probability of Detection for Swerling Case I Target	21
C.	DETECTION PERFORMANCE IN THE PRESENCE OF SEA CLUTTER.	21
1.	K Distributed Clutter Model	21
2.	Detection Performance in K Distributed Clutter	23
IV	ALGORITHM DESCRIPTION	29
A.	SYSTEM CONFIGURATION	29
B.	RADAR DATA SIMULATION	30
C.	HOUGH TRANSFORM BASED DETECTOR	34

1.	Binary Integration Hough Transform	39
2.	Optimal Parameter Selection	39
D.	HOUGH TRANSFORM DETECTION PERFORMANCE	40
1.	Probability of False Alarm	40
2.	Probability of Detection	42
V.	RESULTS	43
A.	TEST CASES DESCRIPTION	43
B.	SINGLE TARGET SCENARIO	44
1.	Additive Rayleigh Noise Case	44
2.	Additive K-Distributed Clutter Case	46
C.	TWO TARGETS TEST CASE SCENARIO	71
D.	DETECTION PERFORMANCE	78
1.	Additive Rayleigh Noise Case	78
2.	Additive K-Distributed Clutter Case	79
E.	PARAMETERS SELECTION	99
1.	Parameter Space	99
2.	Primary and Secondary Thresholds	99
VI.	CONCLUSIONS	103
APPENDIX A.	MATLAB SOURCE CODE	105
A.	HOUGH TRANSFORM	105
B.	INVERSE HOUGH TRANSFORM	106
C.	RADAR DATA PARAMETERS	107
D.	TIME-RANGE MAP GENERATION	108
E.	TARGET SIMULATION	109
F.	RAYLEIGH NOISE SIMULATION	110
G.	K-DISTRIBUTION CLUTTER SIMULATION	110

H.	HOUGH DETECTOR PROBABILITY OF DETECTION	111
I.	HOUGH DETECTOR PROBABILITY OF FALSE ALARM	...	112
J.	ALBERSHEIM METHOD	113
K.	BINARY INTEGRATION THRESHOLD	113
L.	BINARY INTEGRATION PROBABILITY OF DETECTION	..	114
M.	BINARY INTEGRATION DETECTION PERFORMANCE	115
N.	GRAPHICS UTILITY	116
O.	MAIN PROGRAM	118
LIST OF REFERENCES		 119
INITIAL DISTRIBUTION LIST		 121

LIST OF TABLES

Table 1.	Simulated Radar Specifications	43
Table 2.	Single Target Test Cases	44

LIST OF FIGURES

Figure 1.	Track-Before-Detect-Process	6
Figure 2.	Hough Transform for Line Detection.	9
Figure 3.	Time-Range Geometry and the Corresponding Hough Parameters . . .	12
Figure 4.	Hough Parameter Space Corresponding to Figure 3 Data Points	13
Figure 5.	Optimum Unknown Phase Detection Process	15
Figure 6.	System Configuration	29
Figure 7.	Rejection Method for Generating Random Deviate t with a Known PDF $P(t)$	32
Figure 8.	Time-Range Space and Hough Space Configuration	35
Figure 9.	Mesh Plot in Image Space for 20 Knot Target	36
Figure 10.	Time-Range Space for 20 Knot Target with Additive Rayleigh Noise (SNR=5 dB)	37
Figure 11.	Hough Space Corresponding to Time-Range Space of Figure 10 and Backprojection of Detected Target into Time-Range Space	38
Figure 12.	Hough Space of All Ones in Image Space Demonstrating the "Accessible Hough Domain"	41
Figure 13.	Test Case I, SNR=0 dB, ξ =20 dB	47
Figure 14.	Test Case I, SNR=5 dB, ξ =19.5 dB	48
Figure 15.	Test Case I, SNR=0 dB, ξ =18.5 dB	49
Figure 16.	Test Case I, SNR=5 dB, ξ =20 dB	50
Figure 17.	Test Case II, SNR=0 dB, ξ =22 dB	51
Figure 18.	Test Case II, SNR=5 dB, ξ =21 dB	52
Figure 19.	Test Case II, SNR=0 dB, ξ =21 dB	53
Figure 20.	Test Case II, SNR=5 dB, ξ =20 dB	54
Figure 21.	Test Case III, SNR=2 dB, ξ =18 dB	55
Figure 22.	Test Case III, SNR=7 dB, ξ =20 dB	56
Figure 23.	Test Case I, SNR=0 dB, ξ =19 dB	57

Figure 24.	Test Case I, SNR=5 dB, $\xi=19$ dB	58
Figure 25.	Test Case II, SNR=0 dB, $\xi=17$ dB	59
Figure 26.	Test Case II, SNR=5 dB, $\xi=18$ dB	60
Figure 27.	Test Case III, SNR=5 dB, $\xi=16$ dB	61
Figure 28.	Test Case I, With Additive K-Distributed Clutter, SIR=0 dB, $\xi=22$ dB	62
Figure 29.	Test Case I, With Additive K-Distributed Clutter, SIR=5 dB, $\xi=22$ dB	63
Figure 30.	Test Case II, With Additive K-Distributed Clutter, SIR=0 dB, $\xi=23$ dB	64
Figure 31.	Test Case II, With Additive K-Distributed Clutter, SIR=5 dB, $\xi=22$ dB	65
Figure 32.	Test Case III, With Additive K-Distributed Clutter, SIR=5 dB, $\xi=18$ dB	66
Figure 33.	Test Case I, With Additive K-Distributed Clutter, SIR=0 dB, $\xi=22$ dB (With Binary Integration)	67
Figure 34.	Test Case I, With Additive K-Distributed Clutter, SIR=5 dB, $\xi=17$ dB (With Binary Integration)	68
Figure 35.	Test Case II, With Additive K-Distributed Clutter, SIR=0 dB, $\xi=18$ dB (With Binary Integration)	69
Figure 36.	Test Case II, With Additive K-Distributed Clutter, SIR=5 dB, $\xi=19$ dB (With Binary Integration)	70
Figure 37.	Test Case IV, SNR=7 dB, $\xi=16$ dB	72
Figure 38.	Test Case IV, SNR=2 dB, $\xi=12$ dB	73
Figure 39.	Test Case IV, SNR=7 dB, $\xi=16$ dB (With Binary Integration)	74
Figure 40.	Test Case IV, SNR=2 dB, $\xi=12$ dB (With Binary Integration)	75
Figure 41.	Test Case V, SNR=15 dB, $\xi=20$ dB	76
Figure 42.	Test Case V, SNR=15 dB, $\xi=20$ dB (With Binary Integration)	77
Figure 43.	Hough Detector P_{fa} as a Function of Secondary Threshold	80

Figure 44.	Hough Detector P_d as a Function of SNR for a Nonfluctuating Stationary Target with Additive Rayleigh noise Scenario	81
Figure 45.	Hough Detector P_d as a Function of SNR for a Nonfluctuating 5 Knot Target with Additive Rayleigh noise Scenario	82
Figure 46.	Hough Detector P_d as a Function of SNR for a Nonfluctuating 25 Knot Target with Additive Rayleigh Noise Scenario	83
Figure 47.	Binary Integration Hough Detector P_{fa} as a Function of Secondary Threshold	84
Figure 48.	Binary Integration Hough Detector P_d as a Function of SNR for a Nonfluctuating Stationary Target with Additive Rayleigh Noise Scenario	85
Figure 49.	Binary Integration Hough Detector P_d as a Function of SNR for a Nonfluctuating 5 knot Target with Additive Rayleigh Noise Scenario	86
Figure 50.	Binary Integration Hough Detector P_d as a Function of SNR for a Nonfluctuating 25 knot Target with Additive Rayleigh Noise Scenario	87
Figure 51.	P_d as a Function of SNR for a Nonfluctuating Stationary Target with Additive Rayleigh Noise Scenario @ $P_{fa}=3 \cdot 10^{-4}$	88
Figure 52.	P_d as a Function of SNR for a Nonfluctuating Moving Target with Additive Rayleigh Noise Scenario @ $P_{fa}=3 \cdot 10^{-4}$	89
Figure 53.	P_d as a Function of SNR for a Nonfluctuating Stationary Target with Additive Rayleigh Noise Scenario @ $P_{fa}=1 \cdot 10^{-7}$	90
Figure 54.	P_d as a Function of SNR for a Nonfluctuating Moving Target with Additive Rayleigh Noise Scenario @ $P_{fa}=1 \cdot 10^{-7}$	91
Figure 55.	Required SNR to Achieve $P_d=0.9$ as a Function of Target Speed in Knots, for Optimum Detection Process and the Hough Detector	92
Figure 56.	Hough Detector P_{fa} as a Function of Secondary Threshold for the Additive K-Distributed Clutter Case	93
Figure 57.	Hough Detector P_d as a Function of SNR for a Nonfluctuating Stationary Target with Additive K-distributed Clutter Scenario	94

Figure 58.	Hough Detector P_d as a Function of SNR for a Nonfluctuating 5 Knot Target with Additive K-Distributed Clutter Scenario	95
Figure 59.	Hough Detector P_d as a Function of SNR for a Nonfluctuating 25 Knot Target with Additive K-distributed Clutter Scenario	96
Figure 60.	P_d as a Function of SNR for a Nonfluctuating Target with Additive K-distributed Scenario @ $P_{fa}=8 \cdot 10^{-5}$	97
Figure 61.	Required SNR to Achieve $P_d=0.9$ @ $P_{fa}=8 \cdot 10^{-5}$ as a Function of Target Speed in Knots, for Square Law Detection Process and the Hough Detector, (for the Additive K-Distributed Clutter Scenario) . . .	98
Figure 62.	Required SNR as a Function of Parameter Space Granularity @ $P_d=0.9$, $\xi=12$ dB	100
Figure 63.	Required SNR as a Function of Primary Threshold @ $P_d=0.9$, $\xi=12$ dB	101

I. INTRODUCTION

A. BACKGROUND

Detection of small targets in the presence of noise and sea clutter interference, presents a formidable task in a radar system design. A small Radar Cross Section (RCS) target (order of 1 m^2 or less) should be detected in the presence of wide dynamic range non-Gaussian sea clutter and thermal noise. As we recall from radar theory, radar detectability is proportional to the amount of energy returned from the target. Conventional noncoherent radar signal processing techniques, compare the range azimuth-elevation cell return against a threshold and make a detection decision based upon the results of this comparison. No past data is usually saved after the decision process, although some information about the target might be contained in the discarded data. Detection improvement in those systems is usually achieved by using a high range resolution waveform combined with a high speed scanning antenna (60-300 RPM), to perform scan-to-scan integration. The target is extracted from the clutter background using the fact that target returns tend to correlate from scan to scan, while the clutter returns tend to decorrelate from scan to scan. Spectral discrimination techniques using Doppler processing [Ref. 2], are not appropriate for the detection of relatively slow targets since the target may be stationary or have zero velocity relative to the local mean surface waves. Detection performance improvement is required to enable successful operation in the modern environment of reduced RCS targets and restricted Electromagnetic Emission Control Policy (EECP), which implies brief periods of radar operation.

One approach that shows promise uses a high speed digital processor to implement a type of processing known as track-before-detect [Ref. 3,4,6,7,23]. As presented in greater detail in the following chapters, the track-before-detect method uses data taken prior to thresholding (or detection) which is processed into feasible tentative tracks on a scan-to-scan, or revisit-to-revisit basis. Measures of the track strength, track quality and other track parameters are generated for each tentative track, tracks are declared or when appropriate

thresholds are exceeded. Detection sensitivity improvement using this method comes from avoiding loss of information caused by premature thresholding and discarding data processed on prior data scans or revisits. In this way information that takes longer than one scan, or revisit, to develop can be exploited. Some approaches to the track-before-detect method were offered by Reed [Ref. 3], and Barniv [Ref. 4], which applied dynamic programming to the track-before-detect problem.

Carlson, Evans and Wilson [Ref. 1] introduced a new method for track-before-detect which results in improved target detection and applied the method to an air-traffic control problem, namely detecting high speed targets in a clutter free environment. This thesis investigates the applicability of this technique for the detection of small low speed targets in the presence of noise and sea clutter. The technique combines the raw data from multiple scans and translates them into multi-dimensional time range space using the Hough transform. The Hough transform which is a curve or a "feature" detector, usually used in image processing, translates targets that appear as hits or points in the time range space to curves or "features" in the Hough domain. The method uses the Hough transform and the inverse Hough transform to extract the detection tracks from the raw radar data. Using this technique creates a track defined by the detected curve in the Hough domain and reduces the need to revisit a detected target to accomplish the acquisition process. The proposed method improves the performance of noncoherent integration from scan-to-scan, from beam-to-beam, and from range cell-to-range cell.

B. OBJECTIVES

The objective of this thesis, is to investigate track-before-detect signal processing, applied to the radar returns of small moving or stationary targets, in an additive noise and high sea clutter background. A major goal is to determine the feasibility of using the Hough transform to accomplish the track-before-detect function.

It is expected that extraction of targets using the track-before-detect process will enhance target detection since all the energy returned from the target is correlated prior

to thresholding. This is equivalent to using a three dimensional filter which is matched to the target trajectories, in addition to the conventional target parameters. The questions to be answered by this thesis concern the effectiveness of the Hough transform in achieving improved radar target detection. The methodology used in this thesis is as follows :

- ▶ An efficient algorithm to perform the Hough transform and inverse Hough transform was derived;
- ▶ The detection performance (i.e., probability of detection (P_d) as a function of Signal to Noise Ratio (SNR) curves, and P_d as a function of probability of false alarm (P_{fa}) curves) using the Hough transform process, were determined parametrically;
- ▶ Benchmark performance of an optimal signal processing (using all the target energy) was determined;
- ▶ Hough transform processing was compared against the optimum detector in Rayleigh interference to determine detection loss; and
- ▶ Hough transform performance as a function of radar and target parameters was determined.

C. THESIS OUTLINE

The analysis and results associated with the investigation of the above described problem are presented in the five subsequent chapters. Chapter II presents the track-before-detect concept and the Hough transform technique as an efficient way to implement track-before-detect in search radars. In Chapter III a theoretical background for radar detection theory of targets in the presence of thermal noise and sea clutter is introduced. Chapter IV introduces the algorithm developed in this thesis. The results obtained using those algorithms and comprehensive comparison between those results and the theoretical results are discussed in Chapter V. Recommendations and conclusions are presented in Chapter VI. Finally, the MATLAB computer code for each algorithm is presented in the appendix.

II. TRACK-BEFORE-DETECT PROCESSING

A. TRACK-BEFORE-DETECT BASIS

Track-Before-Detect (*TBD*) processing [Ref. 21], has a primary objective of enhancing target detectability. In contrast to conventional approaches, *TBD* is an algorithm for detecting trajectories, as opposed to detecting single dwell target returns and assembling trajectories from those returns. As a result, *TBD* is applied over multiple observation intervals, or dwells, of the radar rather than over the multiple pulse repetition intervals that constitute an individual dwell. Consequently, the time between updates in the *TBD* process is typically in the order of seconds. Significant target motion can occur between updates making it necessary to associate, over several updates, the resolution cells that correspond to the target motions. The name track-before-detect is derived from the fact that a sequence of associated resolution cells, comprising a time history of the target or track exists before detection is declared. Considering a coherent search radar, capable of measuring the range, range rate, and azimuth angle of the target, the track-before-detect algorithm consists of the following set of procedures:

- ▶ Integration of the received radar signals over the dwell time of the scanning radar beam;
- ▶ Comparing the integrated signals in each resolution cell on each scan to an amplitude threshold, which is set lower than normal;
- ▶ Over a number of scans N , forming sets of associated cells, called templates, which correspond to possible target motions;
- ▶ In each template count the number of scans for which the amplitude threshold is exceeded, calling this number m ;
- ▶ Applying m out of M test (i.e., declare target detection if in a template $m \geq M$) where M is a selected integer less than N ; and
- ▶ Continue to form new templates and extend those that have yielded detections by repeated application of the rules of association.

Figure 1, introduced by Schleher [Ref.5], illustrates the *TBD* concept implemented as a linear velocity filter for short exposure targets. The figure illustrates normalized target and sea clutter returns, plotted on a scan to scan basis. The *TBD* filter is implemented as a linear velocity template which is matched to a particular target trajectory. One template is required for each realizable target velocity, consistent with the radar range resolution. In this example, detection occurs when at least 9 target responses fall within the linear velocity template set for a target exposure of 6 seconds (12 scans). False alarm occurs when at least nine random sea spikes and noise match the template response. To the human eye, a target track is easily visible. However, if only one data set is viewed at a time it is impossible to tell with much certainty if a target is present or not.

In an automatic detection system [Ref. 6], a detection decision can be made by thresholding a score that is a function of all the amplitudes along each potential target

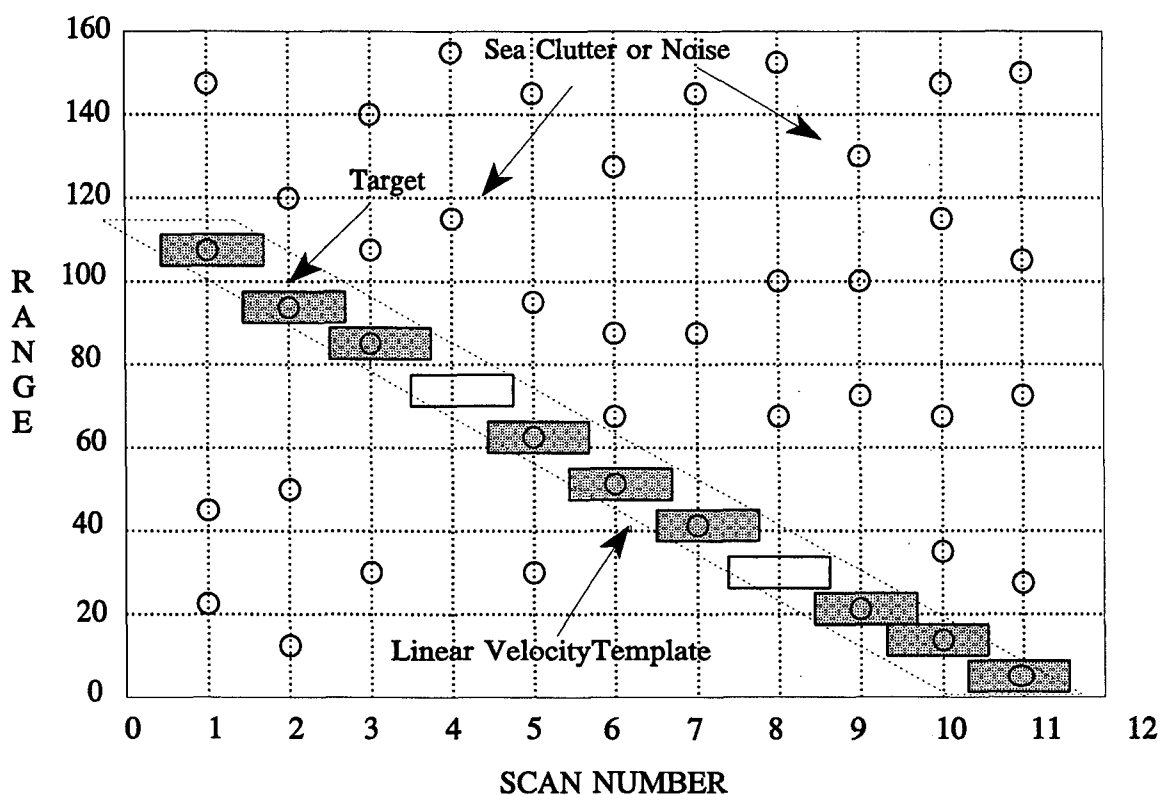


Figure 1. Track-Before-Detect Process.

trajectory, rather than thresholding after each dwell or revisit, and then trying to make a decision based on a single data point. A simple scoring function can be defined by noncoherent integration along the candidate trajectory, in which case the *TBD* functions as an adaptive noncoherent integrator which follows the target motion. Thus, the *TBD* can be applied in cases where conventional noncoherent integration would be inefficient because of target motion. *TBD* exploits the fact that, because of target motion constrains, the position cell of the target return will be correlated from dwell to dwell, whereas the positions of the noise spikes will not.

B. THE HOUGH TRANSFORM

The Hough transform, (*HT*) was first introduced by Paul Hough [Ref. 8] in 1961 as a method of detecting complex patterns in binary image processing. It achieves this by determining specific values of parameters which characterize these patterns. Spatially extended patterns are transformed, so that they produce spatially compact features in a space of possible parameter values. The *HT* converts a difficult global detection problem in image space into a more easily solved local peak detection problem in a parameter space. The key idea behind the *HT* can be illustrated by considering sets of collinear points in an image. A set of image points (x,y) , which lie on a straight line can, be defined by a relation f , such that

$$f(\hat{m},\hat{c}),(x,y))=y-\hat{m}x-\hat{c}=0, \quad (2.1)$$

where m and c are two parameters, the slope and intercept, which characterize the line. Equation (2.1) maps each value of the parameter combination (m,c) to a set of image points. The *HT* uses the idea that Equation (2.1) can be viewed as a mutual constraint between image points and parameter points, and therefore, it can be interpreted as defining a one to many mapping from an image point to a set of possible parameter values. This corresponds to calculating the parameters of all straight lines, which belong to the set that passes through a given image point (x,y) . This operation is called back-projection of the image point; the definition relation which achieves this is given by

$$g((\hat{x}, \hat{y}), (m, c)) = \hat{y} - \hat{x}m - c = 0. \quad (2.2)$$

In the case of a straight line, each image point (x, y) back-projects or defines a straight line in the (m, c) parameter space. Figure 2a is a typical point image, and Figure 2b shows the parameter lines produced by back-projecting the image points into parameter space using Equation (2.2). Points which are collinear in image space all intersect at a common point in parameter space, as demonstrated in Figure 2c, where the coordinates of this parameter point characterizes the straight line connecting the image points. The *HT* identifies those points of intersection in the parameter space. Determination of the point of intersection in the parameter space is a local operation, which is considerably easier than detecting extended point patterns in image space. The extension of the method to detect parameterically defined image curves, other than straight lines, is straightforward. Image points on a curve, characterized by n parameters a_1, \dots, a_n , can be defined by an equation in the form of

$$f((\hat{a}_1, \dots, \hat{a}_n), (x, y)) = 0. \quad (2.3)$$

By interchanging the roles of the parameters and variables, Equation (2.3) can be used to derive the defining relations for the back-projection mapping of image points to parameter space

$$g((\hat{a}_1, \dots, \hat{a}_n), (x, y)) = 0. \quad (2.4)$$

This back-projection equation maps out a hypersurface in the n -dimensional parameter space. The most probable parameters for image curves are indicated by the intersection of several of those hypersurfaces.

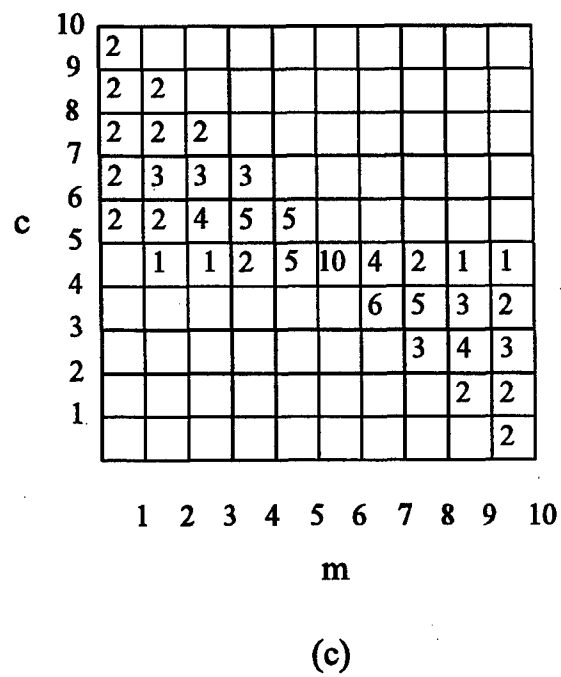
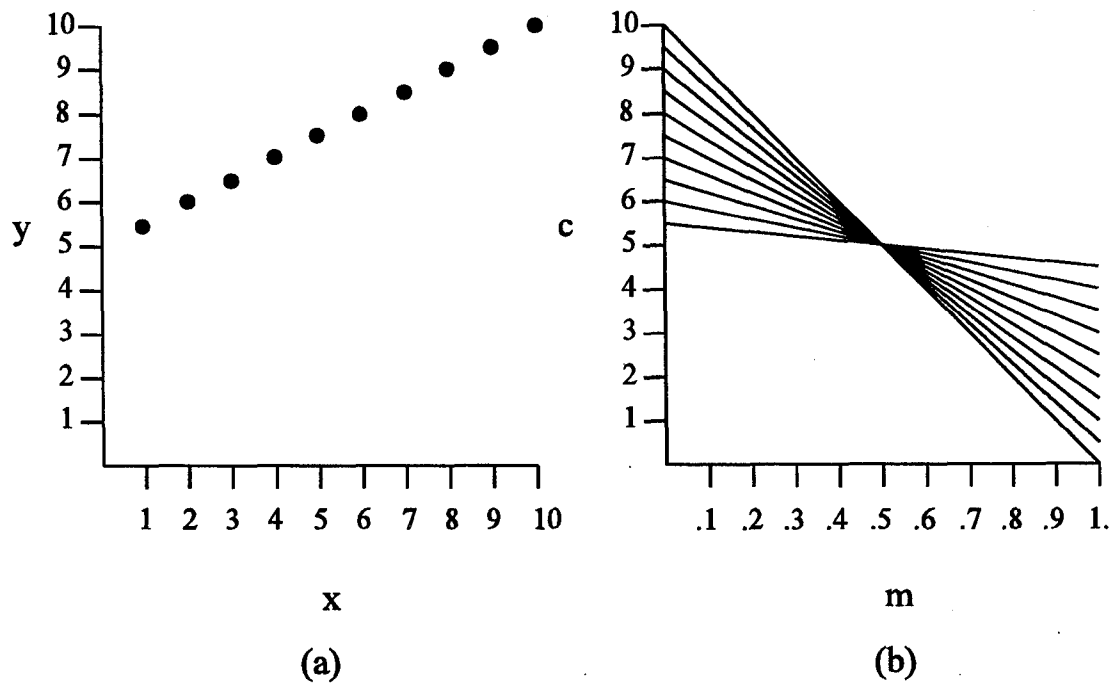


Figure 2. Hough Transform for Line Detection.
 (a) Point Image Space.
 (b) Parameter Space.
 (c) Accumulator Parameter Space.

Duda and Hurt [Ref. 8] suggested that straight lines might be usefully parameterized by the length ρ , and the orientation, θ , of the normal vector to the line from the image origin given as

$$\rho = x \cos(\theta) + y \sin(\theta). \quad (2.5)$$

This has distinct advantage over the (m,c) parameterization which has a singularity for lines with large slopes, i.e., $m \rightarrow \infty$. Using the (ρ, θ) parameters means that image points map into sinusoidal curves in a two parameter space.

Once the *HT* has been accumulated, the pattern of the counts in the accumulator is analyzed to estimate the presence and location of the local peaks. The most common method is to determine a global threshold. Any accumulator cell with more counts than the threshold indicates a possible occurrence of the search for shape. The threshold is chosen either using prior knowledge, or it can be automatically selected by analyzing the distribution of counts in the array, e.g., a fixed fraction of the maximum count on any single accumulator bin. The shortcomings in the *HT*, as presented by Hunt [Ref. 19], are;

- ▶ The *HT* suffers from performance degradation due to presence of noise in the image plane;
- ▶ The *HT* tends to favor long lines at the expense of short lines, that is a result of the peak detection embedded in the back-projection to the image plane; and
- ▶ The *HT* implicitly assumes uniform distribution of the noise.

As a result, image planes that are contaminated with noise, or containing objects with almost but not quite parallel edges, will suffer from performance degradation.

C. USE OF THE HOUGH TRANSFORM IN SEARCH RADAR

Traditional search radars provide range, azimuth, elevation and Doppler data as functions of time, where time is quantized by the scan period, and the coverage sector is searched by sequentially looking in all beam directions. Conventional radars usually apply noncoherent integration and *M-out-of-N* decision rule, so that a target is declared if the returns for a beam position and a range gate are above a predefined threshold. When

considering a moving target that could move from one detection cell to another, the integrating efficiency drops; this problem is known as the range-walk problem. The Hough transform, as discussed in the previous subsection, is a curve or a "feature" detection method which is well suited to locating lines in a plane of noise. When using conventional maritime radars, the effective information is usually obtained through time domain analysis, where features are mainly due to sea clutter and clutter characteristics which makes the discrimination between the target and the clutter a difficult task. Sampling of a radar power returns from a target and analyzing them in the time-range plane, leads to a curve which represents the target trajectory (where the amplitude of the curve represents the returns power level). Detection of this curve reveals all the current information about the detected targets. Figure 3 shows an example of a 20 knots radial velocity target in the time-range plane for a particular beam and Doppler bin. The slope of the line is determined by the velocity of the target. Stationary target, or stationary clutter, would appear as horizontal lines in this space. All moving targets would have some finite slope approaching zero, as the target moves faster. The time axis runs from the past to the current time and contains the number of scans integrated. The target movement, which defines a line in the time-range domain, can be defined by the angle θ of its perpendicular, from the origin and the distance ρ from the origin to the line along the perpendicular, as demonstrated in Figure 3. The Hough transform map points in the time-range space into curves in the Hough parameter space (θ, ρ) by

$$\rho = r \cos\theta + t \sin\theta. \quad (2.6)$$

The r and t in this equation are measured from the origin of the time-range space. The mapping to the Hough space is done by stepping through θ from 0° to 180° and calculating the corresponding ρ . Carlson, Evans and Wilson [Ref 1] have shown that by trigonometric manipulation, Equation (2.6) can be expressed as

$$\rho = \sqrt{r^2 + t^2} \sin(\theta + \tan^{-1} \frac{r}{t}). \quad (2.7)$$

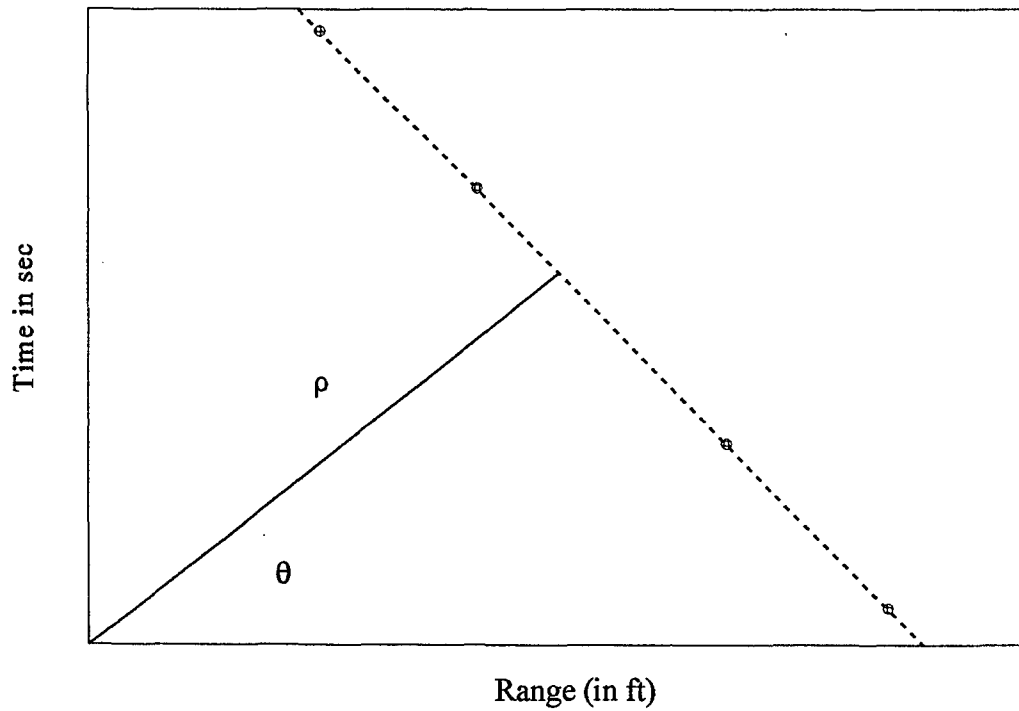


Figure 3. Time-Range Space Geometry and the Corresponding Hough Parameters.

Equation (2.7) leads to a sinusoid with amplitude and phase depending on the r - t value of the mapped data point. Figure 4 shows the Hough transformation of the data points in Figure 3. It can be observed that each ρ - θ point in the Hough space represents a single straight line in the r - t space with the corresponding ρ - θ value. Each of the curves in the Hough space represents the set of all possible lines in the r - t space that cross the corresponding data point. The line in the r - t domain that connects all the data points corresponds to the point of intersection of all the mapped sinusoid in the Hough space. The time-range space is divided into cells equal to the number of range gates times the number of scans being considered. Convenient way for mapping the time -range space to the Hough space using simple matrix multiplication was offered by Carlson, Evans and Wilson [Ref 1] as follows:

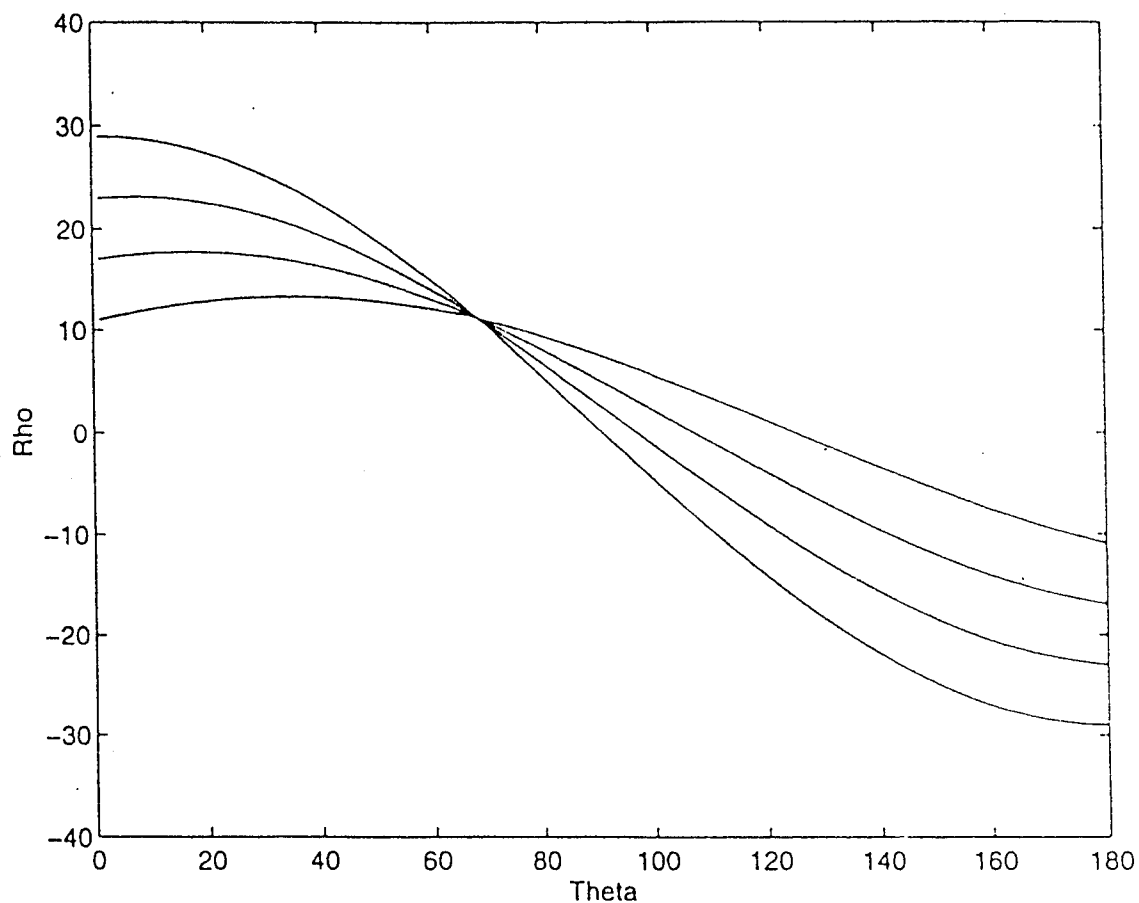


Figure 4. Hough Parameter Space Corresponding to Figure 3 Data Points.

A data matrix RT comprised of radar returns in the time-range space is defined, such that the columns contain I radar range returns and the corresponding time value for a particular antenna direction

$$RT = \begin{bmatrix} r_1 & r_2 & r_3 & \cdots & r_I \\ t_1 & t_2 & t_3 & \cdots & t_I \end{bmatrix} \quad (2.8)$$

Now a transformation matrix H is defined as the combination of all the sines and cosines, as defined in Equation (2.6)

$$H = \begin{bmatrix} \cos\theta_1 & \sin\theta_1 \\ \cos\theta_2 & \sin\theta_2 \\ \cdot & \cdot \\ \cdot & \cdot \\ \cos\theta_N & \sin\theta_N \end{bmatrix}, \quad (2.9)$$

where θ takes N values from 0° to 180° using predefined resolution cells. Determination of the resolution cells is resolved by the simulation and will be discussed in Chapter IV. The multiplication of RT and H gives a N by I matrix R containing the values of ρ for the different data points. The subscripts of ρ values represent the index numbers of the data point transformed and the angle θ used in the Hough mapping

$$R = H * RT = \begin{bmatrix} \rho_{1,\theta_1} & \cdot & \cdot & \rho_{I,\theta_1} \\ \cdot & \cdot & \cdot & \cdot \\ \cdot & \cdot & \cdot & \cdot \\ \rho_{1,\theta_N} & \cdot & \cdot & \rho_{I,\theta_N} \end{bmatrix}. \quad (2.10)$$

Each column of the matrix R represents the N ρ values for each one of the Hough space sinusoid. It is clear that the more data points in the image plane we have the bigger R and RT will be, resulting in heavier computational load. The transformation matrix is precomputed, and its size depends only on the parameter space quantization.

III. RADAR DETECTION THEORY

A. OPTIMUM DETECTION PROCESS

An optimum receiving process for a return signal of known form with unknown phase, which may be used as a reference for comparison of radar detection performance, is diagrammed in Figure 5.

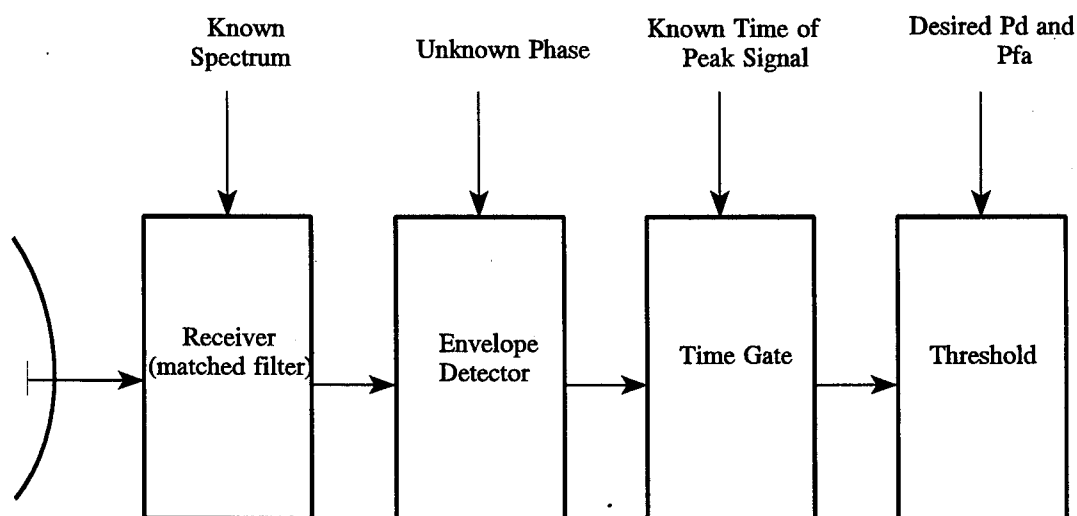


Figure 5. Optimum Unknown Phase Detection Process.

All signal parameters, except carrier phase, are known exactly. The receiving filter is matched to the signal spectrum. When the signal envelope out of the filter reaches its maximum value, the signal to noise average power ratio is equal to the ratio of total received signal energy to the noise spectral density. The ratio of signal power at the peak of the carrier cycle to rms noise is twice as great and is taken into account in setting the

detection threshold. This system will be used to establish the detection performance of a conventional detection process and enables comparison to the Hough based detectors.

1. Detection Performance of an Optimum Detection Process.

Consider a sine wave signal present, along with Gaussian noise (with mean a and variance σ_n^2), in the input to an IF filter. The resulting output of an envelope detector (with amplitude r) is Ricean, i.e., the density function for R is

$$p_R(r) = \frac{r}{\sigma_n^2} \exp\left(-\frac{r^2 + a^2}{2\sigma_n^2}\right) I_0\left(\frac{ar}{\sigma_n^2}\right), \quad (3.1)$$

where $I_0(z)$ is the modified Bessel function of zero order and argument z . We use the transformations

$$R = \frac{a^2}{2\sigma_n^2}, \quad y = \frac{r^2}{2\sigma_n^2}, \quad (3.2)$$

where R corresponds to the signal to noise ratio and y to the normalized output of a square law device. Probability of detection is defined as the probability of y exceeding a threshold level ξ , given x and is obtained by the equation

$$P[y > \xi | R] = \int_{\xi}^{\infty} \exp[-(y+R)] I_0(2\sqrt{Ry}) dy. \quad (3.3)$$

In the absence of target, i.e., noise-only case, $R=0$ and we obtain the probability of false alarm as

$$P_{fa} = \int_{\xi}^{\infty} \exp(-y) dy. \quad (3.4)$$

If instead of a single observation, N observations y_n , $n=1, 2, \dots, N$, of the output of a square law device with corresponding signal to noise ratio are made and summed, then

the probability that the sum $y = \sum_{n=1}^N y_n$ exceeds a threshold ξ for specified R_n is given by

$$P_n(\hat{R}, \xi) \triangleq P(Y > \xi | R_1, R_2, \dots, R_N) = \int_{\xi}^{\infty} \left(\frac{y}{N\hat{R}} \right)^{\frac{N-1}{2}} \exp[-(y - N\hat{R})] I_{N-1}(2\sqrt{N\hat{R}y}) dy, \quad (3.5)$$

where

$$\hat{R} \triangleq \frac{1}{N} \sum_{n=1}^N x_n. \quad (3.6)$$

2. Albersheim's Detection Equation

Walter Albersheim [Ref. 9] derived a simple formula for signal to noise ratio, which is required to achieve a given level of performance for envelope detection of nonfluctuating signal, in narrow band noise. Despite its simplicity, this empirical equation is remarkably accurate. The equation replaces the use of many graphs and cumbersome calculations. The Albersheim equation is given as

$$SNR = -5 \log_{10} M + \left(6.2 + \frac{4.54}{\sqrt{M+0.44}} \right) \log_{10}(A + 0.12AB + 1.7B), \quad (dB) \quad (3.7)$$

where

$$\begin{aligned} A &= \ln \left(\frac{0.62}{P_f} \right), \\ B &= \ln \left(\frac{P_d}{1 - P_d} \right) = \ln(P_d) - \ln(1 - P_d). \end{aligned} \quad (3.8)$$

M is the number of independent pulses, P_d detection probability and P_{fa} the false alarm probability.

3. Collapsing Loss

Practical radar systems can seldom preserve their full RF signal through the integration and thresholding process. Consider n video samples containing signal plus noise integrated along with m extra samples of noise alone. Collapsing loss [Ref. 19] is defined as the additional signal to noise ratio required to provide a specific detection

performance (P_d , P_{fa}) for the $n+m$ signal plus noise variates, as compared to that required in the case of n signal plus noise variates and is given as

$$L_c = 10 \log \left(\frac{R_2}{R_1} \right), \quad (3.9)$$

where R_1 is the required signal plus noise ratio with m extra noise variates and R_2 is the signal to noise ratio required with no extra noise variates. The resulting collapsing ratio ρ is defined as

$$\rho = \frac{n+m}{n} = 1 + \frac{m}{n}. \quad (3.10)$$

Several empirical methods are available for estimating the collapsing loss. The most highly developed method is Batron's method [Ref. 10], which uses the concept of an empirically determined detector loss function. To carry on with the Barton method, it is necessary to introduce a quantity called the detectability factor, which is defined as the ratio of single pulse energy to noise power per unit bandwidth, that provides stated probabilities of detection and false alarm. The notation for the detectability factor is $D_i(n)$, where $i=0, 1, 2, 3, 4$ identifies either a steady case (0) or a Swerling type fluctuating target (1, 2, 3, 4), while n indicates the number of pulses which are incoherently integrated. The detectability factor for a fully coherent detection is $D_c(n)$. The empirically determined detector loss $C_n(x)$ is given by

$$C_x(n) = \frac{[D_0(n) + 2.3\rho]}{D_0(n)}. \quad (3.11)$$

From the definition of the detector loss, the n -th pulse incoherently integrated detectability factor is given by

$$D_0(n) = \frac{D_c(1) C_x(n)}{n}. \quad (3.12)$$

Substituting Equation(3.11) into Equation (3.12) and solving for $D_0(n)$ results in

$$D_0(n) = \frac{D_c(1)}{2n} \left[1 + \sqrt{\frac{1+9.2n\rho}{D_c(1)}} \right] \quad (3.13)$$

The additional signal to noise ratio required, as compared to coherent integration, can be expressed in terms of integration loss given by

$$L_i(n) = \frac{nD_0(n)}{D_0(1)} = \frac{1 + \sqrt{1 + \frac{9.2n}{D_c(1)}}}{1 + \sqrt{1 + \frac{9.2}{D_c(1)}}} \quad (3.14)$$

This can be used to find the collapsing loss which is given by

$$L_c(\rho n) = \frac{L_i(\rho n)}{L_i(n)} = \frac{1 + \sqrt{1 + \frac{9.2n\rho}{D_c(1)}}}{1 + \sqrt{1 + \frac{9.2n}{D_c(1)}}} \quad (3.15)$$

A coherent detection curve for $D_c(1)$, in terms of P_d and P_{fa} is achieved using empirical results and are given in [Ref. 10].

B. DOUBLE THRESHOLD PROCESS DETECTION PERFORMANCE

Double threshold, or *M-out-of-N* detection algorithm, is widely applied in search radars. In this process, a fixed group of N pulses is applied to a detector threshold ξ . A detection is declared if the number of threshold crossings within the group exceeds a secondary threshold M . For a nonfluctuating target, it was shown that the *M-out-of-N* probability of detection P_D , is related to the single pulse probability of detection p_d , by the binomial relation

$$P_D = \sum_{k=M}^N \binom{N}{k} (p_d)^k (1-p_d)^{N-k}. \quad (3.16)$$

In the absence of a signal, the probability of a false M -out-of- N detection, due to noise, P_{FA} , is similarly related to the single pulse probability of detection p_{fa} by

$$P_{FA} = \sum_{k=M}^N \binom{N}{k} (p_{fa})^k (1-p_{fa})^{N-k}. \quad (3.17)$$

The single pulse probability of false alarm is related to the threshold level ξ by

$$p_{fa} = \exp(-\eta), \quad (3.18)$$

where

$$\eta = \frac{1}{2} \left(\frac{\xi}{\sigma_n} \right)^2. \quad (3.19)$$

σ_n is the standard deviation of the noise, and ξ the threshold setting. Since it is developed in the absence of any signal except for that due to system noise, Equation (3.17) is directly valid for all target fluctuation cases (Swerling cases).

1. Probability of Detection for Nonfluctuating Target

The nonfluctuating target has been modeled by Marcum [Ref. 11], wherein each pulse of a group of N pulses is of constant amplitude. The probability density function of such a process is Ricean distributed and may be written in terms of the single pulse probability of detection

$$P_d = \int_{\xi}^{\infty} \frac{r}{\sigma_n^2} \exp \left(-\frac{r^2 + a^2}{2\sigma_n^2} \right) I_0 \left(\frac{ar}{\sigma_n^2} \right) dr. \quad (3.20)$$

Equation (3.20) can be recognized as the Marcum Q function. Thus, it follows from

Equations (3.16) and (3.20) that for the nonfluctuating case

$$P_{DM}(s) = \sum_{k=M}^N \binom{N}{k} [Q(R,\eta)]^k [1-Q(R,\eta)]^{N-k}, \quad (3.21)$$

where $Q(R,\eta)$ is the Marcum Q function, and R normalized signal to noise ratio as defined by Equation (3.2).

2. Probability of Detection for Swerling Case I Target

The slowly fluctuating target has been described by Swerling as one in which pulses are perfectly correlated within the integration time but are scan to scan independent. For this analysis, the Swerling case I target may be considered to be a series of N Marcum model pulses accruing successively but with statistically independent amplitudes from scan to scan. If we assume that statistics of this amplitudes variation are Rayleigh distributed, we can write

$$P_{DI} = \int_0^{\infty} \frac{R}{G} \exp\left(-\frac{R^2}{2G}\right) P_{DM}(R) dR, \quad (3.22)$$

where $P_{DM}(s)$ is the Marcum case detection probability, and G the average power signal to noise ratio. Combining Equations (3.21) and (3.22), we obtain P_{DI} , the detection probability for Swerling case I target

$$P_{DI} = \int_0^{\infty} \frac{R}{G} \exp\left(-\frac{R^2}{2G}\right) \sum_{k=M}^N \binom{N}{k} [Q(R,\eta)]^k [1-Q(R,\eta)]^{N-k} dR. \quad (3.23)$$

C. DETECTION PERFORMANCE IN THE PRESENCE OF SEA CLUTTER

1. K Distributed Clutter Model

For radars in which the dimension of the range resolution cell is much greater than the sea swell wavelength with grazing angles greater than about 10° , it is well known that the clutter amplitude is Rayleigh distributed [Ref. 12]. This is the consequence of the central limit theorem, since the results can be thought of as being the vector sum of two

randomly phased components from a large number of independent scatterers. As the radar resolution is increased and for a smaller grazing angle, the clutter amplitude is observed to develop a longer "tail", and the returns are often described as becoming spiky [Ref. 12, 13, 14]. It has been found from practical measurements over a wide range of conditions that the clutter returns for a high resolution radar can be well modeled by two components. The first component is an underlying mean level obeying a chi distribution. This mean level has a long temporal decorrelation period, which characterizes for example, the mean level variation in clutter spikes, or the periodic variation in amplitude as seen when looking up or down the sea swell. The second component is termed the "speckle" component. This speckle component has a mean level determined by the first component of the clutter model. The K distribution is derived by averaging the speckle components over all possible values of the mean level

$$p(r) = \int_0^{\infty} p(r/u)p(u)du, \quad (3.24)$$

where $p(r)$ is the overall Probability Density Function (*PDF*) of the clutter returns, $p(u)$ is the *PDF* of the clutter mean level, and $p(r/u)$ is the *PDF* of the speckle component. The speckle component is Rayleigh distributed so that

$$p(r/u) = \frac{\pi r}{2u^2} \exp\left(-\frac{\pi r^2}{4u^2}\right), \quad r \geq 0, \quad (3.25)$$

where u obeys a chi distribution and $p(u)$ is given by

$$p(u) = \frac{2b^{2v}}{\Gamma(v)} u^{2v-1} \exp(-b^2 u^2), \quad u \geq 0, \quad (3.26)$$

where Γ is the gamma function, v is a shape parameter, $b^2 = v/\Omega$ and $\Omega = E[u^2]$ is the average power of the clutter. Substituting Equations (3.25) and (3.26) into Equation (3.24) yields the K-distribution

$$p(r) = 4 \frac{c^{v+1}}{\Gamma(v)} r^v K_{v-1}(2cr), \quad (3.27)$$

where $K_\nu(x)$ is the $(\nu-1)$ -th order modified Bessel function of the third kind, and $c=b/\sqrt{2}$ is the distribution scale parameter. For high resolution sea clutter, values of ν are generally observed in the region $0.1 \leq \nu \leq \infty$, where $\nu \approx 0.1$ represents a very spiky and $\nu = \infty$ represents thermal noise. An empirical derived shape factor for an x band radar is offered by Watts [Ref. 12] and given by

$$\log(\nu) = \log \left[\frac{2}{3} \log(\phi_g) + \frac{5}{8} \log(l) + \psi - k \right], \quad (3.28)$$

where ϕ_g is the grazing angle in degrees, l is the cross range resolution in meters, ψ is the aspect dependency, which takes value of $-\frac{1}{3}$ for up or down swell directions, $\frac{1}{3}$ for across swell and 0 for intermediate directions, or no swell, and k describes the polarization effect and takes the value 1 for vertical polarization and $\frac{1}{7}$ for horizontal polarization.

2. Detection Performance in K Distributed Clutter

The analysis for the detection performance in K-distributed clutter [Ref. 15, 16] assumes that the detection processing consists of a linear bandpass filter and a square law detector, followed by a pulse to pulse integrator. This receiver is not optimal for the K-distributed clutter, but it is widely used in practice, since the detection is easy to implement. The output of a square law detector is sampled in turn at time intervals $t=iT$ ($i=0,1,\dots,N-1$) and then integrated. A test statistic V is compared with a threshold η to decide whether or not a target exists. The output of the receiver can be represented by

$$r(t) = S(t) + C(t) + n(t), \quad (3.29)$$

where $S(t)$, $C(t)$ and $n(t)$ represent signal, K-distributed clutter and receiver noise, respectively. They can be expressed as

$$\begin{aligned}
S(t) &= a(t)\cos(\omega_c t) - b(t)\sin(\omega_c t), \\
C(t) &= x_c(t)\cos(\omega_c t) - y_c(t)\sin(\omega_c t), \\
n(t) &= x_n(t)\cos(\omega_c t) - y_n(t)\sin(\omega_c t),
\end{aligned} \tag{3.30}$$

where $a(t)$, $b(t)$, $x_c(t)$, $x_n(t)$ and $y_n(t)$ represent the inphase and the quadrature component of the signal, clutter, and noise, respectively. They are mutually independent random processes. Equation (3.29) can be rewritten as

$$r(t) = [a(t) + x(t)]\cos(\omega_c t) - [b(t) + y(t)]\sin(\omega_c t), \tag{3.31}$$

where

$$\begin{aligned}
x(t) &= x_c(t) + x_n(t), \\
y(t) &= y_c(t) + y_n(t),
\end{aligned} \tag{3.32}$$

are the inphase and quadrature of the clutter plus noise. The average power of $x(t)$ or $y(t)$ is given by

$$E[x^2(t)] = E[y^2(t)] = \int_0^\infty (u^2 + \beta_n^2) p(u) du = \frac{v}{b^2} + \beta_n^2 = \Omega + \beta_n^2, \tag{3.33}$$

where β_n^2 is the average power of white noise component, and Ω is the average power of the clutter. The Average Clutter to Noise Ratio (CNR) is given by

$$\Lambda = \frac{v}{b^2 \beta_n^2} = \frac{\Omega}{\beta_n^2}. \tag{3.34}$$

The test statistic can be defined as

$$V = \frac{1}{2\beta_n^2} \sum_{i=0}^{N-1} [(x_i + a_i)^2 + (y_i + b_i)^2], \tag{3.35}$$

where x_i, y_i, a_i and b_i ($i=0,1,\dots,N-1$) are the samples of $x(t)$, $y(t)$, $a(t)$ and $b(t)$, respectively.

For the convenience of the analysis, u in Equation (3.25) will be regarded as a random variable. Based on this assumption, the conditional *PDF*'s of the inphase and quadrature components of the clutter plus noise can be expressed as

$$p(x/y) = \frac{1}{\sqrt{2\pi(u^2 + \beta_n^2)}} \exp\left[-\frac{x^2}{2(u^2 + \beta_n^2)}\right],$$

$$p(y/u) = \frac{1}{\sqrt{2\pi(u^2 + \beta_n^2)}} \exp\left[-\frac{y^2}{2(u^2 + \beta_n^2)}\right].$$
(3.36)

The Moment Generation Function (*MGF*), defined as the Laplace transform of the *PDF* of the statistic V in the presence of nonfluctuating target, can be obtained by [Ref. 10]

$$L_V(z/u, R) = \frac{1}{\left[1 + \left(1 + \frac{u^2}{\beta_n^2}\right)z\right]^N} \exp\left[-\frac{NRz}{1 + \left(1 + \frac{u^2}{\beta_n^2}\right)z}\right].$$
(3.37)

In the case of a fading target the R in (3.37) is a random variable. For a chi square family of fluctuating targets the *PDF* of R is given by

$$p(R) = \frac{1}{\Gamma(k)} \left(\frac{k}{\bar{R}}\right)^k R^{k-1} \exp\left(-\frac{kR}{\bar{R}}\right),$$
(3.38)

where \bar{R} is the average of R over target fluctuations and $k > 0$ is a fluctuating parameter representing the degree of signal fading. The smaller k corresponds to a deeper signal fading. k can be related to the Swerling's fluctuating model, where $k=1, N, 2, 2N$ and $k=\infty$ corresponds to Swerling cases 1, 2, 3, 4 and constant target, respectively. The *MGF* of test statistic V of the chi square family of fluctuating target can be written as

$$L_V(z/u) = \int_0^\infty L_V(z/u, R) p(R) dR. \quad (3.39)$$

Solving the integral leads to

$$L_V(z/u) = \frac{\left[1 + \left(1 + \frac{u^2}{\beta_n^2} \right) z \right]^{k-N}}{\left[1 + \left(1 + \frac{u^2}{\beta_n^2} + \frac{NR}{K} \right) z \right]^k}. \quad (3.40)$$

In the absence of target, i.e., $R=0$, the *MGF* becomes

$$L_0(z/u) = \frac{1}{\left[1 + \left(1 + \frac{u^2}{\beta_n^2} \right) z \right]^N}. \quad (3.41)$$

The conditional false alarm probability can be obtained using the residue technique to solve the inverse Laplace transform

$$P_{fa}(u) = -\sum_{k0} \text{res} \left[L_0(z/u) \frac{\exp(\eta z)}{z}, z_{k0} \right], \quad (3.42)$$

where $\text{res} [\cdot]$ denotes residue, η is a decision threshold and z_{k0} ($k0=1,2,\dots$) are the poles of $L_0(z/u)$ lying in the left half plane. Solving Equation (3.42) results in

$$P_{fa}(u) = \sum_{n=0}^{N-1} \frac{\eta^n \exp\left(-\frac{\eta}{1 + \frac{u^2}{\beta_n^2}} \right)}{n! \left(1 + \frac{u^2}{\beta_n^2} \right)}. \quad (3.43)$$

The false alarm probability is then obtained by integrating all possible values of u obeying chi-distribution in Equation (3.26)

$$P_{fa} = \int_0^{\infty} (u) p(u) du. \quad (3.44)$$

Solving the integral results in the following equation for P_{fa}

$$P_{fa} = \frac{2b^{2v}}{\Gamma(m)} \sum_{n=0}^{N-1} \frac{\eta^n}{n!} \int_0^{\infty} \frac{u^{2v-1}}{\left(1 + \frac{u^2}{\beta_n^2}\right)^n} \exp\left(-b^2 u^2 - \frac{\eta}{1 + \frac{u^2}{\beta_n^2}}\right) du, \quad (3.45)$$

Calculation of the conditional probability of detection $P_d(u)$ is done similarly with $R \neq 0$

$$P_d(u) = - \sum_{kl} \text{res} \left[L_v(z/u) \frac{\exp(\eta z)}{z}, z_{kl} \right], \quad (3.46)$$

where z_{kl} are the poles of $L_v(z/u)$ lying in the left half plane. Using Equation (3.46), we obtain the following equations:

$$P_d(u) = A \exp\left(-\frac{\eta}{1 + \frac{u^2}{\beta_n^2}}\right) + B \exp\left(-\frac{\eta}{1 + \frac{u^2}{\beta_n^2} + \frac{NR}{k}}\right), \quad 1 \leq k \leq N, \quad (3.47)$$

where A and B are defined as

$$A = \sum_{m=0}^{N-k-1} \binom{N-m-2}{k-1} \frac{(-1)^k \left(1 + \frac{u^2}{\beta_n^2} + \frac{NR}{k}\right)^{N-k-m-1}}{\left(\frac{NR}{k}\right)^{N-m-1}} \sum_{n=0}^m \frac{\eta^n \left(1 + \frac{u^2}{\beta_n^2}\right)^{k-n}}{n!}, \quad (3.48)$$

$$B = \sum_{i=0}^{k-1} \binom{N-i-2}{n-K-1} \frac{\left(-1 + \frac{u^2}{\beta_n^2}\right)}{\left(\frac{NR}{k}\right)^{N-i-1}} \sum_{j=0}^i \frac{\eta^j \left(1 + \frac{u^2}{\beta_n^2} + \frac{NR}{k}\right)^{N-k-j}}{j!}.$$

In the case of $K \geq N$,

$$P_d(u) = \sum_{m=N-1}^{k-1} \binom{k-N}{k-m-1} \sum_{n=0}^m \frac{\eta^n \left(1 + \frac{u^2}{\beta_n^2} + \frac{NR}{k}\right)^{N-k-n}}{n! \left(\frac{NR}{k}\right)^{N-m-1}} \exp\left(-\frac{\eta}{1 + \frac{u^2}{\beta_n^2} + \frac{NR}{k}}\right). \quad (3.49)$$

The detection probabilities are obtained by averaging Equations (3.48) and (3.49) over all possible values of u that is

$$P_d = \int_0^{\infty} p_d(u) p(u) du. \quad (3.50)$$

where $p(u)$ is given by Equation (3.26).

IV. ALGORITHM DESCRIPTION

A. SYSTEM CONFIGURATION

This chapter discusses the system implementation and the design considerations of the various parameters used in the simulation. The system block diagram is presented in Figure 6.

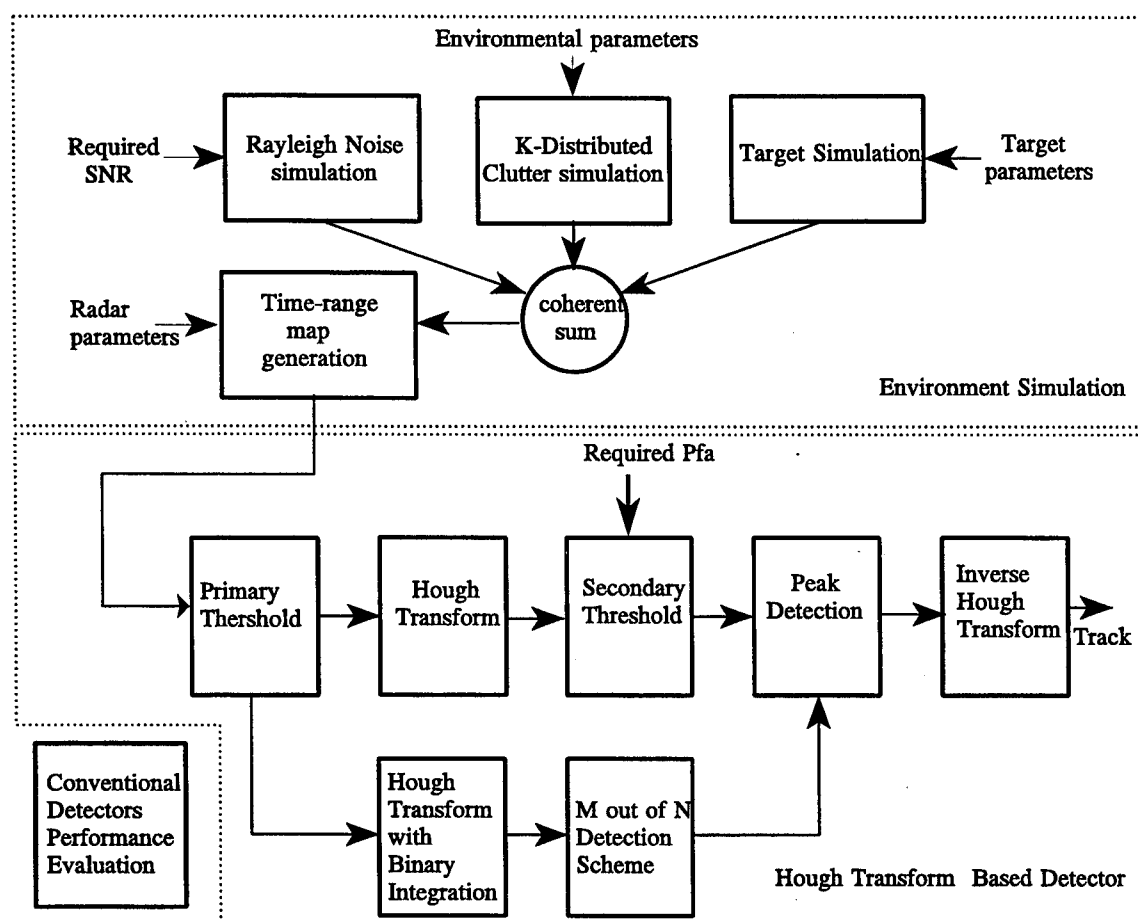


Figure 6. System Configuration.

The algorithm is comprised of three main blocks. The first block is the radar data simulation, responsible for generating the time range data map. This block accepts the following inputs:

- ▶ Radar system parameters, such as Pulse Width (PW), antenna scan rate, peak power and system losses;
- ▶ Environmental conditions such as sea state, radar grazing angle and sea swells characteristics. Those parameters determine the clutter behavior, as discussed in Section B; and
- ▶ Target characteristics, which define the target radar cross section, Swerling case type, location in space and maneuvering information.

The output of this function is a random variable generated as the coherent sum of the three components of the radar returns, namely target signal, noise and sea clutter. The output from the first block serves as the input to the Hough based detector function. This block performs the task of the Hough transform, inverse Hough transform and system detection performance evaluation. Conventional detection schemes performance evaluation is done at the third part of the system and establishes a reference baseline for detection performance comparison.

B. RADAR DATA SIMULATION

To simulate a maritime radar data map, we need to generate the three main components of the radar returns, i.e., target signal, noise and sea clutter. We generate signal plus interference random variable given by

$$rms = \sqrt{(vs - rn_i)^2 + rn_q^2}, \quad (4.1)$$

where vs is the steady signal voltage, rn_i and rn_q are the inphase and quadrature components of the interference respectively. Two types of targets are considered in this work; the non fluctuating target and the Swerling type I target. The nonfluctuating target is modeled as a constant signal, whose amplitude is determined by the radar equation given as

$$S = \frac{P_i G^2 \lambda^2 \sigma L}{(4\pi)^3 R^4}, \quad (4.2)$$

where P_i is the radar peak power, G the antenna gain, σ the target cross section, R the detection range and L the overall system losses. To simulate a Swerling I target, we use a model [Ref. 18] which describes the fluctuation in target amplitude caused by the changes in target aspect angle, rotation or vibration of target scattering sources, or changes in radar wavelength. The Swerling case 1 model assumes a Rayleigh target amplitude fluctuation, which results in an exponential cross section distribution given by

$$w(\sigma, \bar{\sigma}) = \frac{1}{\bar{\sigma}} \exp\left(-\frac{\sigma}{\bar{\sigma}}\right), \quad (4.3)$$

where $\bar{\sigma}$ is the target mean radar cross section.

The clutter addressed in this work is sea clutter and considered to be K distributed. A method of simulating K-distributed clutter introduced by Schleher [Ref. 17], suggests that the K-distributed random variable is given by

$$r = u \sqrt{-2 \ln(x)}, \quad (4.4)$$

where x is a uniformly distributed variable (0-1), u is root gamma (chi) variable defined as

$$u = \frac{\sqrt{t}}{b}, \quad (4.5)$$

where b is a scale parameter, defined by Equation (3.34), and t is a gamma random variable whose PDF is given by

$$p(t) = \frac{t^{v-1} e^{-t}}{\Gamma(v)}, \quad t \geq 0. \quad (4.6)$$

Equation (4.6) implies that K-distributed clutter simulation requires the generation of a gamma random variable of order v . This is done by first generating a gamma deviate of integer order k and then a second gamma deviate of order $v-k$, such that, $a = v-k < 1$.

The sum of the two gamma variates provides a gamma variable of order v . A gamma variable of integer order k can be achieved by adding up k exponentially distributed waiting times, i.e., the logarithms of uniform deviates given by

$$tI_k = -\ln(x_1 * x_2 * \dots * x_k), \quad (4.7)$$

where x_i are uniformly distributed random variables (0-1) and $tI_k = 0$. The second Gamma random variable of order $v-k$ is generated using the rejection method, which is a general technique for generating random variables whose PDF is known and computable. Figure 7 demonstrates the geometrical argument on which the rejection method is based.

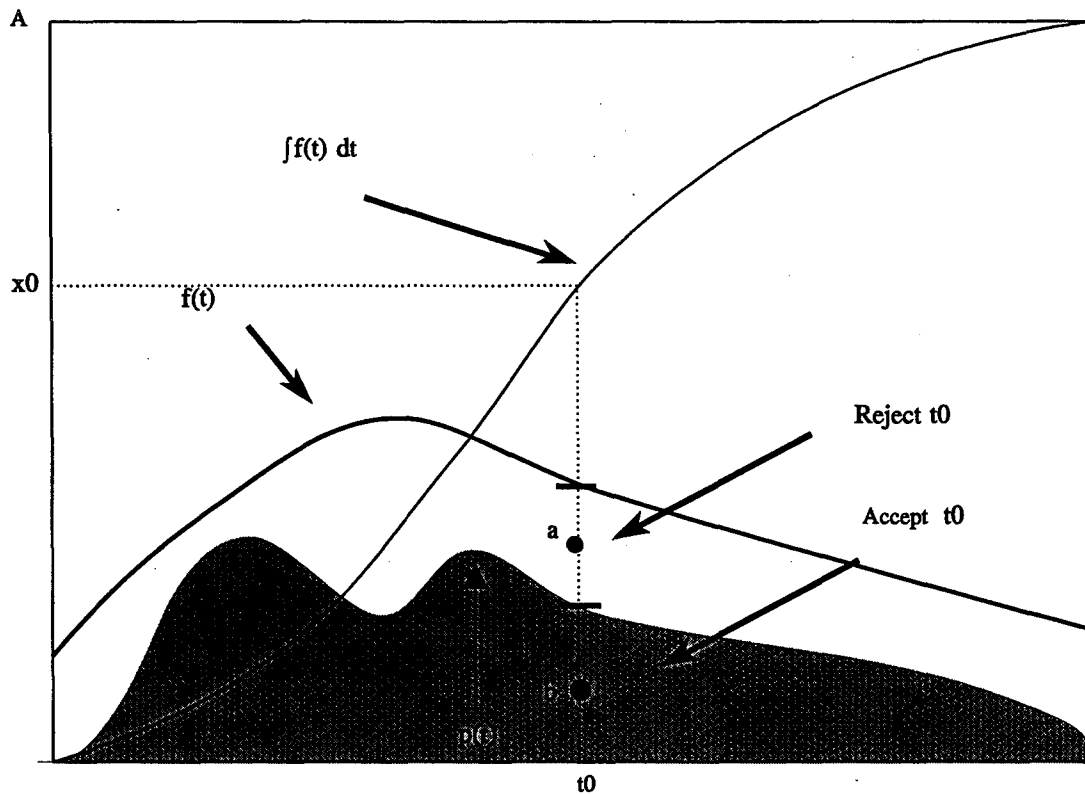


Figure 7. Rejection Method for Generating Random Deviate t with a Known PDF $p(t)$.

We consider a known PDF, $p(t)$ denoted as the shadowed region in Figure 7. The first step in the rejection method consists of selecting an arbitrary invertible function $f(t)$, defined as the comparison function, which lies everywhere above the original probability function. Next consider a point in two dimensions that is uniform in the area under the comparison function (points a and b in Figure 7). If the test point lies outside the original probability function, the point will be rejected; if it lies inside the area, it will be accepted. The accepted points are uniform in the accepted area, so their t values have the desired distribution. To choose a random point in two dimensions, a test random t is generated from the comparison function, using a uniform deviate ranging from zero to A, where A is the area under the comparison function. A second uniform deviate (0-1) is generated and tested against the ratio $q = \frac{p(t)}{f(t)}$. If the deviate is less than q , the variable t is accepted; otherwise it is rejected. An efficient comparison function for the gamma random variable is

$$f(t) = \begin{cases} \frac{t^{a-1}}{\Gamma(a)} & 0 \leq t \leq 1 \\ \frac{e^{-t}}{\Gamma(a)} & t \geq 1 \end{cases} \quad (4.8)$$

Random variables t can be generated from $f(t)$ using the transformation method

$$t(x) = F^{-1}(t), \quad (4.9)$$

where $F^{-1}(t)$ is the inverse function of the indefinite integral of $f(t)$. Applying Equation (4.8) to (4.9) and solving results in

$$t = \begin{cases} a\Gamma(a)x^{\frac{1}{a}} & 0 < t < 1 \\ a\Gamma(a)(1 - \ln(x)) & t \geq 1 \end{cases} \quad (4.10)$$

The rejection criteria is then obtained by computing $q = \frac{p(t)}{f(t)}$ which leads to

$$q = \begin{cases} e^{(-t)} & 0 < t < 1 \\ t^{a-1} & t \geq 1 \end{cases} \quad (4.11)$$

At this point, receiver noise is introduced into the simulation. The noise amplitude is assumed to be Rayleigh distributed; and therefore, the noise power amplitude is exponentially distributed (we assume a square law envelope detector). Since the noise envelope is independent of the clutter, its variance adds to that of the clutter. The resulting random variable simulating k-distributed clutter with receiver noise is given by

$$rn = \sqrt{\left(u^2 + \frac{P_n}{2}\right)(-2 \ln(x))}, \quad (4.12)$$

where P_n is the noise power. Substituting Equation (4.12) into Equation (4.1) and (4.4), yields the target plus interference random variable given as

$$rns = \sqrt{(vs - rn \cos(2\pi x_1))^2 + (rn \sin(2\pi x_1))^2}, \quad (4.13)$$

where x_1 is uniform distributed random variable.

C. HOUGH TRANSFORM BASED DETECTOR

The Hough transform algorithm transforms data from the time-range space to the Hough space, using the formulation of Chapter III. Figure 8 presents the configuration of the time-range space and the Hough space parameters used for the simulations. The time range space is divided into 128 range gates and a time history composed of 100 scans, with scan time defined by the radar parameters. This leads to time-range space dimensions of 128 by 100 for a total of 12800 data cells.

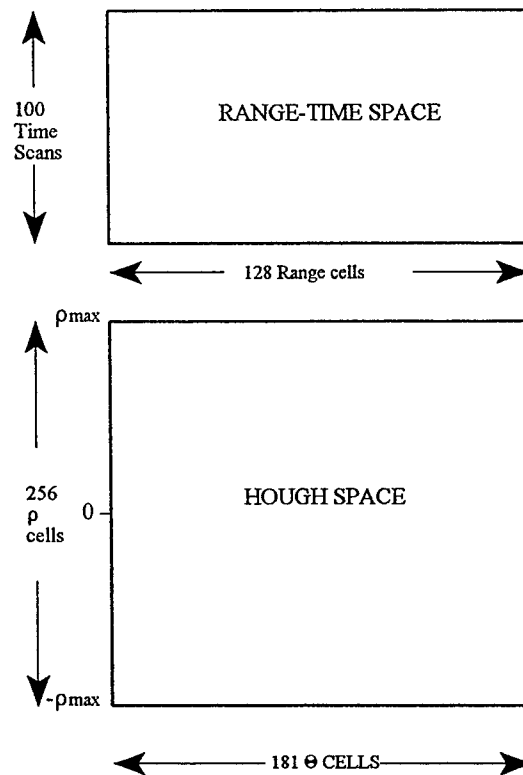


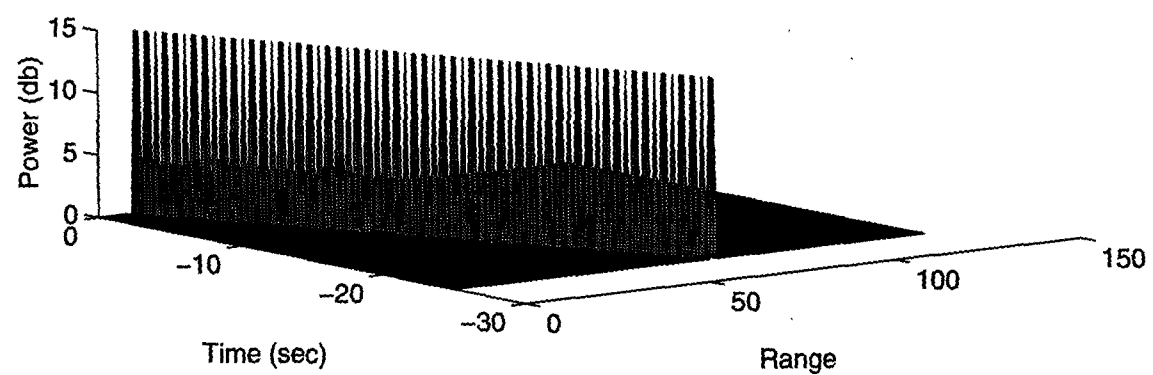
Figure 8. Time-Range Space and Hough Space Configuration.

Figure 9a is a time-range mesh plot example of an approaching constant target with a radial velocity of 20 knots and heading of 45° , relative to the line of sight. Figure 9b is the same target with additive Rayleigh noise. The raw data is compared against a primary threshold whose level is determined by the requirement that the initial probability of false alarm, which is applied to the data at this point, must allow most of the target returns through with some noise spikes. The main objective of the primary threshold is to reduce the computation load, which is linearly proportional to the number of time-range cells crossing the primary threshold. The primary threshold level, η , is determined by the desired value of the initial probability of false alarm (per pulse) in the time-range domain, P_{fa} , given (for the case of

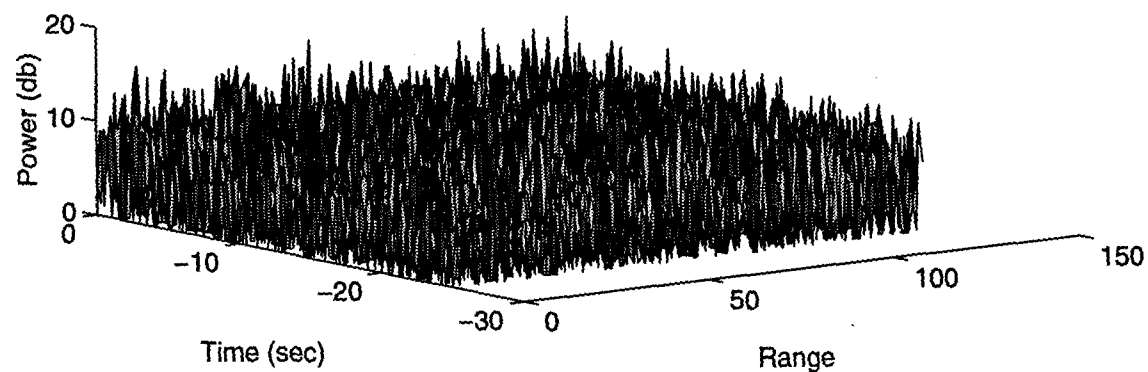
additive Rayleigh noise) by

$$\eta = -\ln(P_{fal}). \quad (4.14)$$

A gray scale plot of the time-range space for a target signal, with additive noise before and after applying a primary threshold corresponding to P_{fal} of 10^{-2} , is shown in Figures 10a and 10b, respectively, where only the region of interest is shown, i.e., the range cells in which the target exists.



(a)



(b)

Figure 9. Mesh Plot in Image Space for a 20 Knot Target.
(a) Without Noise.
(b) With Additive Rayleigh Noise (SNR=2dB).

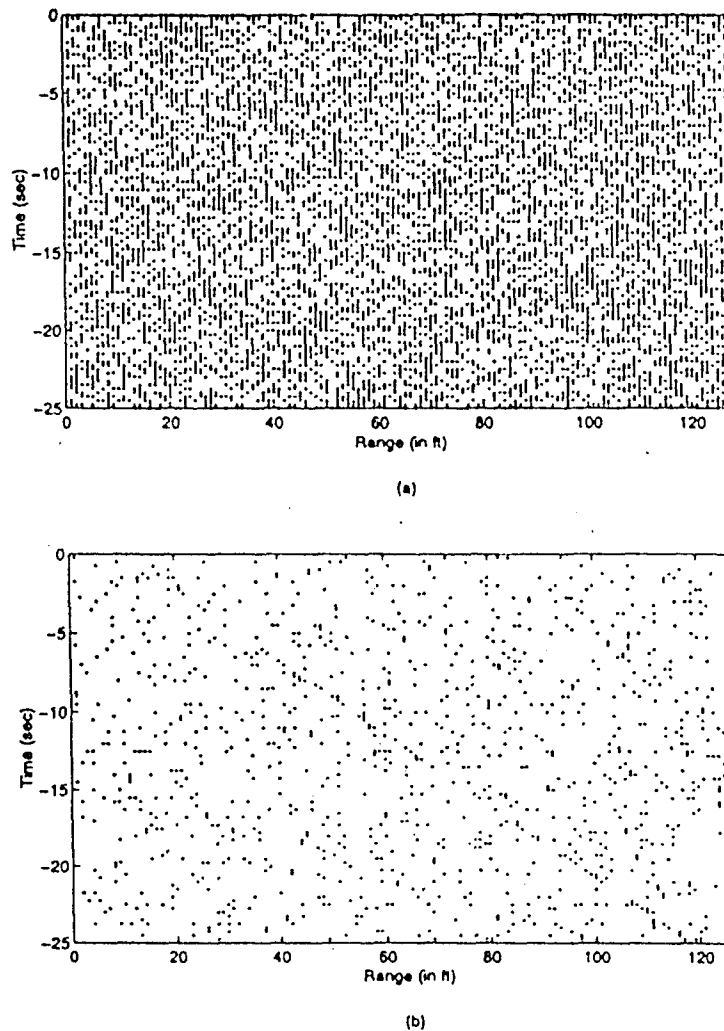


Figure 10. Time-Range Space for 20 Knot Target with Additive Rayleigh Noise (SNR=5 dB).
 (a) Before Primary Threshold.
 (b) After Primary Threshold.

The time-range data is now transformed to the Hough parameter domain using the procedure described in Chapter III. The signal power associated with the sinusoidal curve segments in each cell is now summed noncoherently to give a total cell power. Figure 11a shows the Hough parameters mesh plot corresponding to the data presented in Figure 9b. The major peak matches the target trajectory while the smaller peaks are related to the noise; each peak produces a straight line in the time-range space. Applying a secondary threshold in

the parameter space leads to target peak detection. The ρ and θ values of the peak are used for the back-projection into the time-range space, as demonstrated in Figure 11b.

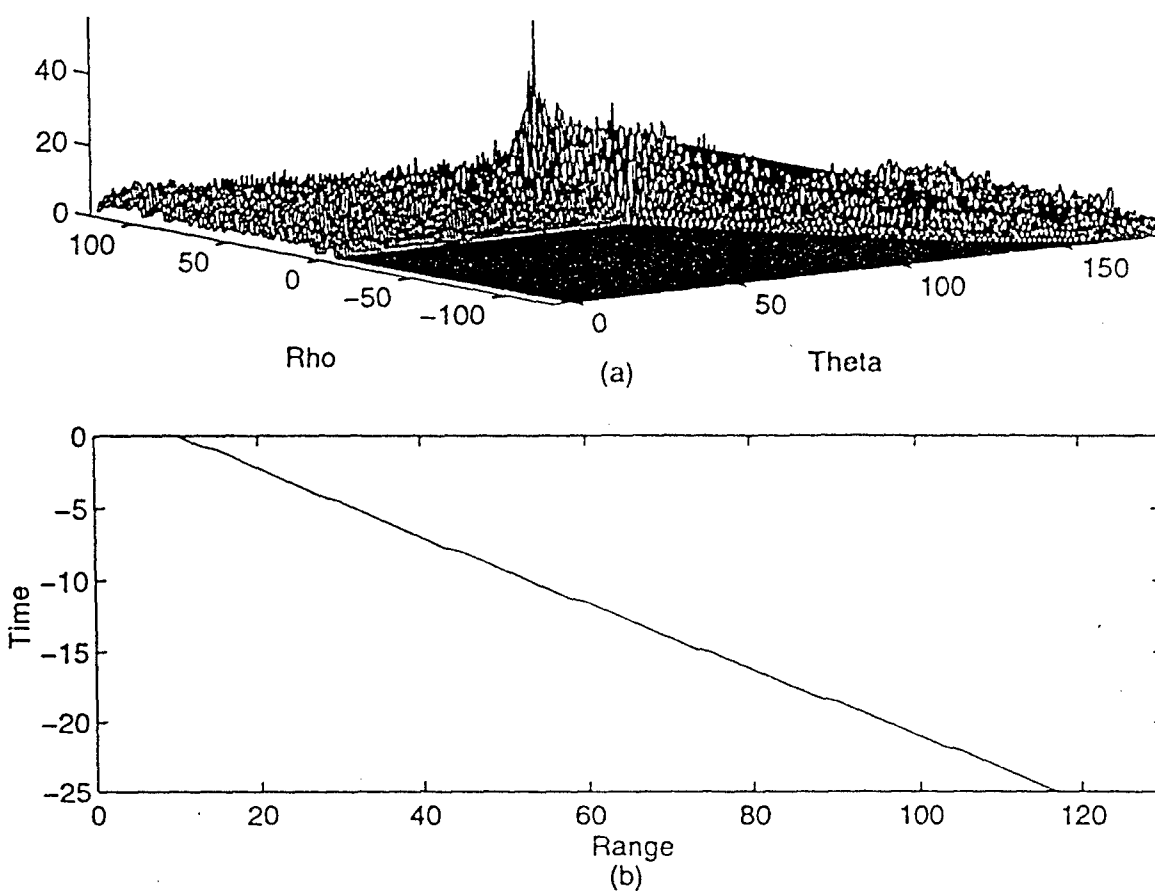


Figure 11. (a) Hough Space Corresponding to Time-Range Space of Figure 10.
(b) Back-Projection of Detected Target into Time-Range Space.

1. Binary Integration Hough Transform

Implementing the Hough transform when more than one target is present in the observed area might result in dynamic range problem [Ref. 1]. If one target is larger than the other, we get masking of the small target by the large target in the Hough space. This results from the Hough transform integration approach using the (which performs a noncoherent summation of the signal power), whereby, a large target peak in the Hough domain will be much higher than the small target peak. Setting the threshold low enough to detect the small target will increase the number of false alarms, while increasing the threshold results in losing the small target. As a result choosing a threshold that allows detection of small targets, while avoiding detection of false targets, might be a difficult task. Similar problems occur if we detect targets that have crossing trajectories; as a result the peak of one target will mask the other target peak. One possible way, discussed by Carlson, Evans and Wilson [Ref 1], to avoid this problem is to use binary integration in the Hough space. In this method, all the data points that cross the primary threshold in the time-range space are assumed to have a value of one and mapped into the Hough space accordingly. This eliminates the difference between the targets due to their size and results in a target size in the Hough space relative to the targets trajectory length. Numerous conventional detection schemes which employ a fixed threshold, or use *aM-out-of-N* secondary threshold might be used to detect the target peaks. Using the binary integration method has some disadvantages, since noise or clutter peaks that cross the primary threshold level might cause a false alarm.

2. Optimum Parameter Selection

Several parameters can affect the performance of the Hough based detector. The first one is granularity of the parameter space. The optimum granularity is the one that achieves the desired P_{fa} without choosing too fine a granularity that splits the target between more than one cell in the Hough domain. This issue was investigated by applying different granularity to the Hough transform and observing the effect on the system performance. Other parameters that should be addressed are the primary and secondary threshold value

selection. We can choose high primary threshold values, which result in fewer data points crossing the threshold and less points transformed into the Hough domain. In this case, we have to use low values for the secondary values, as the target trajectory is comprised of less points. The other alternative is to use low primary threshold values, which will cause most of the time-range points to be transformed into the Hough domain and determine high secondary threshold values to avoid false alarms. Finding the optimum values for detection is done by using different values of threshold in the simulations and evaluating their detection performance. Those results are presented in Chapter V.

D. HOUGH TRANSFORM DETECTION PERFORMANCE

Efficient evaluation of the Hough transform based detectors, and a measure of comparison to the more conventional detectors, is achieved by determining the detection statistics (i.e., probability of detection as a function of the input SNR for a given P_{fa}). This is done for specific radar parameters and for predefined target, noise and sea clutter signal levels. The detection statistics will enable us to evaluate the target detection range in a given scenario.

1. Probability of False Alarm

The first step in evaluating the detector performance consists of determining the probability of false alarm as a function of secondary threshold. False alarm in the Hough detector is defined as finding a line, or a trajectory, in the Hough domain where no target exists in the time-range space. To find the probability of false alarm, we use the concept of "accessible Hough space" introduced by Carlson, Evans and Wilson [Ref. 1] . This quantity is found by putting a one in all the range time cells of the image space, and then Hough transforming them. The resulting mesh plot is shown in Figure 12 for the Hough parameters defined in Section B . It can be observed that some cells in the Hough domain have a zero value which results from the fact that not all the cells in the Hough domain can be backprojected into the time-range domain , in other words those cells match non-existing trajectories. " The accessible Hough space" is parameter dependent and has to be calculated

according to the granularity of the time-range and the Hough dimensions. To determine the P_{fa} as a function of secondary threshold, a time-range map with Rayleigh noise was generated using the simulation procedure described in chapter V. The primary threshold in the time-range domain is set to a predefined value (several values were tested), and the Hough transform is applied to this data. The number of secondary threshold crossings, divided by the total number of cells in the accessible Hough space, yields the probability of false alarm. The secondary threshold is then varied to determine the probability of false alarm, as a function of the secondary threshold.

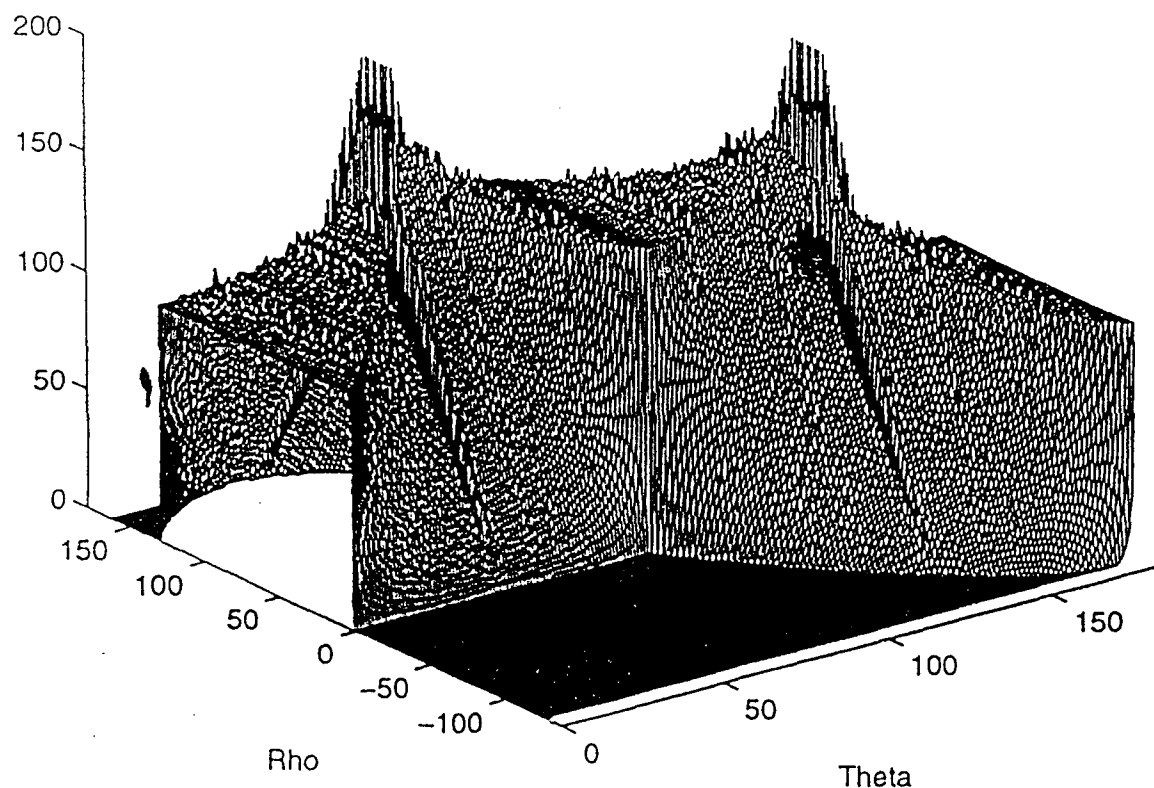


Figure 12. Hough Transform of All Ones in Image Space, demonstrating the "Accessible Hough Domain".

2. Probability of Detection

Detection for the Hough based detector is defined as finding a predefined target trajectory in the time-range space. To evaluate the detection performance of the system, we first define a scenario and then test it under those conditions. In the scenario definition, we simulate a target trajectory in the time-range space, and then combine the simulated Rayleigh noise and sea clutter with the target according to the desired SNR. Transformation to parameter space then gives the corresponding accumulator cell values in Hough space. Probability of detection is calculated by counting the number of detections achieved in the appropriate Hough cell divided by the overall number of simulations. As was proposed by Carlson, Evans and Wilson [Ref. 1], an n by n grid about the expected Hough cell location is considered, where n is an integer defined in the simulation, and detection is declared as any secondary threshold crossing within this grid. The proper value for n is determined in the simulation. The procedure is repeated for different secondary threshold values, corresponding to different values of P_{fa} , which will give the system probability of detection as a function of the SNR for a given P_{fa} .

V. RESULTS

A. TEST CASES DESCRIPTION

The simulated radar parameters, specified in Table 1, are typical for land based high resolution radars. These types of radar are mainly used for small target detection in the presence of sea clutter and, as such, are potential candidates for the Hough detector implementation. The algorithm was applied to different scenarios generated in accordance with the radar parameters, chosen to enable comprehensive evaluation of the system performance and efficiency. The parameter space for this simulation is taken as 256 by 180 for the ρ and θ dimensions. Those parameters, as shown in subsection E, are close to the optimum choice for the granularity of the parameter space.

Table 1. Simulated Radar Specifications.

Center Frequency	9 GHZ
Pulse Repetition Frequency (PRF)	1000
Pulse Width (PW)	10 nsec
Peak Power	10 MW
Antenna Gain	35 dB
Antenna Speed Table 1.	240 RPM
System Losses	6 dB
Grazing Angle	2°
Polarization	Horizontal

Two main test scenarios are considered in this work. The first one consists of a single target, nonfluctuating or Swerling 1 type, embedded in Rayleigh noise or K-distributed sea clutter. Several target speeds, heading directions and SNR's are considered to determine the system sensitivity to those parameters. The second scenario consists of multiple targets with additive noise and K-distributed sea clutter, with variation in the

targets relative size, speed and headings. This scenario is intended to evaluate the performance of the algorithm in which multiple targets present in the time-range space.

B. SINGLE TARGET SCENARIO

1. Additive Rayleigh Noise Case

A simple but important test case is a single constant velocity target with additive Rayleigh noise. The target is tested for different speeds and heading directions, where those parameters define the target trajectory in the time-range space and affect the system performance. The different test cases for this scenario are summarized in Table 2, where R_0 denotes the target range, V_0 is the target velocity, a_0 the target acceleration and α denotes the targets heading direction relative to the radar site. The SNR is assumed to be constant during the integration time, due to the low target speed and the resulting small crossing distance. The primary threshold in the time-range space was chosen to give a time-range P_{fa} of $\frac{1}{30}$ and the secondary threshold value, ξ , which is taken as a fraction of the maximum value of the accumulator cell in the parameter space.

Table 2. Single Target Test Cases

Test Case I	Stationary Target	Nonfluctuating	$R_0=20$ Nm, $V_0=0$
Test Case II	Constant Velocity Target	Swerling I type	$R_0=20$ Nm, $V_0=25$ Knots, $\alpha=90^\circ$
Test Case III	Accelerating Target	Swerling I type	$R_0=20$ Nm, $V_0=5$ Knots, $\alpha=45^\circ$ $a_0=0.1$ ft/sec ²

Figures 13a-14a are the time-range space maps after primary threshold for test case I, with SNR of 0 and 5 dB, respectively, and ξ matched to the peak value. Figures 13b-14b present the true target trajectory and the Hough detector time-range back-projection, while Figures 13c-14c show the corresponding Hough parameter space. The longest possible trajectory for this particular time-space map is 162, occurring at the diagonal line, while the maximum target trajectory length, which corresponds to this test case, is 100. We can

observe the false detection declared in the case of SNR=0 dB. These occur because the detector prefers the longer lines created by the noise. In the case of 5 dB SNR, the peak in the parameter space is higher, and the target is easily detected. The effect of choosing an unmatched threshold is shown in Figures 15-16, where the optimal threshold is reduced by 1 dB and applied to the test case I target, with SNR's of 0 and 5 dB, respectively. The resulting false tracks demonstrates the sensitivity of the detector to the secondary threshold level.

Test case II has a diagonal trajectory in the time-range space, which corresponds to the longest line possible in the time-range map. Figures 17-18 show the time-range space map and the corresponding parameter space for SNR's of 0 and 5 dB, respectively, with matched ξ . Again we can observe the clear peak in the Hough domain corresponding to the target trajectory. The effect of unmatched ξ is tested again and is presented in Figures 19-20 for secondary threshold setting of 0.5 and 1 dB lower than the optimal one. Test case III consists of a target changing its speed by a radial acceleration over the data history. In order to detect this type of target, we need to map the data into a 3-D Hough space. A 2D detector, like the one implemented in this thesis, can be used, and the results of applying the algorithm to test case III are shown in Figures 21-22 for SNR of 2 and 7 dB, respectively. A lower threshold level is used, and we can see that several lines are mapped back into the image space. Each of those lines represent a section along the actual curved path. The true trajectory is tangent to those lines along the inside edge. Although some uncertainty results from using a 2D system to detect a 3D space, it is not extreme, and it is much easier to implement.

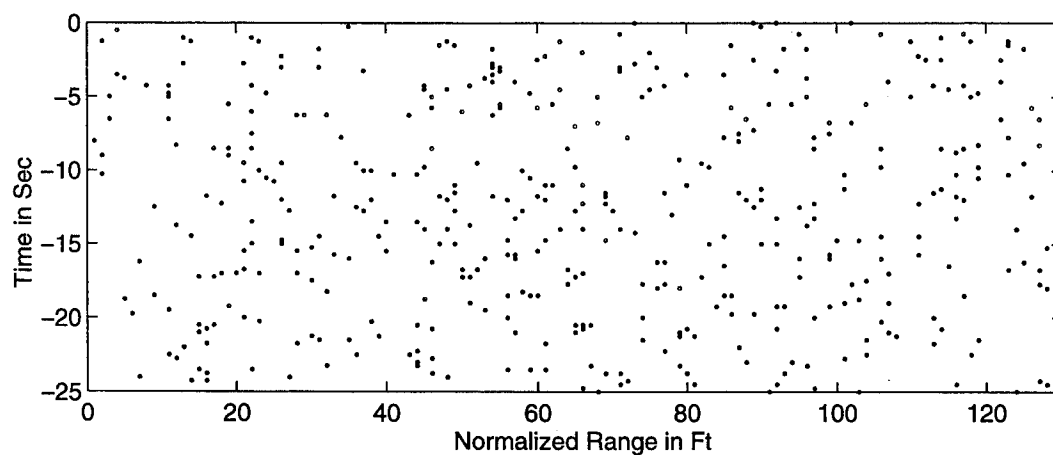
As discussed in Chapter IV, the Binary-Integration (BI) Hough detector has some advantages in the multiple target scenarios and might be used as a preferred detection scheme. To evaluate the effectiveness of this scheme, the BI Hough detector was applied to test cases I-III, and the results are shown in Figures 23-27 for SNR's of 0 and 5 dB and matched ξ . The detection performance reflected from those plots seems to be lower than those obtained using the Hough detector itself, although for SNR's of 5 dB the original target trajectory is being detected in all the test cases. Quantitative results for the

performance degradation using this method, as compared with the results using the basic algorithm, are presented in Section D.

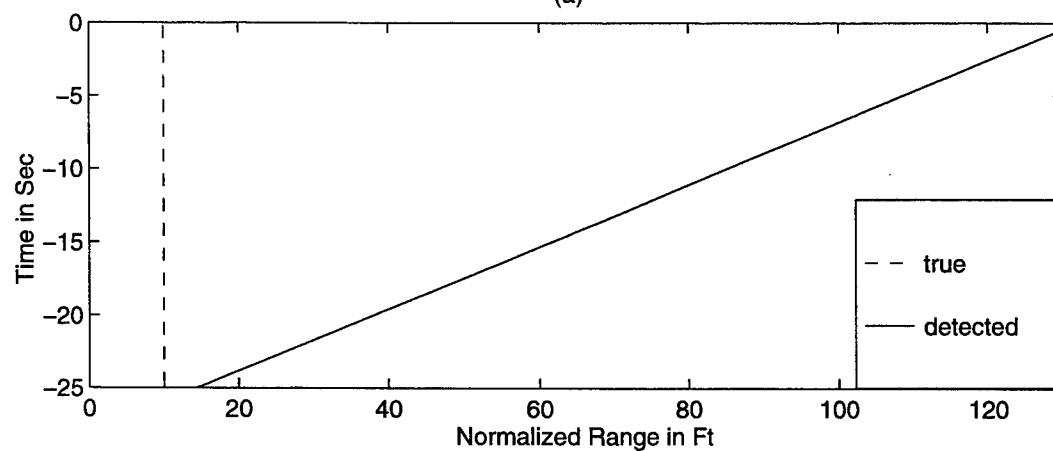
2. Additive K Distributed Clutter Case

A more realistic scenario is the case of one target in the presence of sea clutter. The clutter was simulated in accordance with the procedure described in Chapter IV, where the clutter characteristics are simulated using Equation (3.28), in accordance with the radar parameters and assuming up/down swell direction. We tested the algorithm against test cases I-II for different interference levels where interference power is defined as $I = P_c + P_n = P_n(1 + \text{CNR})$, P_c and P_n are the noise and clutter power, and CNR defines the clutter to noise ratio. Figures 29-30 present the results obtained for test case I with additive K-distributed clutter for signal to interference ratio (SIR) of 0 and 5 dB, respectively, and matched ξ . Similar results to the additive noise case are obtained for this case, although the clutter has spikier nature than the noise. We can observe that the target trajectory is detected in the case of SIR of 5 dB, while no detection is declared in the case of 0 dB.

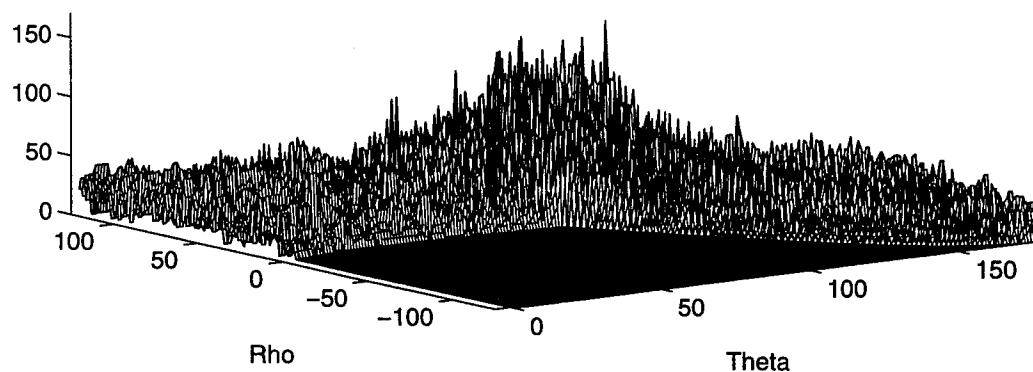
The results for test case 2 are presented in Figures 31 and 32 for SIR'S of 0 and 5 dB, respectively, with matched ξ . The effect of unmatched threshold is demonstrated in Figures 33-36 for test cases I-II and the two tested SIR's. The overall performance of the detector in the presence of K-distributed clutter is close to the performance in the noise-only case, so that the effect of the sea spikes, which affect the performance of conventional detectors, has been eliminated.



(a)

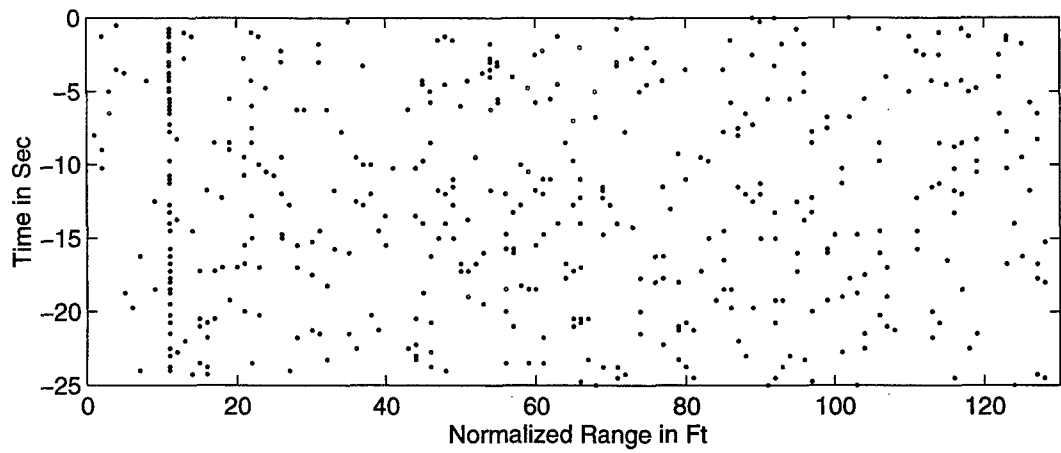


(b)

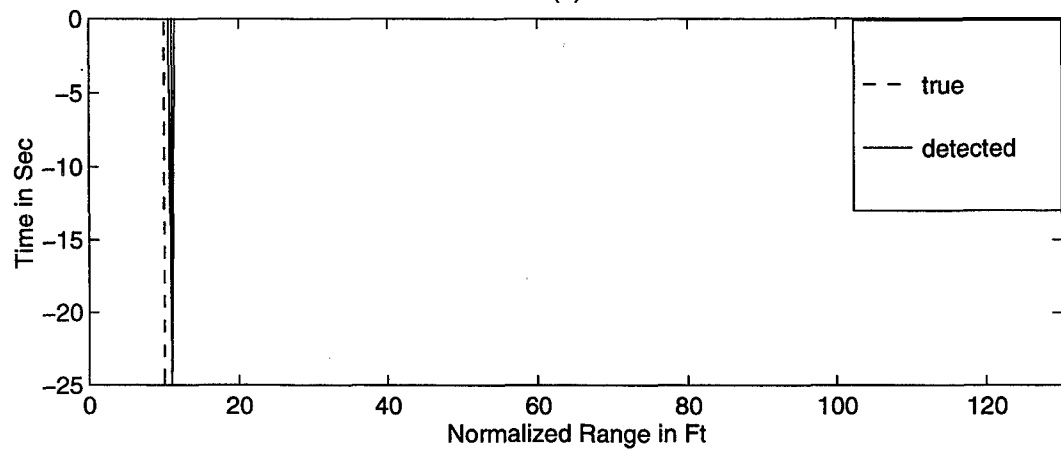


(c)

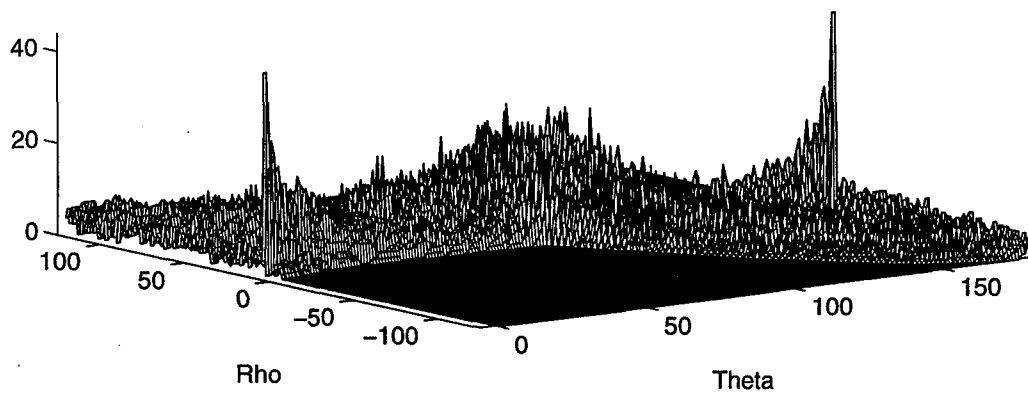
Figure 13. Test Case I, SNR=0 dB, $\xi=20$ dB.
 (a) Time Range Space after Primary Threshold.
 (b) True and Detected Target Trajectory in Image Space.
 (c) Parameter Space Mesh Plot.



(a)

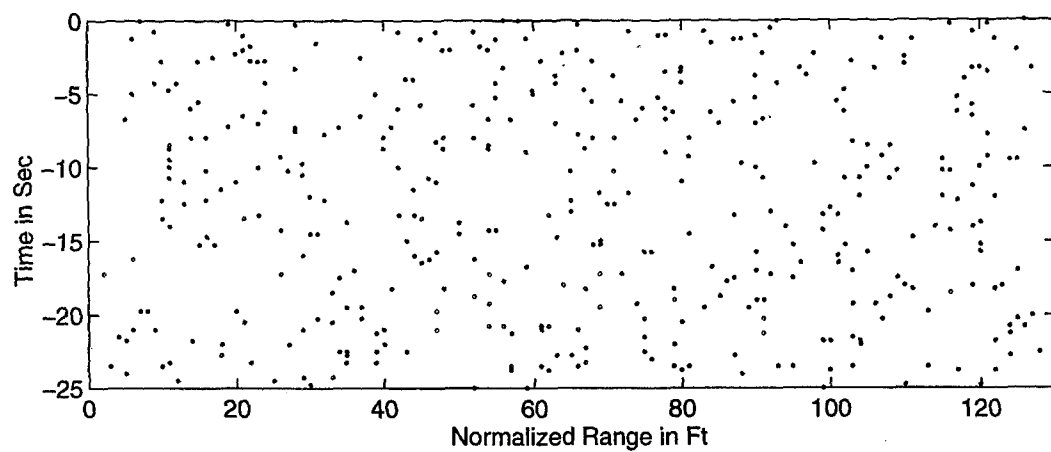


(b)

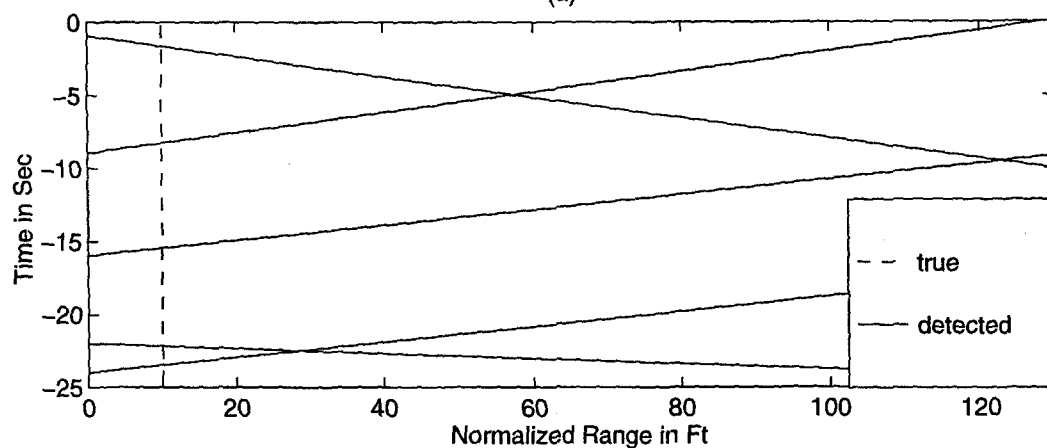


(c)

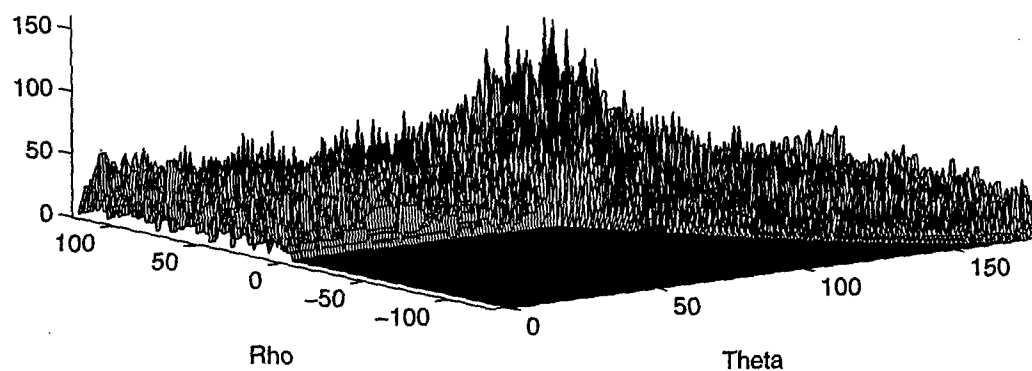
Figure 14. Test Case I, SNR=5 dB, $\xi=19.5$ dB.
 (a) Time Range Space after Primary Threshold.
 (b) True and Detected Target Trajectory in Image Space.
 (c) Parameter Space Mesh Plot.



(a)

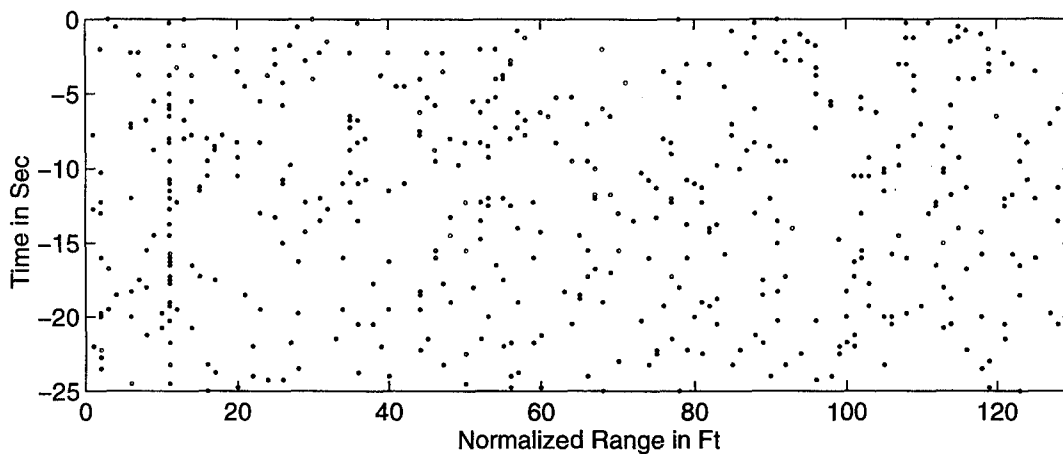


(b)

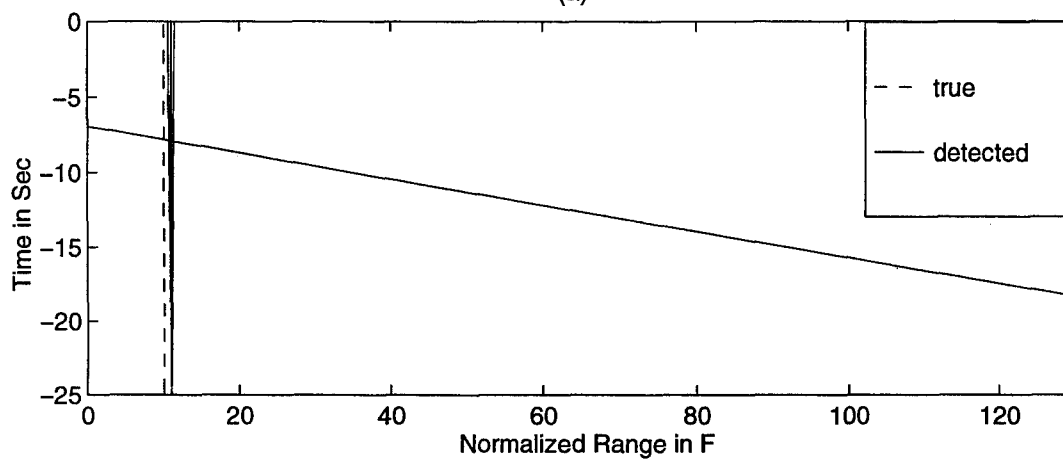


(c)

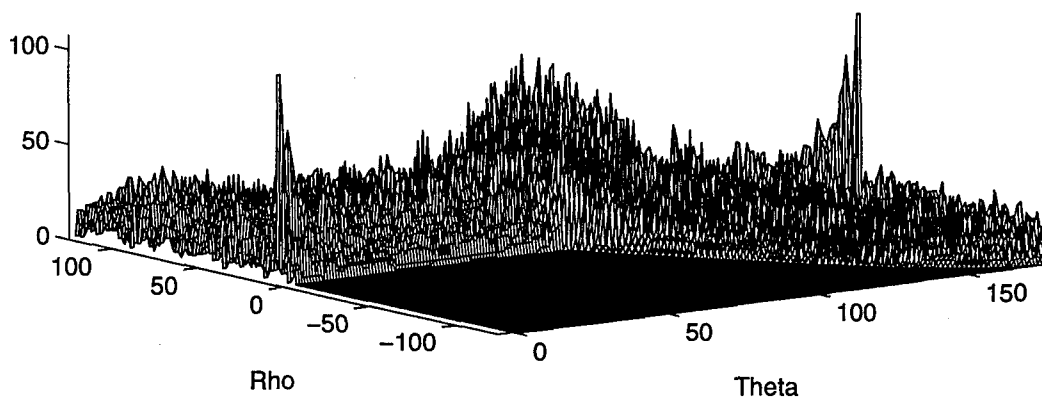
Figure 15. Test Case I, SNR=0 dB, $\xi=18.5$ dB.
 (a) Time Range Space after Primary Threshold.
 (b) True and Detected Target Trajectory in Image Space.
 (c) Parameter Space Mesh Plot.



(a)



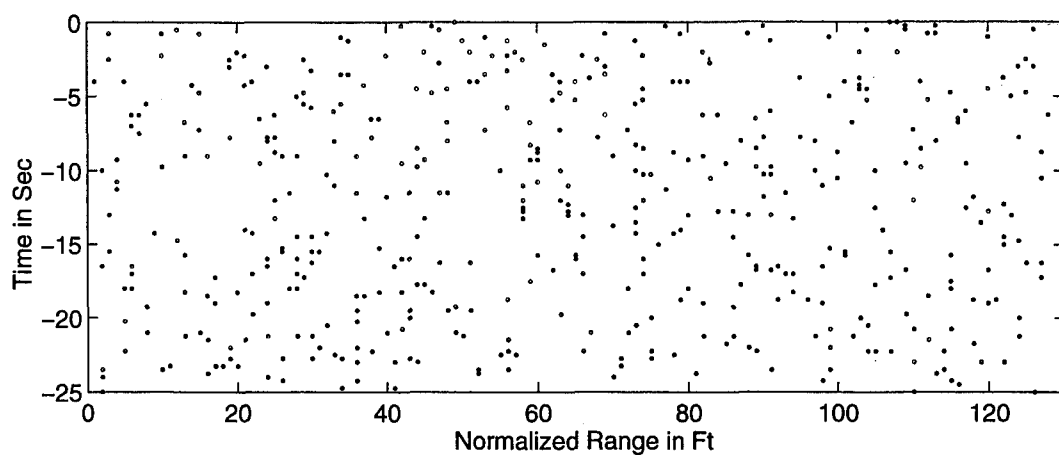
(b)



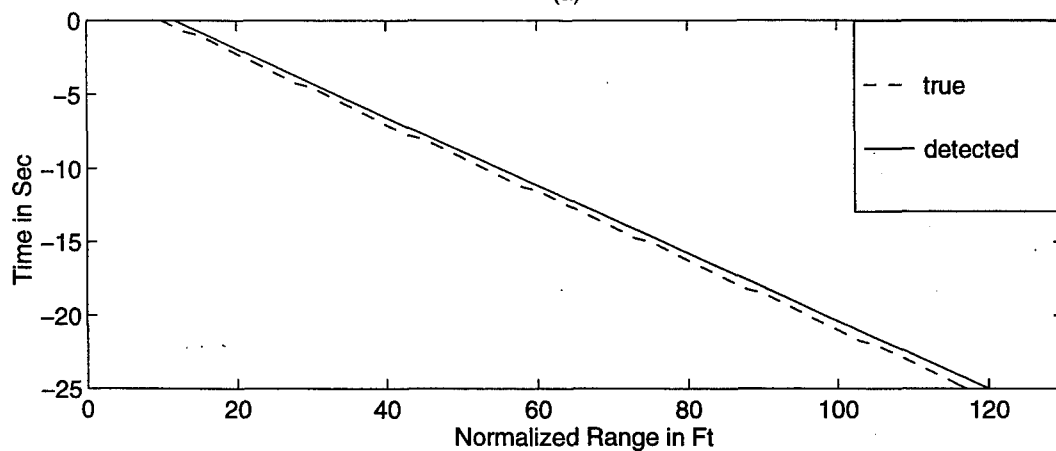
(c)

Figure 16. Test Case I, SNR=5 dB, $\xi=18.5$ dB.

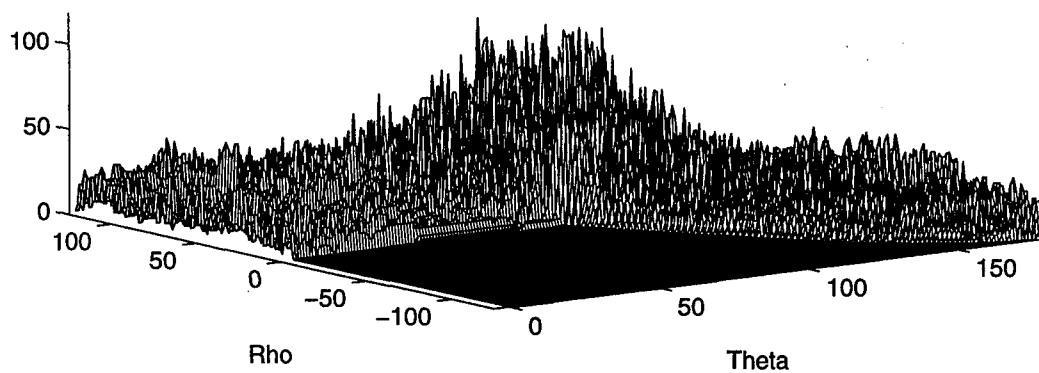
- (a) Time Range Space after Primary Threshold.
- (b) True and Detected Target Trajectory in Image Space.
- (c) Parameter Space Mesh Plot.



(a)

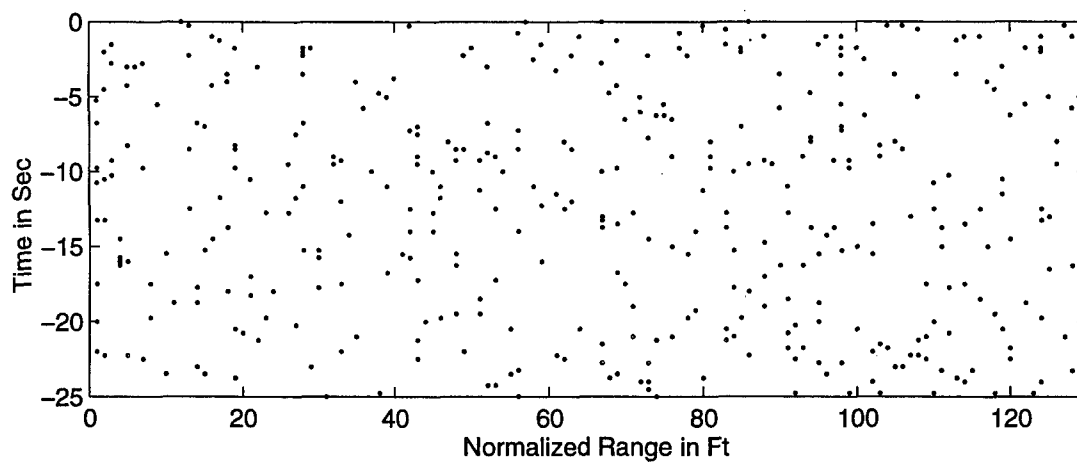


(b)

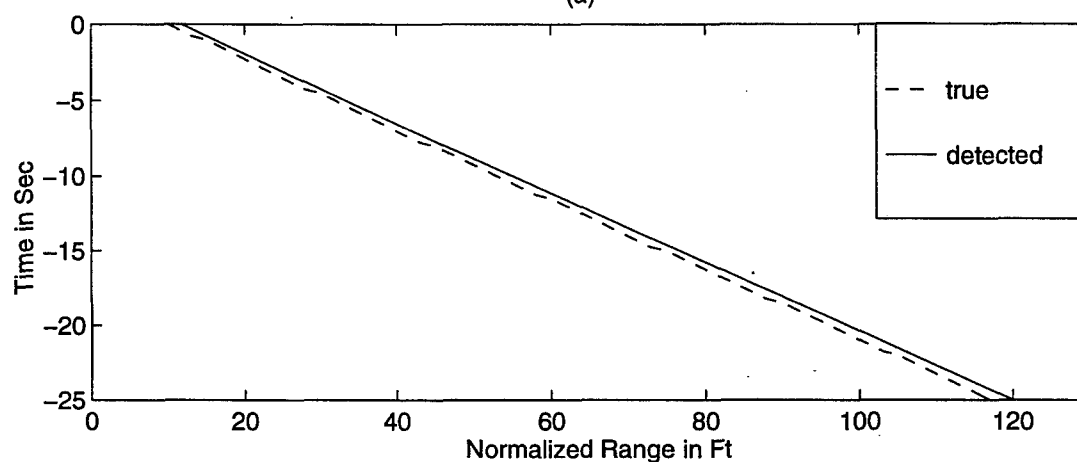


(c)

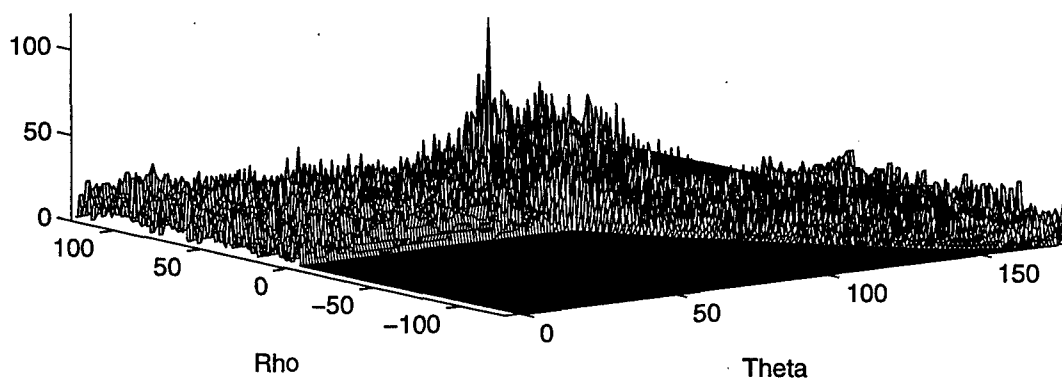
Figure 17. Test Case II, SNR=0 dB, $\xi=22$ dB.
 (a) Time Range Space after Primary Threshold.
 (b) True and Detected Target Trajectory in Image Space.
 (c) Parameter Space Mesh Plot.



(a)



(b)



(c)

Figure 18. Test Case II, SNR=5 dB, $\xi=21$ dB.

- (a) Time Range Space after Primary Threshold.
- (b) True and Detected Target Trajectory in Image Space.
- (c) Parameter Space Mesh Plot.

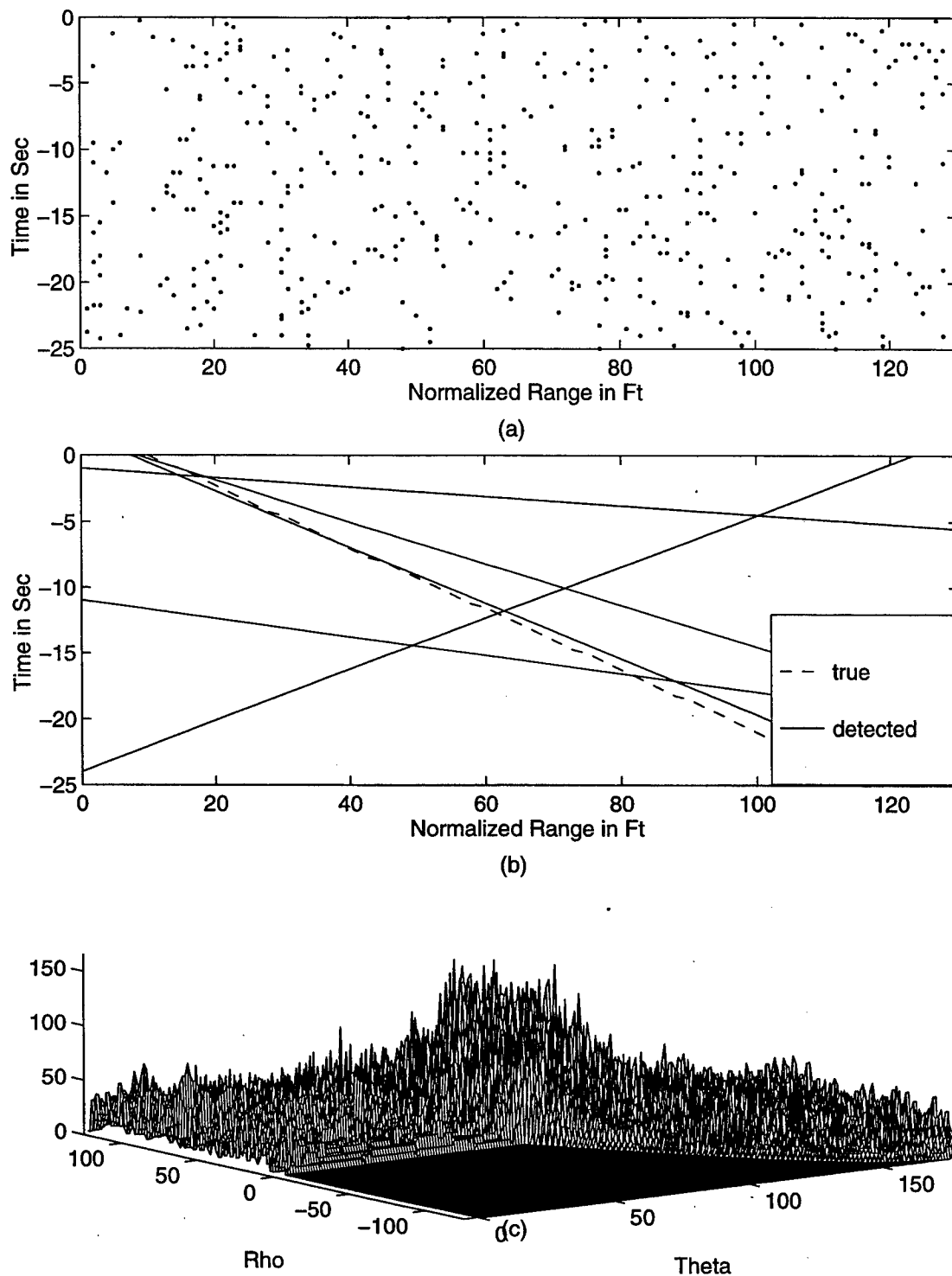


Figure 19. Test Case II, SNR=0 dB, $\xi=21$ dB.
 (a) Time Range Space after Primary Threshold.
 (b) True and Detected Target Trajectory in Image Space.
 (c) Parameter Space Mesh Plot.

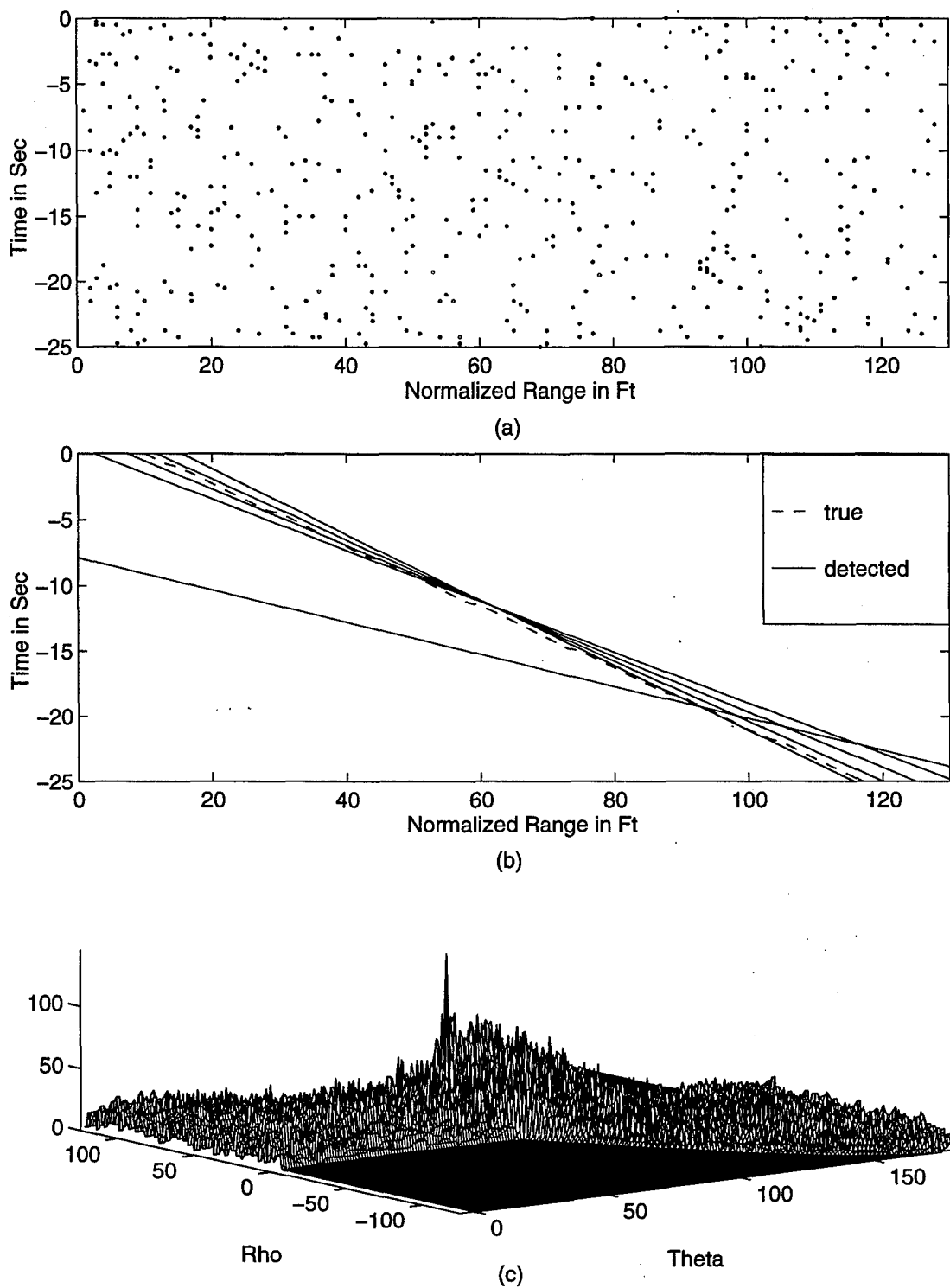


Figure 20. Test Case II, SNR=5 dB, $\xi=20$ dB.
 (a) Time Range Space after Primary Threshold.
 (b) True and Detected Target Trajectory in Image Space.
 (c) Parameter Space Mesh Plot.

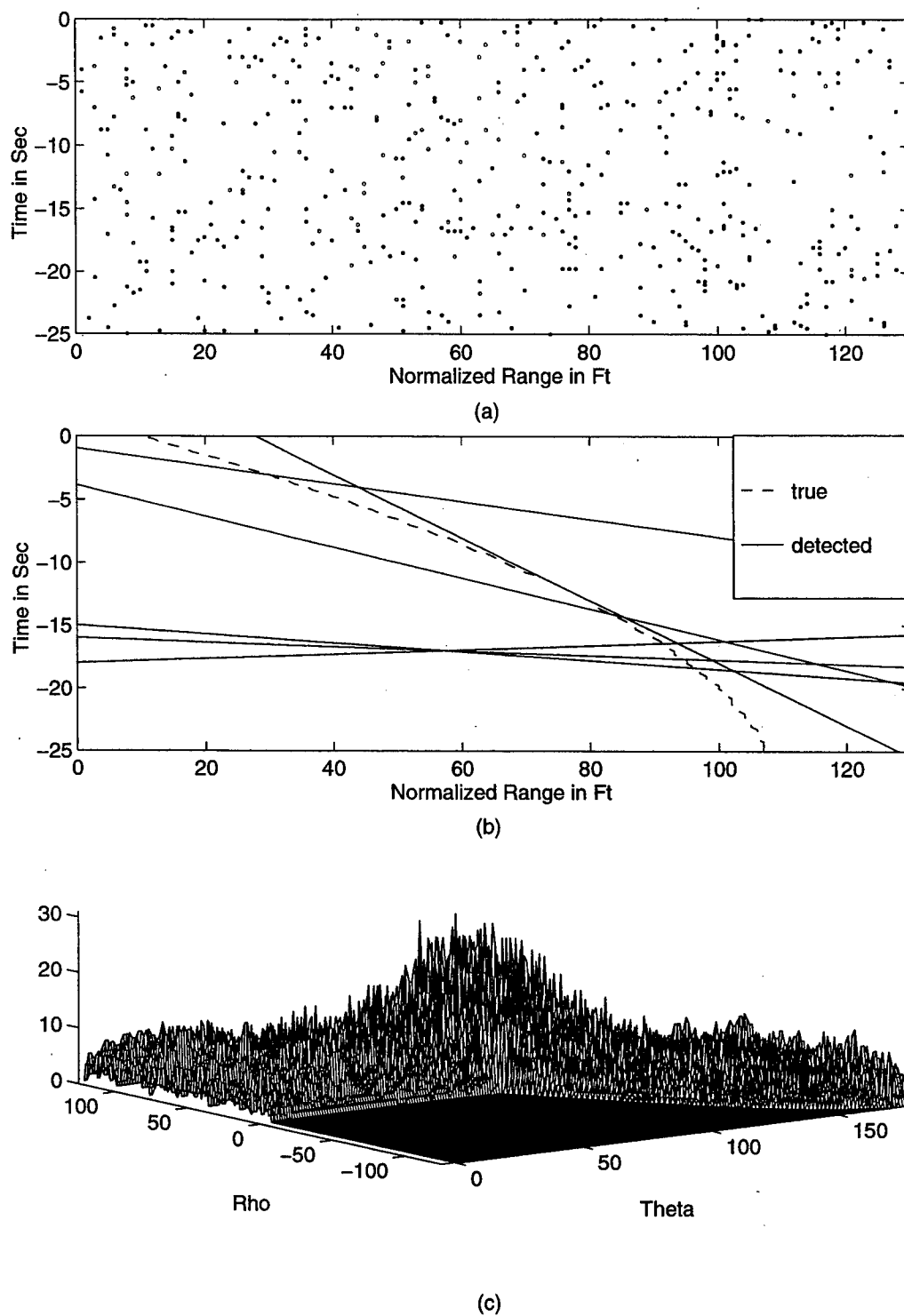


Figure 21. Test Case III, SNR=2 dB, $\xi=16$ dB.
 (a) Time Range Space after Primary Threshold.
 (b) True and Detected Target Trajectory in Image Space.
 (c) Parameter Space Mesh Plot.

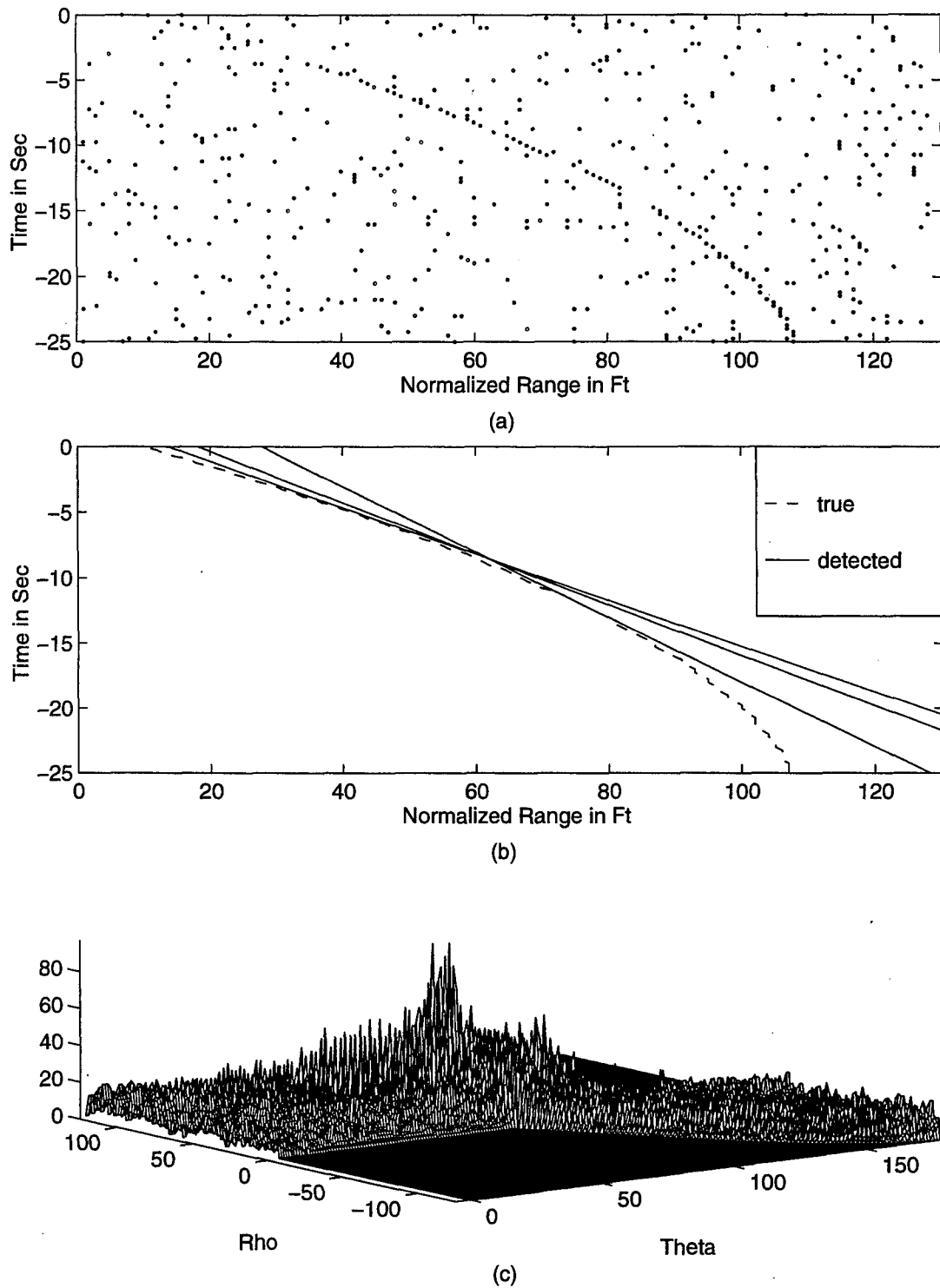


Figure 22. Test Case III, SNR=7 dB, $\xi=20$ dB.
 (a) Time Range Space after Primary Threshold.
 (b) True and Detected Target Trajectory in Image Space.
 (c) Parameter Space Mesh Plot.

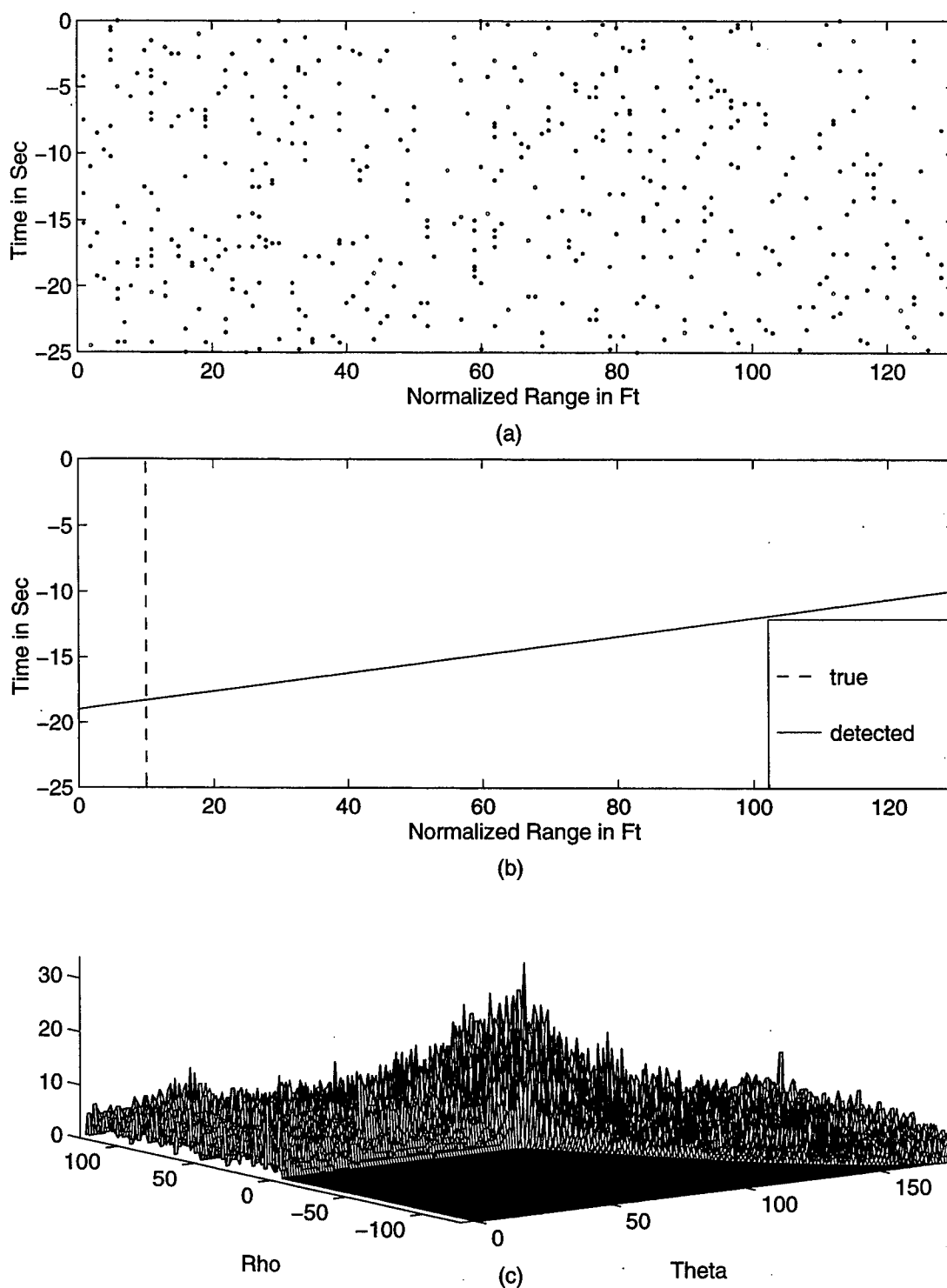


Figure 23. Test Case I, SNR=0 dB, $\xi=19$ dB.
 (a) Time Range Space after Primary Threshold.
 (b) True and Detected Target Trajectory in Image Space.
 (c) Parameter Space Mesh Plot (with Binary Integration).

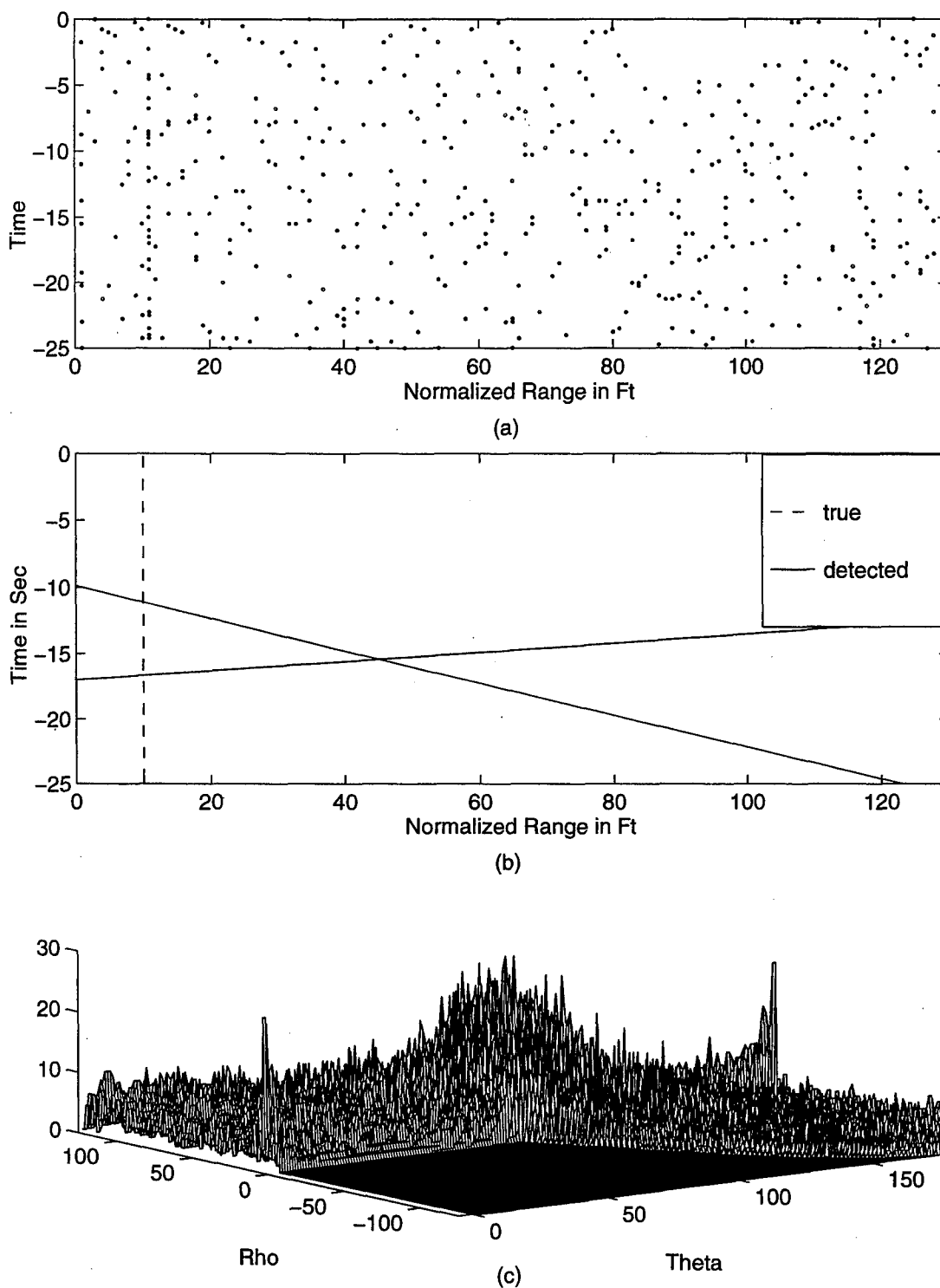


Figure 24. Test Case I, SNR=5 dB, $\xi=19$ dB.
 (a) Time Range Space after Primary Threshold.
 (b) True and Detected Target Trajectory in Image Space.
 (c) Parameter Space Mesh Plot (with Binary Integration).

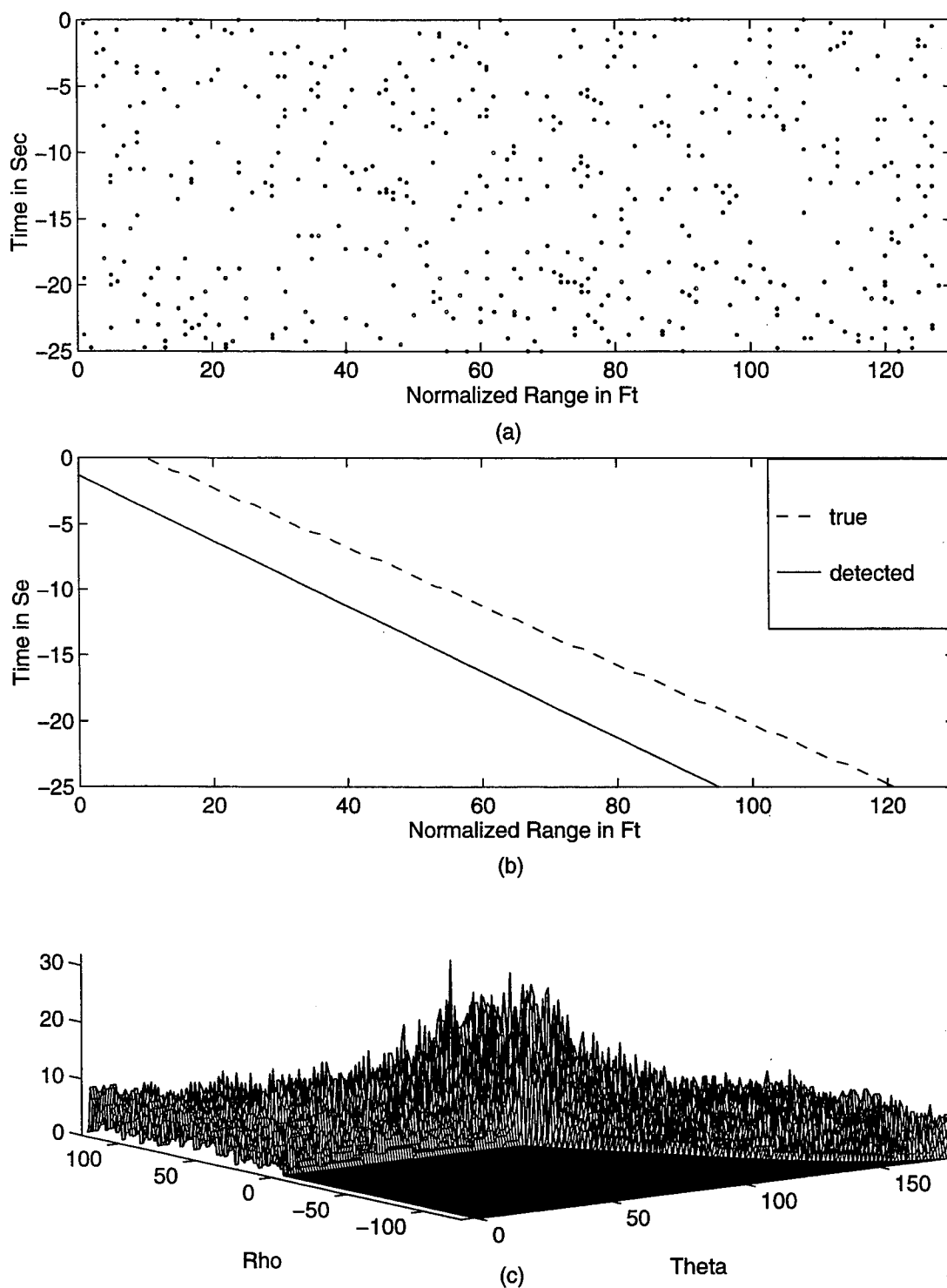
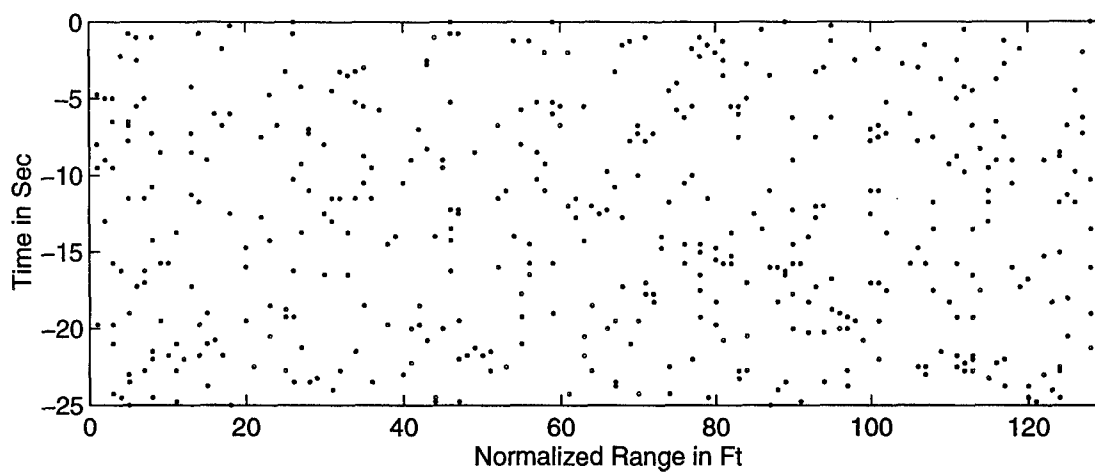
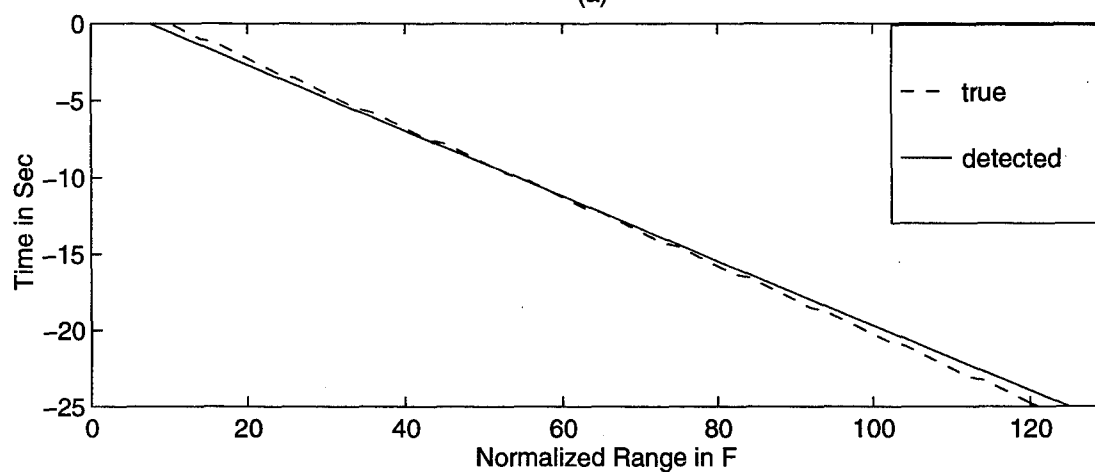


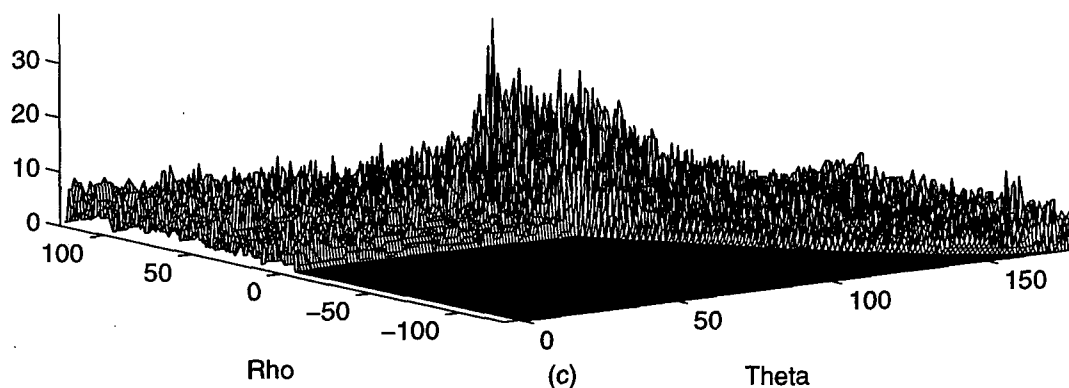
Figure 25. Test Case II, SNR=0 dB, $\xi=17$ dB.
 (a) Time Range Space after Primary Threshold.
 (b) True and Detected Target Trajectory in Image Space.
 (c) Parameter Space Mesh Plot (with Binary Integration).



(a)



(b)



(c)

Figure 26. Test Case II, SNR=5 dB, $\xi=18$ dB.
 (a) Time Range Space after Primary Threshold.
 (b) True and Detected Target Trajectory in Image Space.
 (c) Parameter Space Mesh Plot (with Binary Integration).

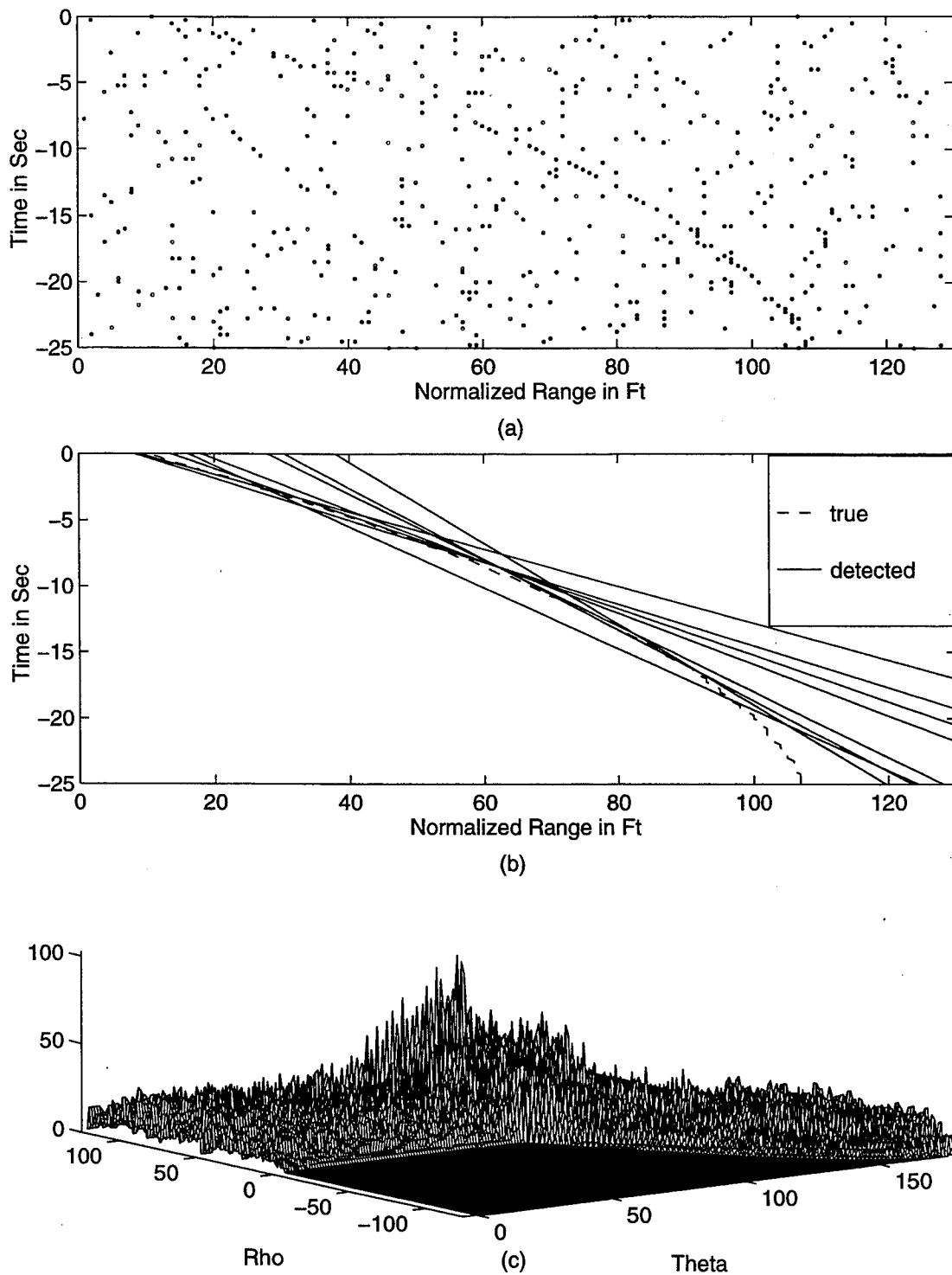


Figure 27. Test Case III, SNR=5 dB, $\xi=16$ dB.
 (a) Time Range Space after Primary Threshold.
 (b) True and Detected Target Trajectory in Image Space.
 (c) Parameter Space Mesh Plot (with Binary Integration).

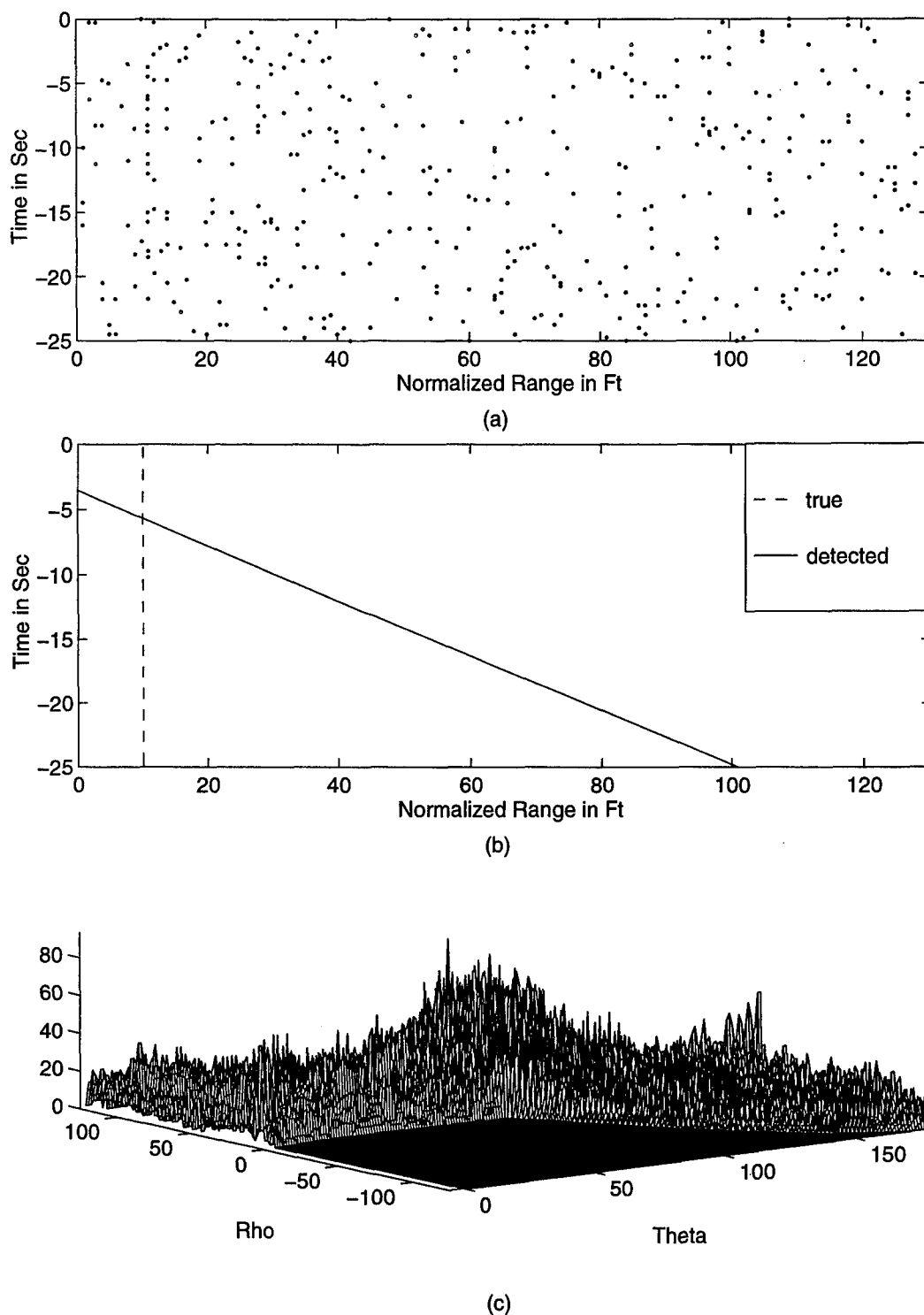


Figure 28. Test Case I, with Additive K-distributed Clutter, $SIR=0$ dB, $\xi=22$ dB.
 (a) Time Range Space after Primary Threshold.
 (b) True and Detected Target Trajectory in Image Space.
 (c) Parameter Space Mesh Plot.

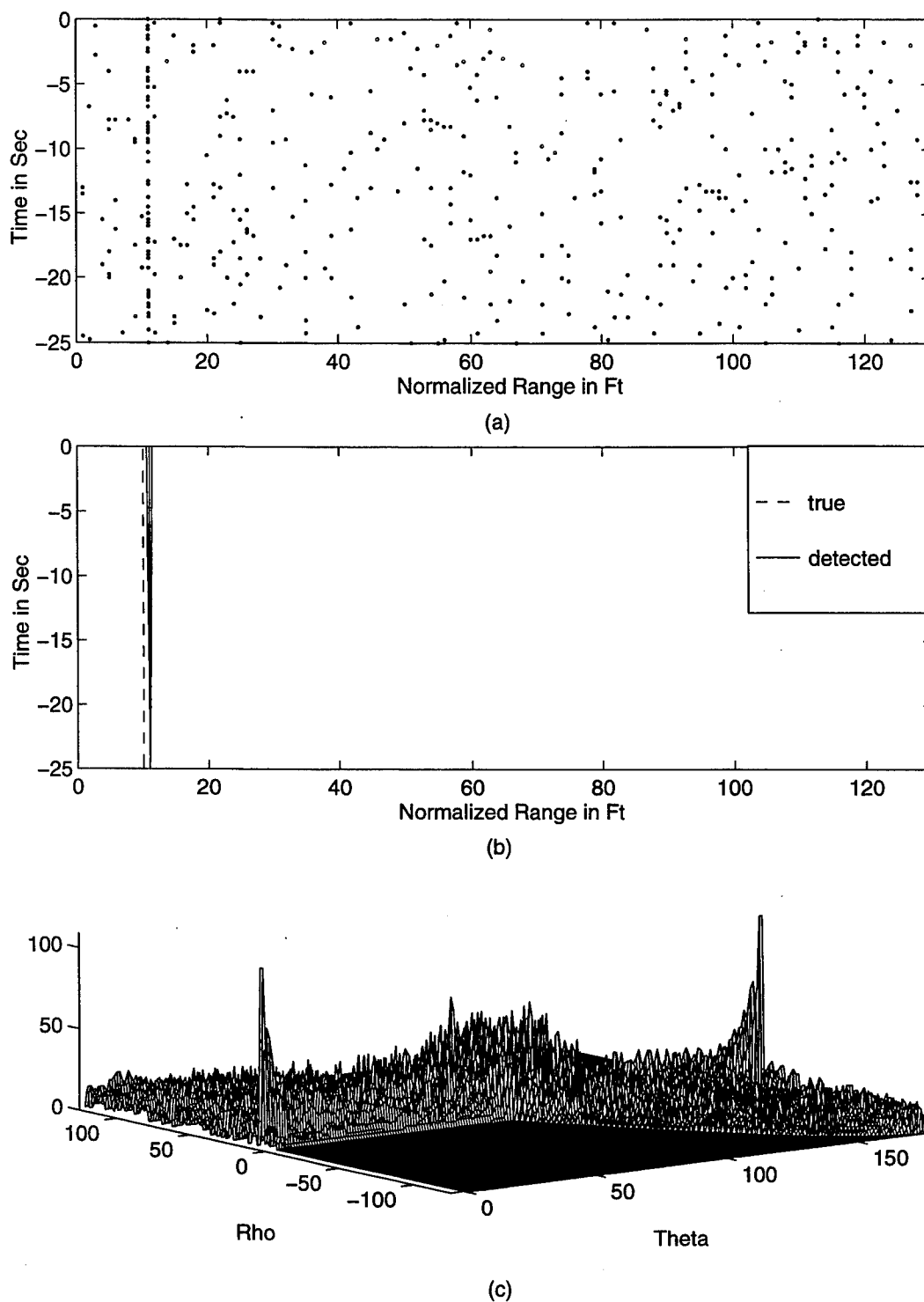
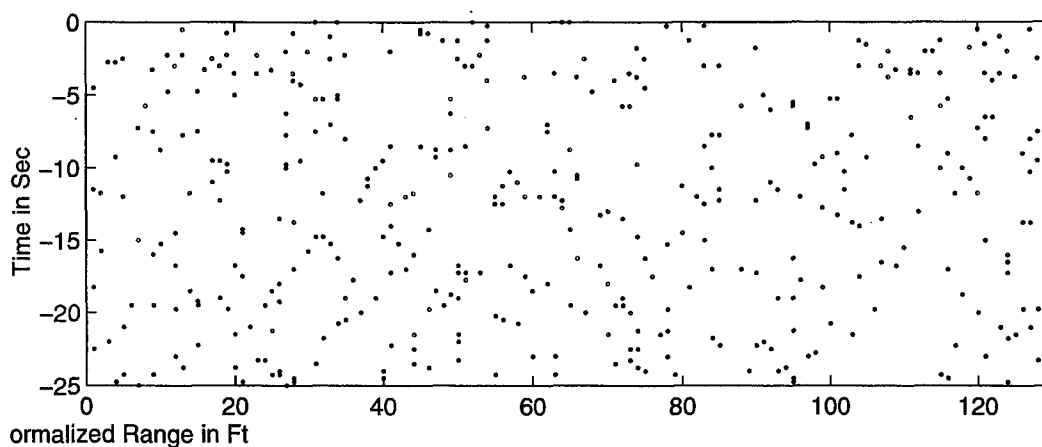
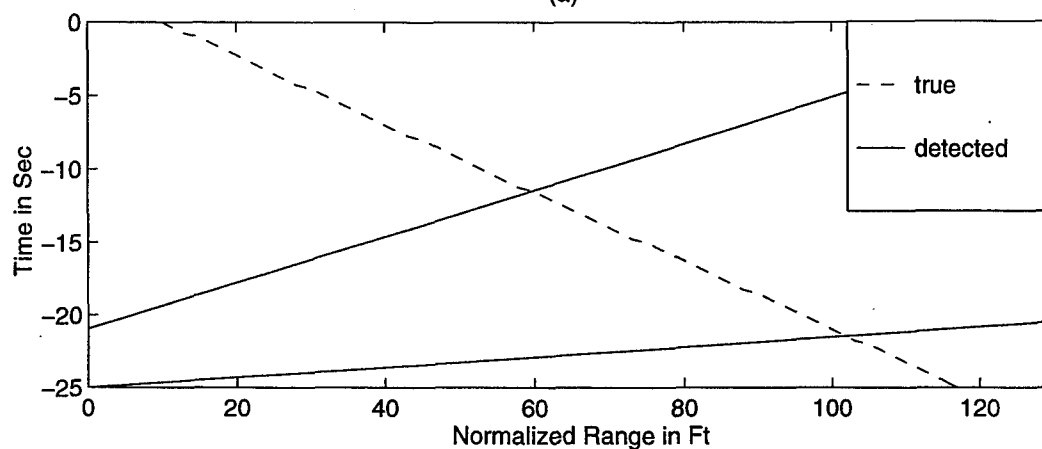


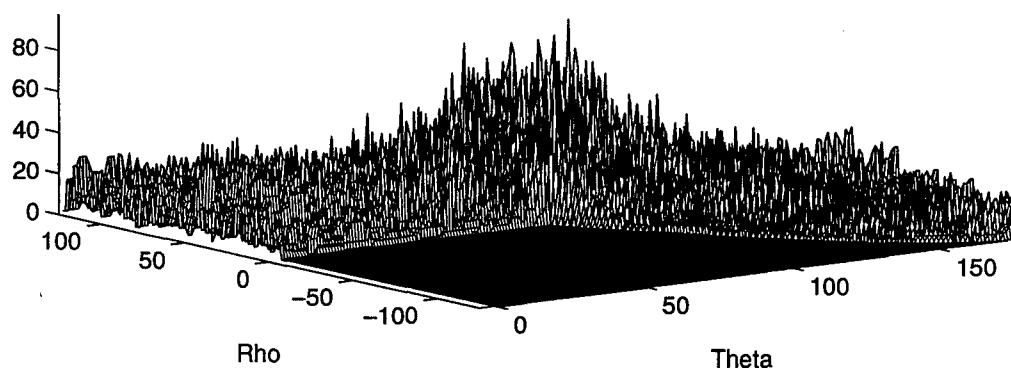
Figure 29. Test Case I, with Additive K-distributed Clutter, SIR=5 dB, $\xi=21$ dB.
 (a) Time Range Space after Primary Threshold.
 (b) True and Detected Target Trajectory in Image Space.
 (c) Parameter Space Mesh Plot.



(a)



(b)



(c)

Figure 30. Test Case II with Additive K-distributed Clutter, SIR=0 dB, $\xi=23$ dB.
 (a) Time Range Space after Primary Threshold.
 (b) True and Detected Target Trajectory in Image Space.
 (c) Parameter Space Mesh Plot.

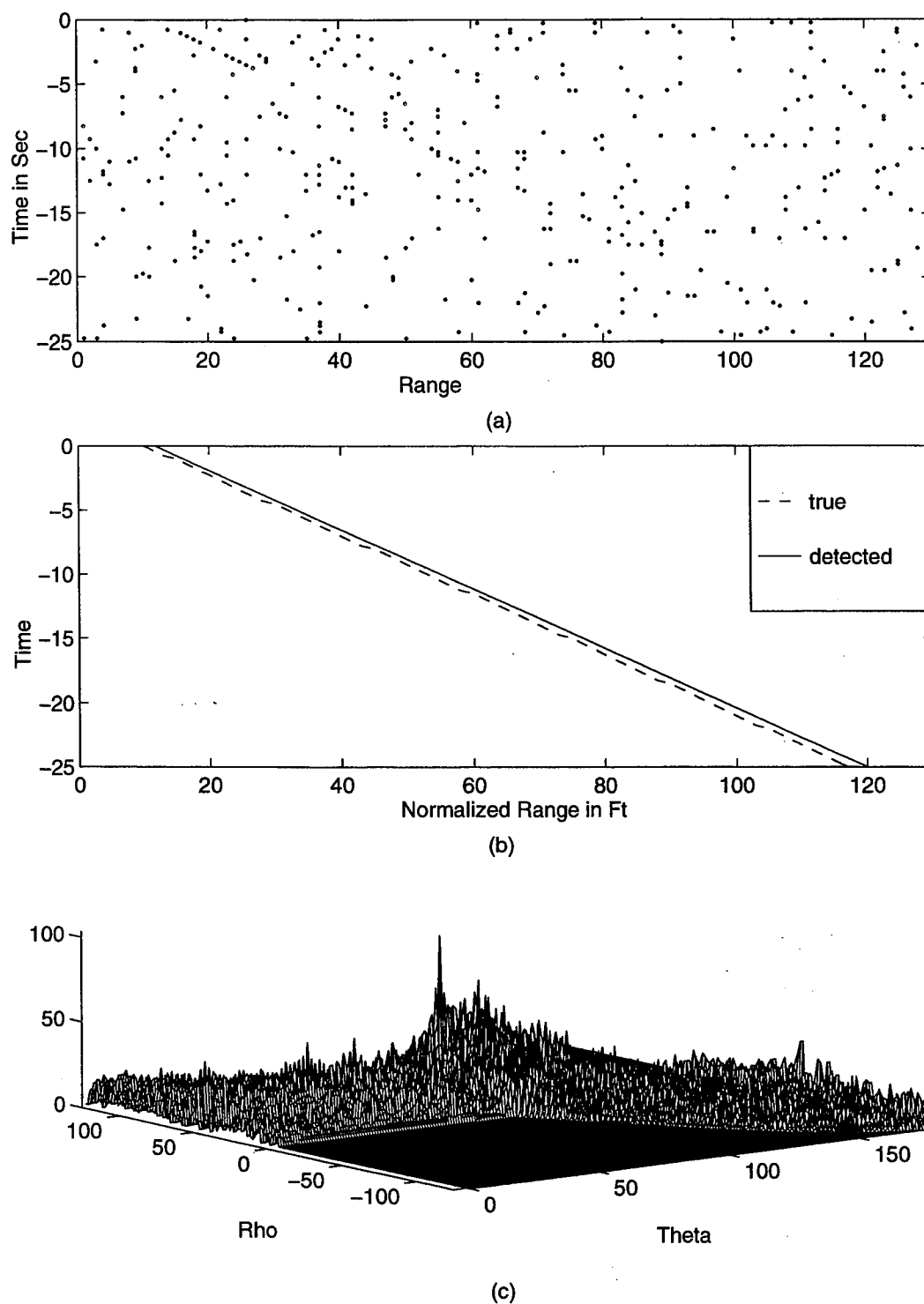


Figure 31. Test Case II, with Additive K-distributed Clutter, $SIR=5$ dB, $\xi=22$ dB.
 (a) Time Range Space after Primary Threshold.
 (b) True and Detected Target Trajectory in Image Space.
 (c) Parameter Space Mesh Plot.

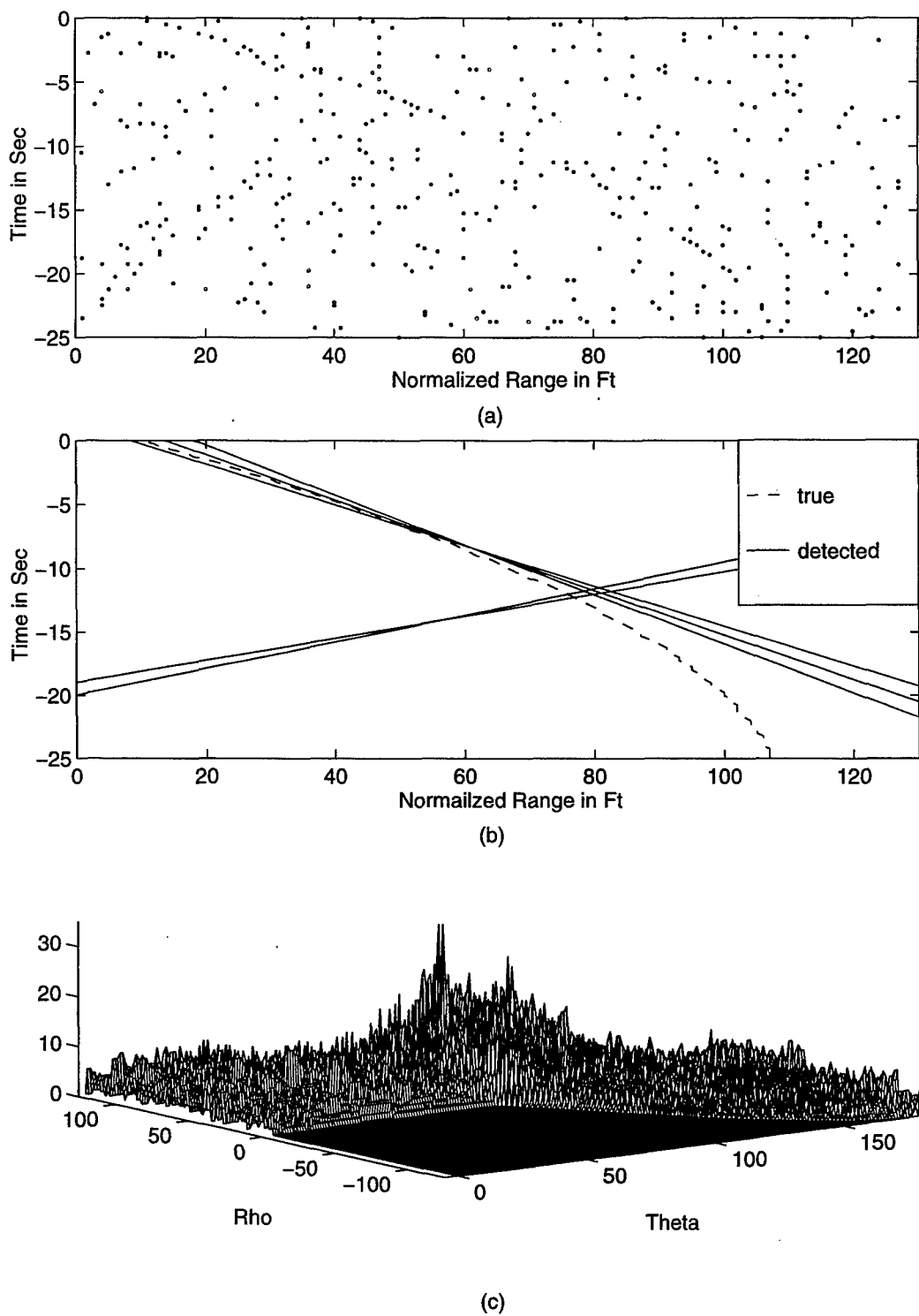


Figure 32. Test Case III, with Additive K-distributed Clutter, $SIR=5$ dB, $\xi=22$ dB.
 (a) Time Range Space after Primary Threshold.
 (b) True and Detected Target Trajectory in Image Space.
 (c) Parameter Space Mesh Plot.

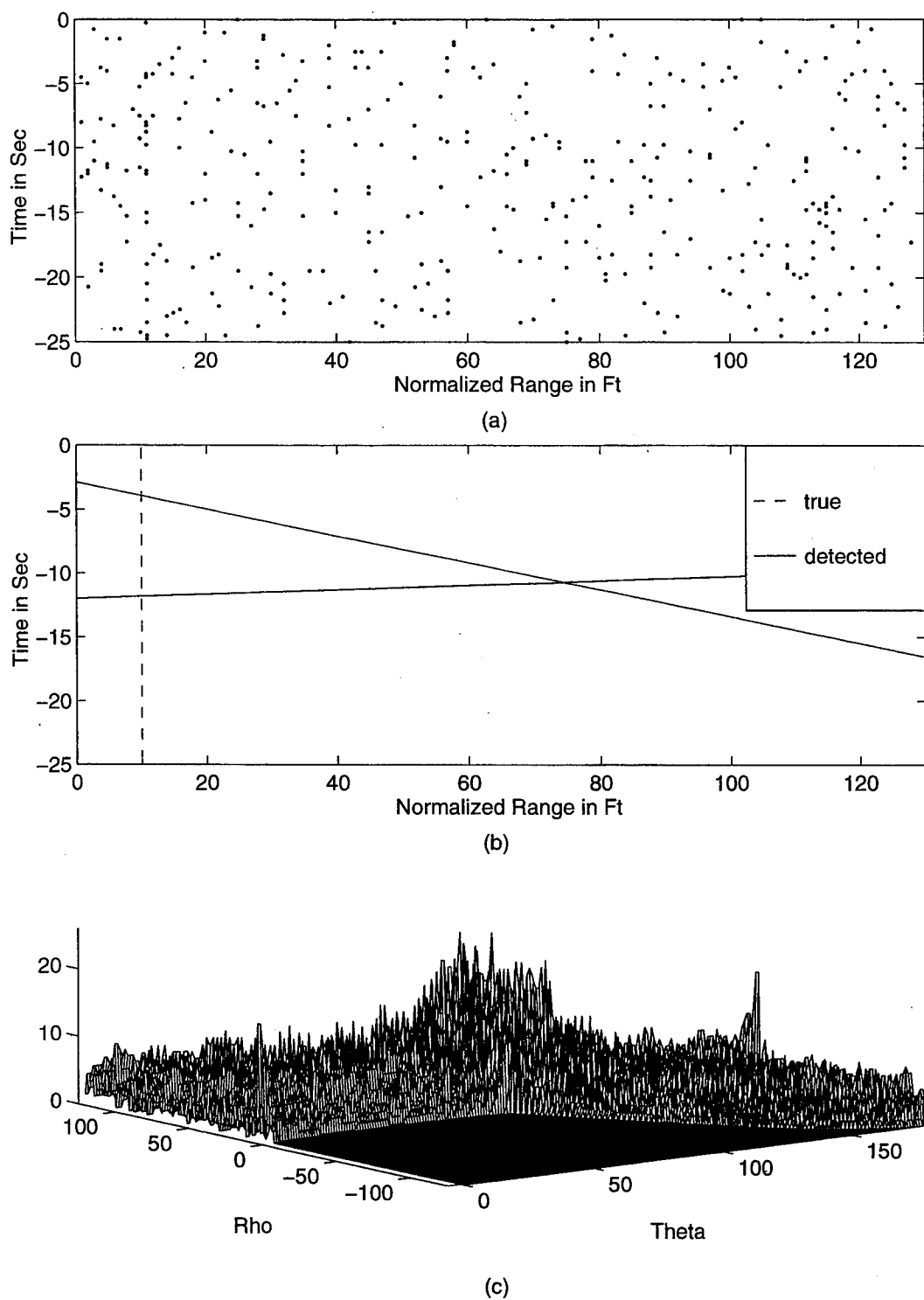


Figure 33. Test Case I with Additive K-distributed Clutter, $SIR=0$ dB, $\xi=16$ dB.
 (a) Time Range Space after Primary Threshold.
 (b) True and Detected Target Trajectory in Image Space.
 (c) Parameter Space Mesh Plot (with Binary Integration).

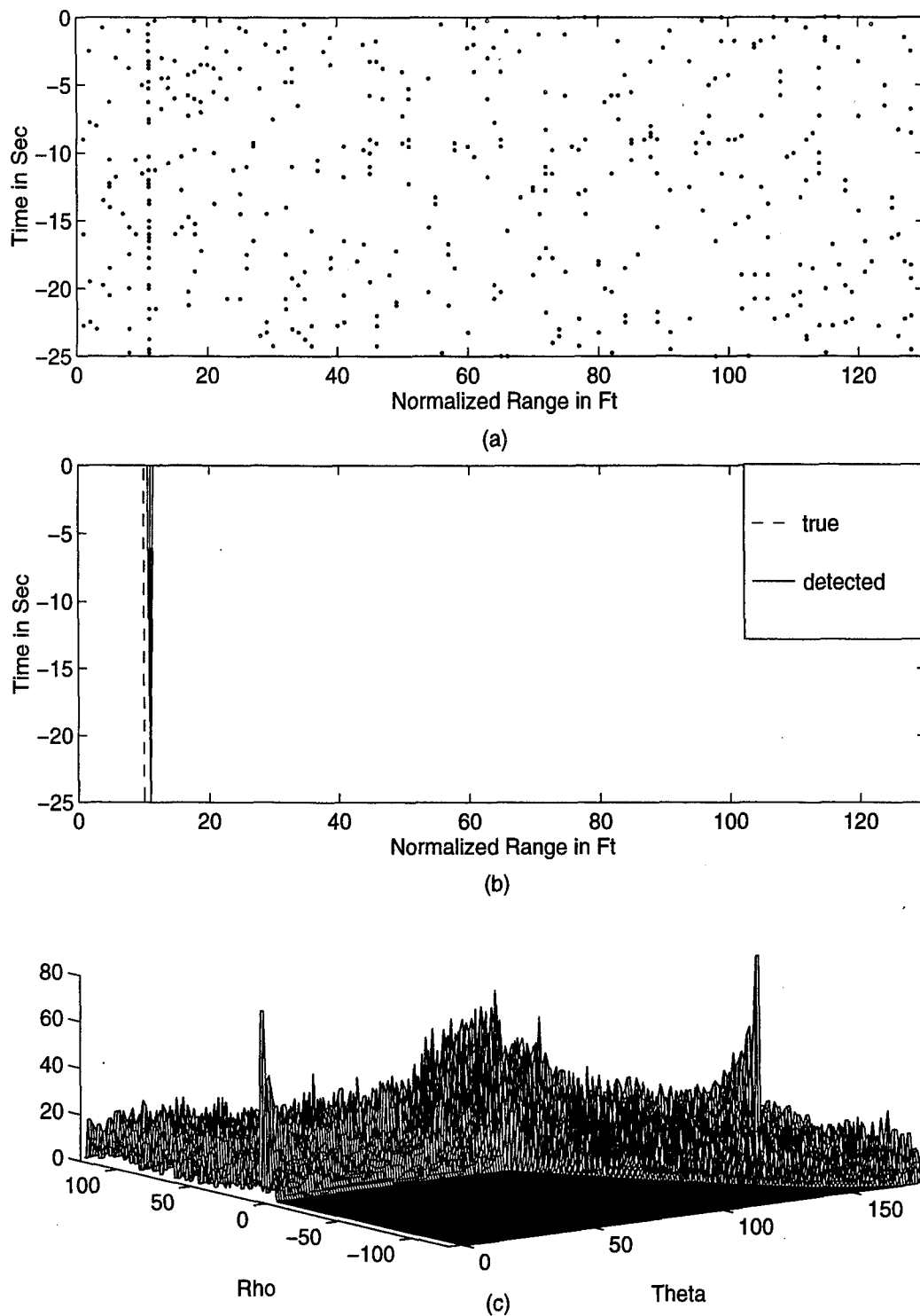


Figure 34. Test Case I, with Additive K-distributed Clutter, $SIR=5$ dB, $\xi=17$ dB.
 (a) Time Range Space after Primary Threshold.
 (b) True and Detected Target Trajectory in Image Space.
 (c) Parameter Space Mesh Plot (with Binary Integration).

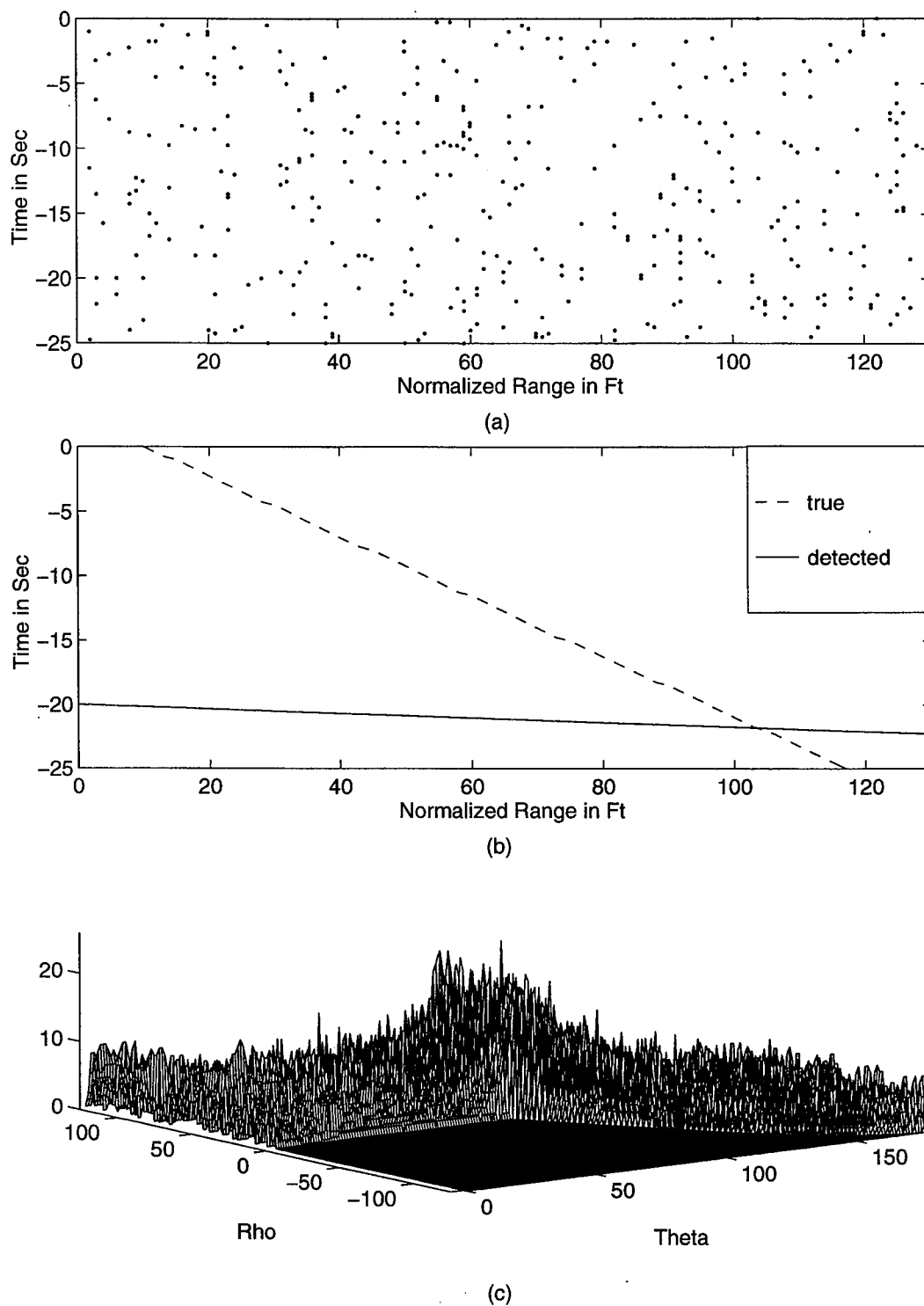


Figure 35. Test Case II with Additive K-distributed Clutter, $SIR=0$ dB, $\xi=18$ dB.
 (a) Time Range Space after Primary Threshold.
 (b) True and Detected Target Trajectory in Image Space.
 (c) Parameter Space Mesh Plot (with Binary Integration).

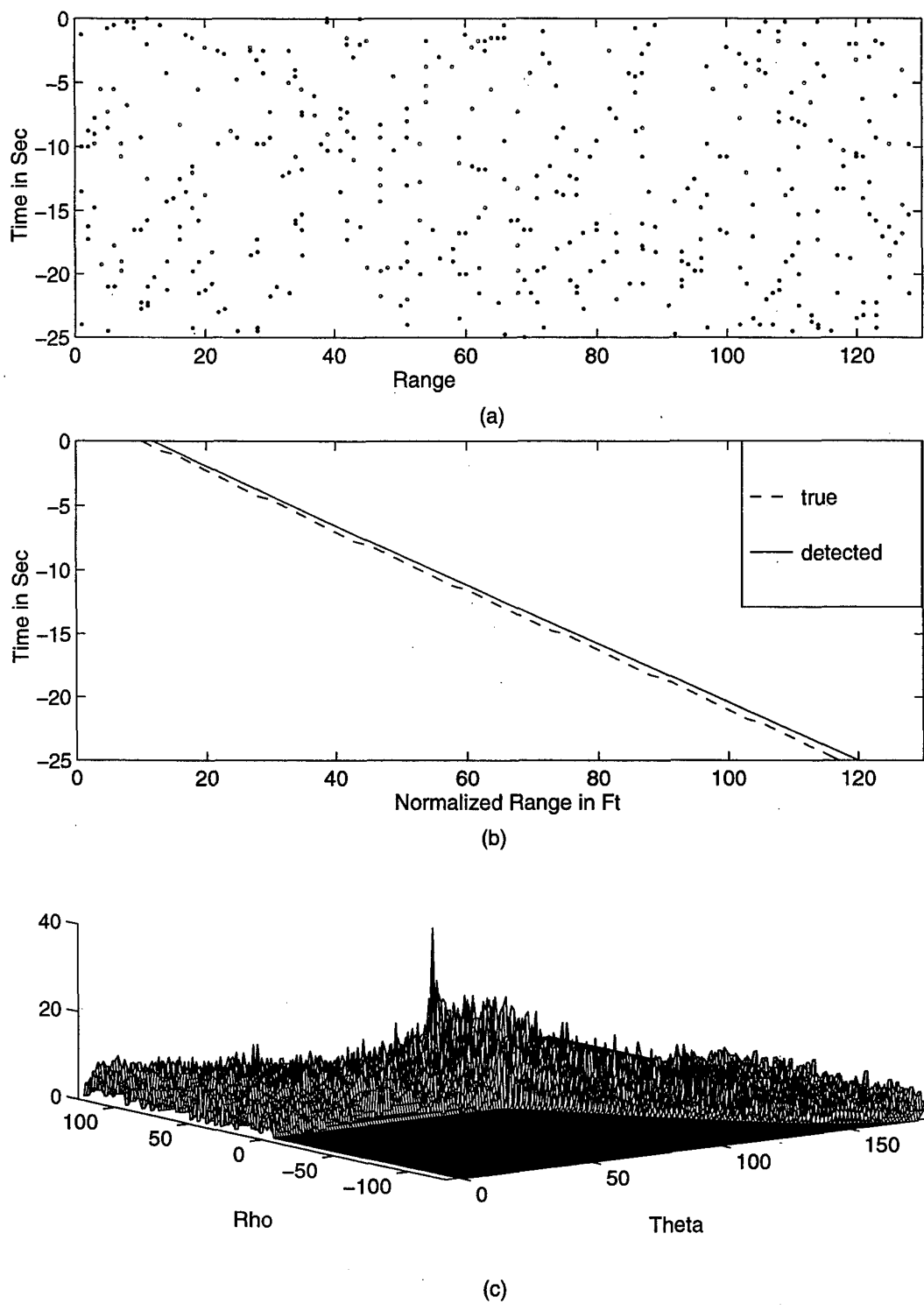


Figure 36. Test Case II, with Additive K-distributed Clutter, $SIR=5$ dB, $\xi=19$ dB.
 (a) Time Range Space after Primary Threshold.
 (b) True and Detected Target Trajectory in Image Space.
 (c) Parameter Space Mesh Plot (with Binary Integration).

C. TWO TARGETS TEST SCENARIO

As discussed in Chapter IV, one of the potential problems using the Hough based detector occurs when integrating time-range maps containing more than one target. Two multiple target scenarios are considered to determine the performance in those cases. The first one, test case IV, defines two targets with crossing trajectories and RCS ratio of 1:4 between the targets. Figure 37 presents the time-space and the corresponding parameter space for test case IV with SNR of 7 dB. Although the target trajectories are similar in length, we can observe the size of the different peaks in the parameter domain resulting from the targets relative size. Due to the high SNR in this test case and with an apriori knowledge about the existence of two targets in the integration area, we can set the secondary threshold, so that the two targets are detected. When we consider the same scenario with low SNR, the small target is masked by the noise, and it is impossible to detect it using a single threshold. This phenomena is demonstrated in Figure 38 for a SNR of 2 dB. Applying the BI Hough detector to the test case IV targets are presented in Figures 40-41 for SNR's of 7 dB and 2 dB, respectively. This results in the emphasis of the small target in the parameter space, and an equal peak size in the parameter space for the two targets is observed. Applying a simple single threshold in this case enables detection of the two targets.

The second case of interest is the case of a small target masking by a very large target. This is defined for the case of high SNR in test case V, which defines two crossing targets with RCS ratio of 1:10 between the targets. Figure 41 shows the time-range domain and the resulting Hough parameter for test case V with SNR of 15 dB. In spite of the fact that the two target trajectories are very close in length, the large target peak masks the small target, since it is much higher in power; and as a result the small target can not be detected. The BI Hough detector was applied to this case, and the results are shown in Figure 42. The level of the two targets peaks in the Hough domain are almost equal now, which enables detection of the two targets using a single threshold. However, the BI Hough transform has some performance degradation for low SNR's, which is discussed in Section C.

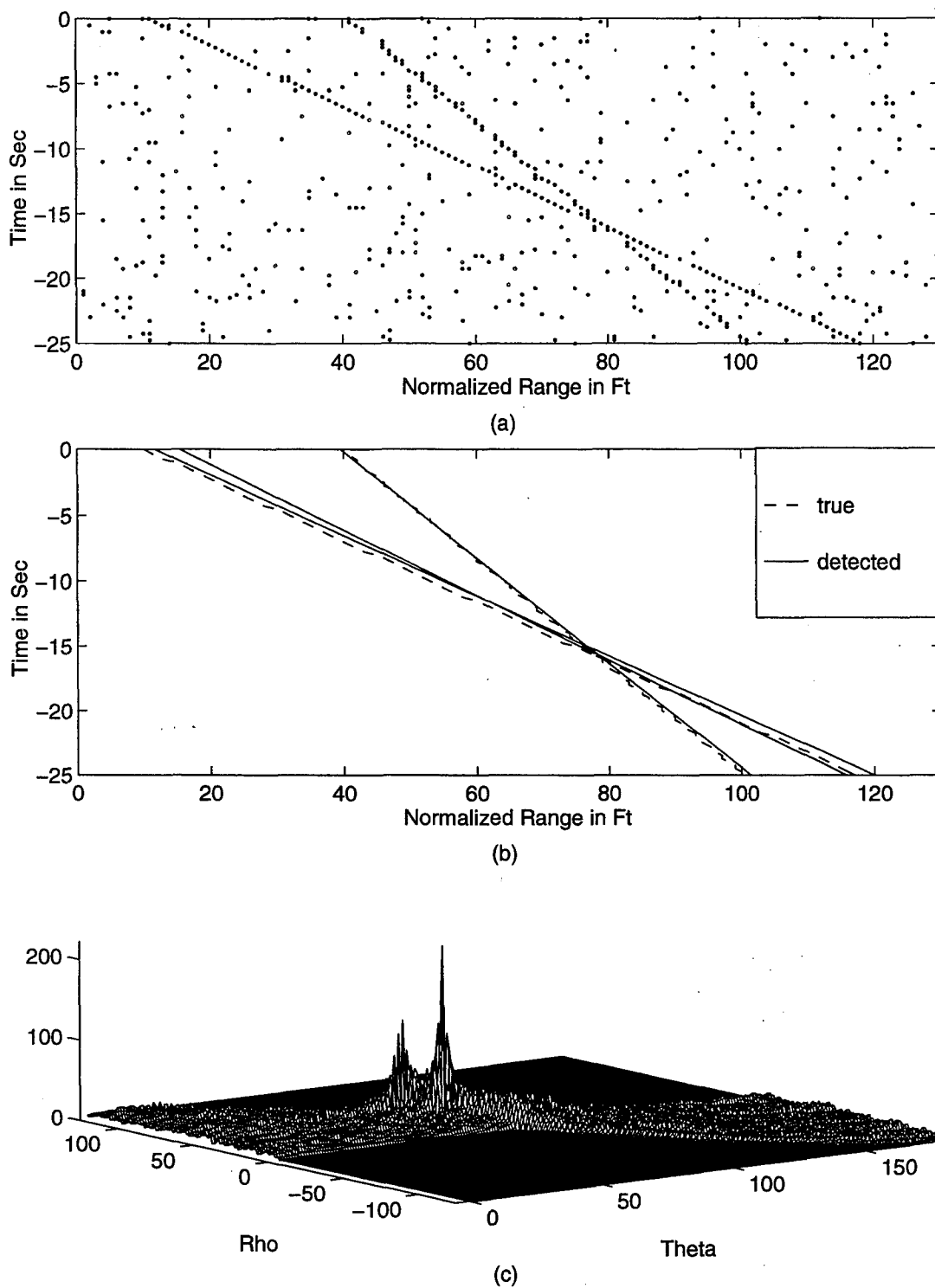


Figure 37. Test Case IV, SNR=7 dB, $\xi=16$ dB.
 (a) Time Range Space after Primary Threshold.
 (b) True and Detected Target Trajectory in Image Space.
 (c) Parameter Space Mesh Plot.

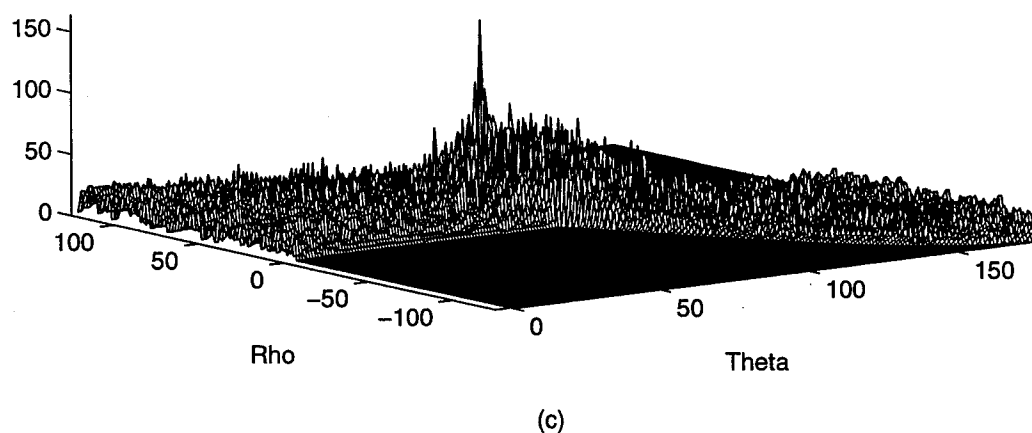
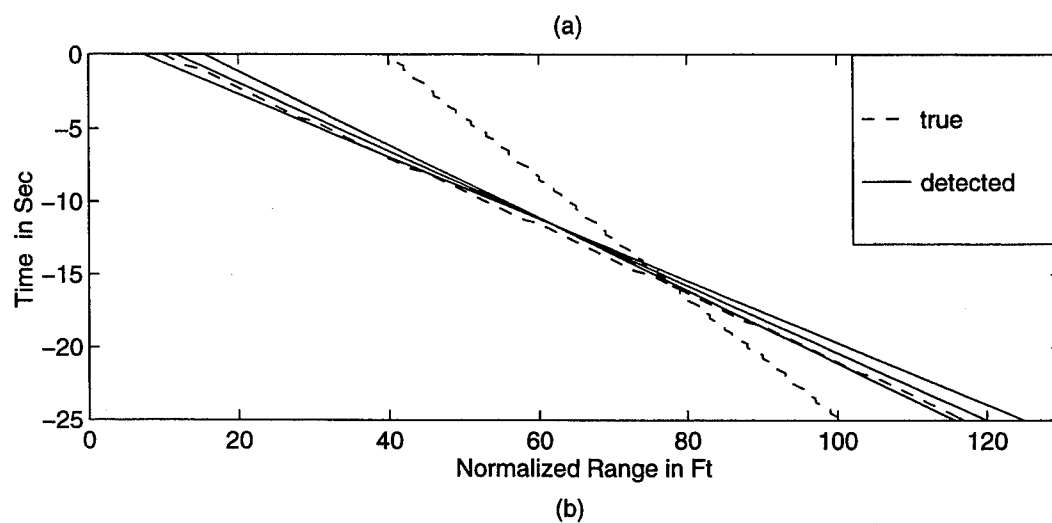
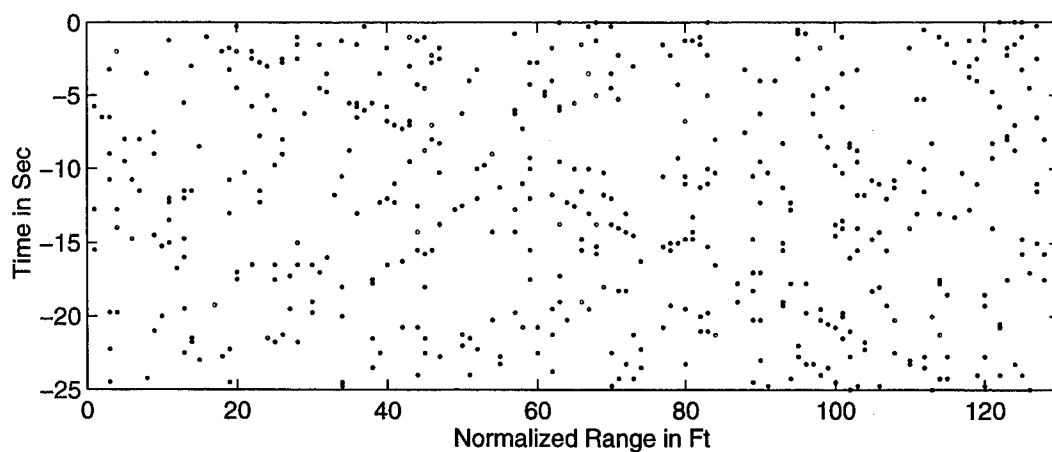
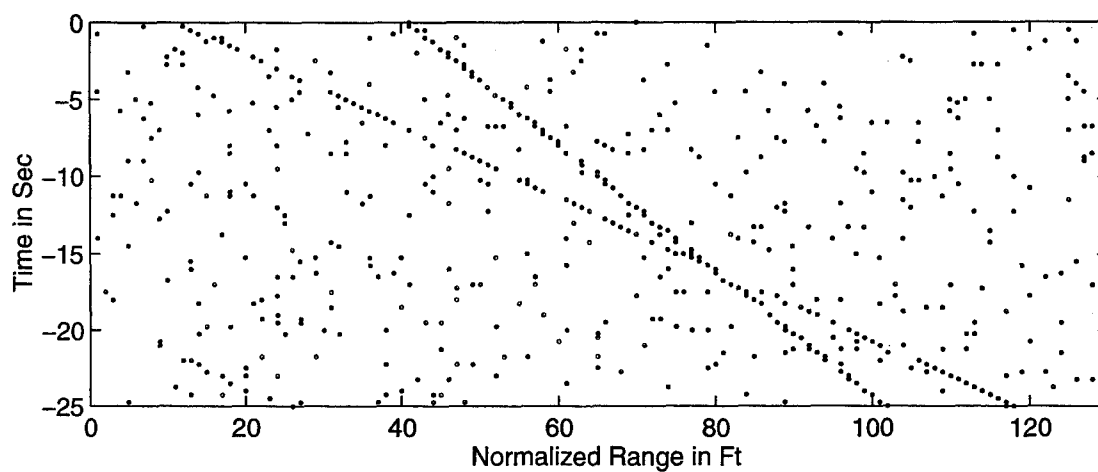
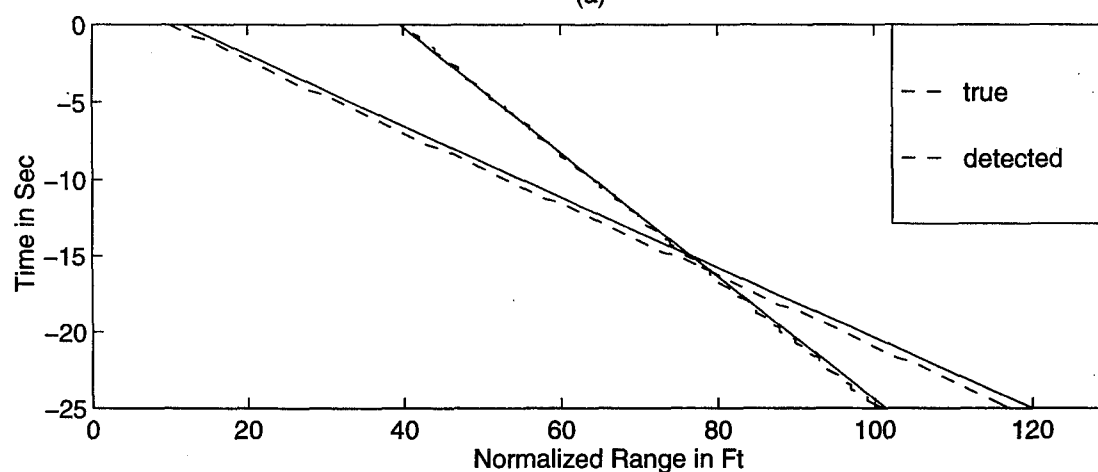


Figure 38. Test Case II, $\text{SNR}=2 \text{ dB}$, $\xi=12 \text{ dB}$.
 (a) Time Range Space after Primary Threshold.
 (b) True and Detected Target Trajectory in Image Space.
 (c) Parameter Space Mesh Plot .



(a)



(b)

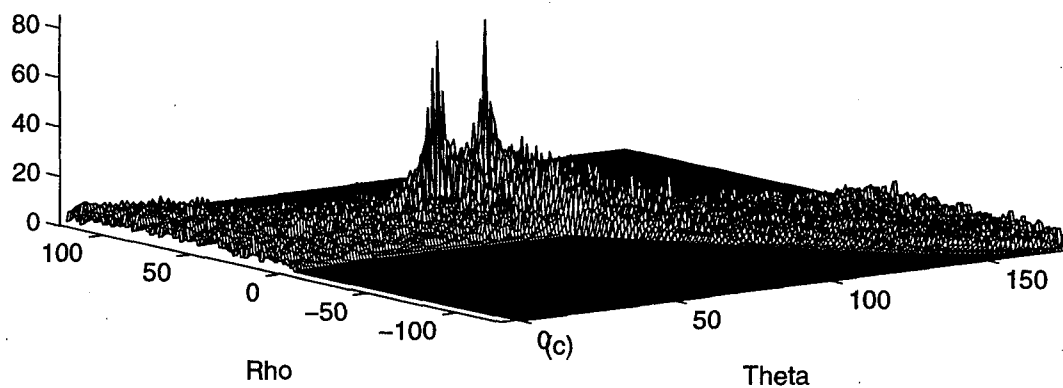


Figure 39. Test Case IV, SNR=7 dB, $\xi=16$ dB.
 (a) Time Range Space after Primary Threshold.
 (b) True and Detected Target Trajectory in Image Space.
 (c) Parameter Space Mesh Plot (with Binary Integration).

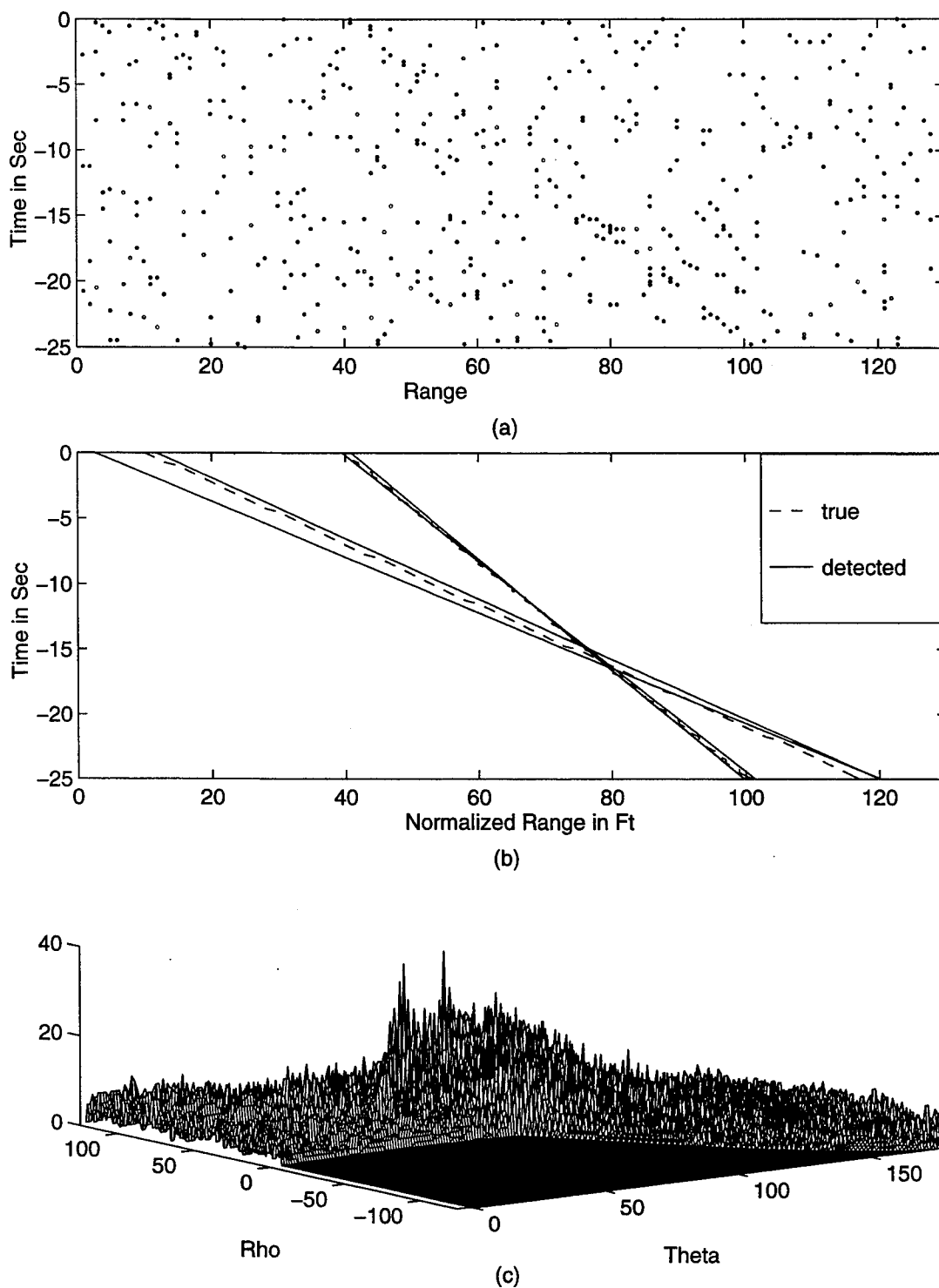
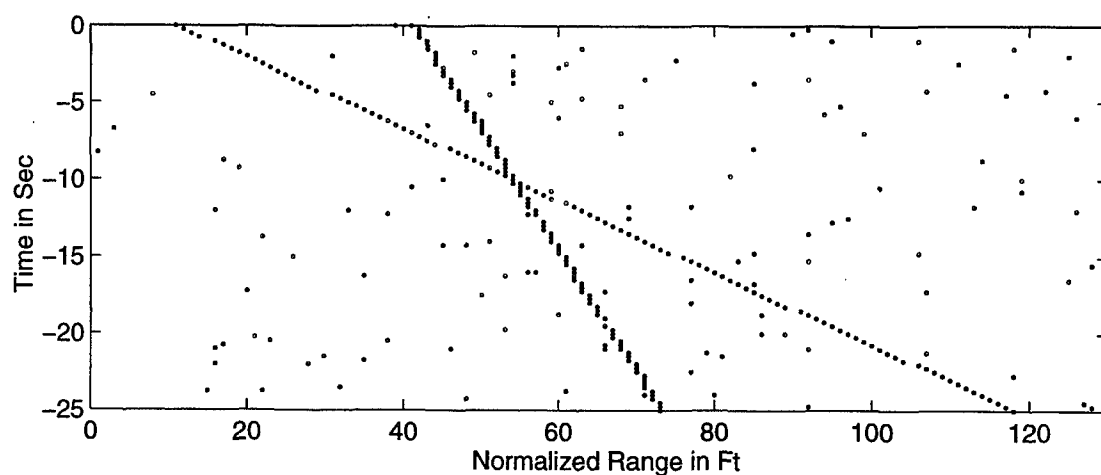
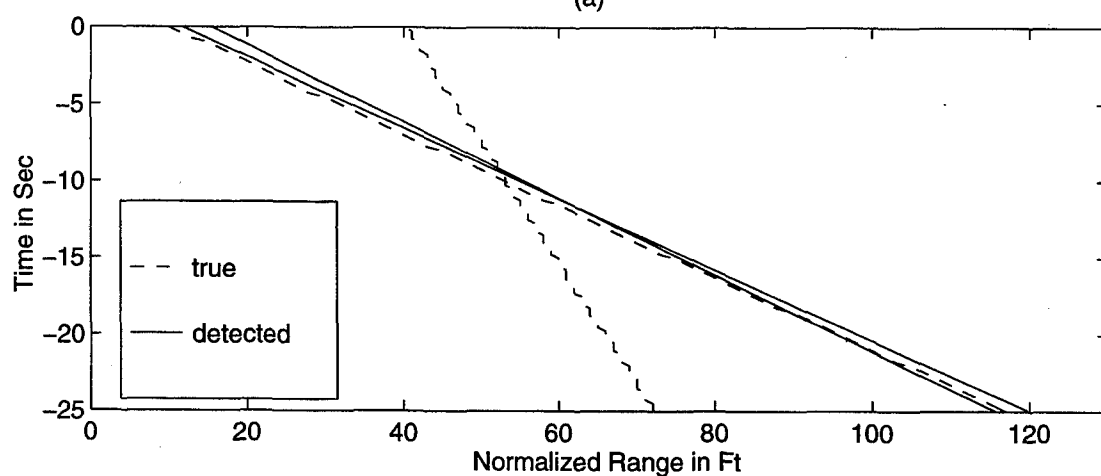


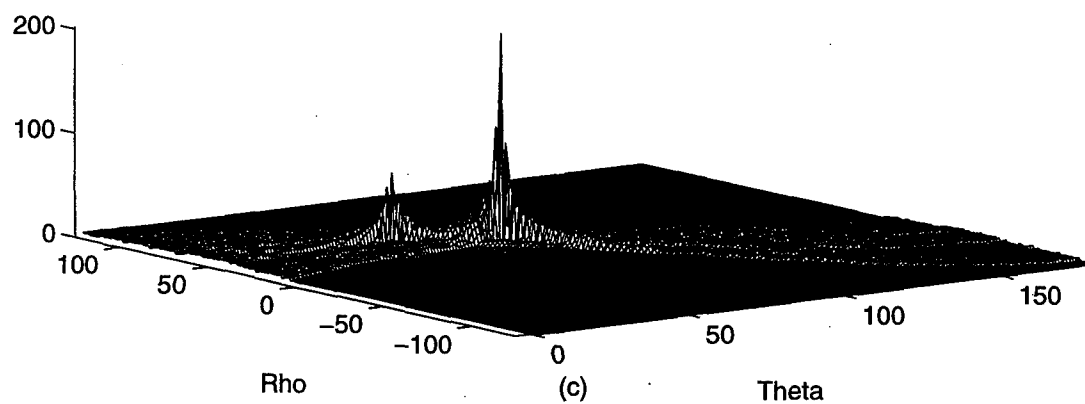
Figure 40. Test Case IV, SNR=2 dB, $\xi=12$ dB.
 (a) Time Range Space after Primary Threshold.
 (b) True and Detected Target Trajectory in Image Space.
 (c) Parameter Space Mesh Plot (with Binary Integration) .



(a)



(b)



(c)

Figure 41. Test Case V, SNR=15 dB, $\xi=20$ dB.
 (a) Time Range Space after Primary Threshold.
 (b) True and Detected Target Trajectory in Image Space.
 (c) Parameter Space Mesh Plot.

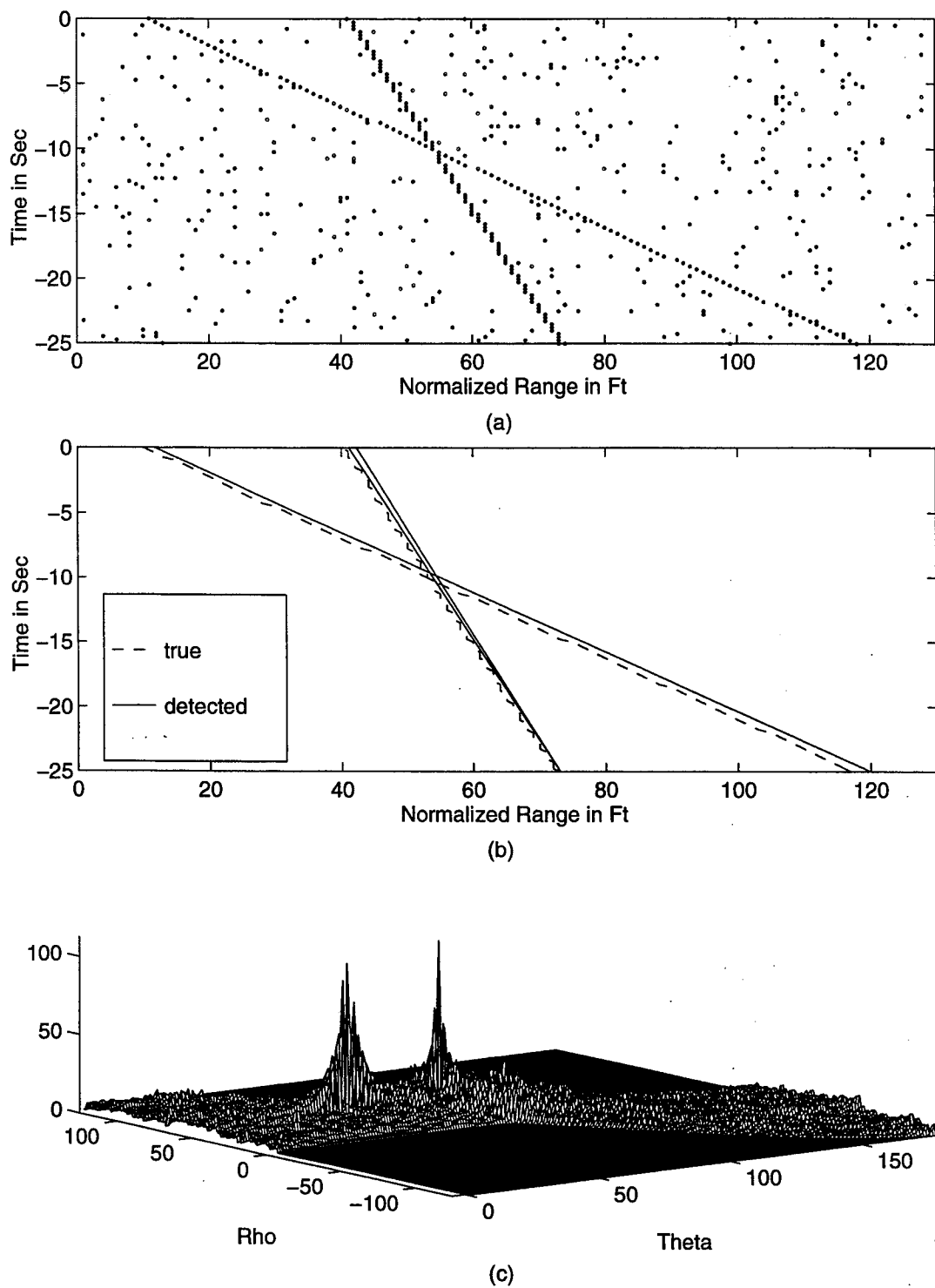


Figure 42. Test Case V, SNR=15 dB, $\xi=20$ dB.
 (a) Time Range Space after Primary Threshold.
 (b) True and Detected Target Trajectory in Image Space.
 (c) Parameter Space Mesh Plot (with Binary Integration) .

D. DETECTION PERFORMANCE

1. Additive Rayleigh Noise Case

The first step in performance evaluation is the determination of the probability of false alarm as a function of the secondary threshold. We simulate Rayleigh noise in image space, with image and parameter space dimensions, as defined in Section A. The number of accessible Hough cells, which is determined by applying all ones in the time-range space, was found to be 8192 for this particular grid choice. The primary threshold was then set to $1/200$, which is chosen to reduce the computational load. To obtain accurate results for the P_{fa} , 5000 simulations were used for each secondary threshold point, and the results were averaged. Figure 43 presents the results for the probability of false alarm as a function of secondary threshold.

To find the probability of detection, a single target was included in the simulation. The test target is modeled as a nonfluctuating target, approaching the radar site with different speeds, corresponding to a diagonal line in the time-range space. To obtain accurate results, the algorithm was tested with different SNR's and 500 repetitions per SNR point. Figures 44-46 show the resulting detection curves for target speeds of 0, 5, and 25 knots, respectively. The different curves in those plots represent different secondary threshold settings corresponding to different P_{fa} 's derived from Figure 43. Figures 48 -50 show the corresponding detection curves for the BI Hough algorithm with P_{fa} , as a function of the secondary threshold derived from Figure 37. Observing the detection curves of the BI Hough algorithm, we find about 1 dB performance degradation relative to the Hough detector. The Hough detector performance is compared against the optimum detection process and binary integration detection process performance. Figure 51 presents the P_d as a function of SNR for a given P_{fa} for a stationary target with a P_{fa} of $3 \cdot 10^{-4}$. Figure 52 presents the performance comparison for target speeds of 5, 15 and 25 knots. Figures 53-54 show the performance comparison for the same scenario with P_{fa} of $1 \cdot 10^{-7}$. The best detection performance for the conventional schemes are achieved, as expected, when the target is stationary. When the target is moving, collapsing loss degrades the detection performance of those detectors. The Hough detector performance

improves as the target speed increases, resulting in longer target line in the time-range domain. Figure 55 shows significant results obtained by estimating the processing gain/loss of the detector, which is compared to the optimal detector for different speeds. This figure shows the range-walk problem exists when applying traditional detection techniques. The Hough detector does not suffer from this problem, and its performance improves as the target speed increases.

2. Additive K-Distributed Clutter Case

Detection performance in the case of additive K-distributed clutter is evaluated in a similar way to the noise only case. The probability of false alarm as a function of the secondary threshold is shown in Figure 56, where the time-range and Hough space parameters are as defined in Subsection 1. Comparing the results obtained in this case to those presented in Figure 43 for the noise-only case, we observe that the P_{fa} , or the same secondary threshold setting, is higher, due to the spiky nature of the clutter.

The probability of detection was determined using the test targets defined in Subsection 1. The number of repetitions in this case was limited to 100 per SNR point, due to the large computational load in the K-distributed clutter simulation. Figures 57-59 present the resulting detection curves for a scenario consisting of target embedded in k-distributed clutter plus noise approaching the radar site in velocities of 0, 5, and 25 knots, respectively. The different curves in those plots represent different secondary thresholds. Comparison of the Hough detector to traditional radars is done by simulating a square law detector and evaluating its performance for the same scenarios. Figure 61 presents the performance comparison for a nonfluctuating stationary target, a 25 knot nonfluctuating target and a P_{fa} of $8 \cdot 10^{-5}$. We observe that the Hough transform performance improves as the target speed increases. The spikier nature of the clutter, which force us to use a higher threshold to achieve predefined P_{fa} level, results in causes degradation in the performance comparing to the noise only case. Figure 60 presents the processing gain/loss for this case, as compared to an envelope detector for different target speeds. We observe that the range-walk problem is solved in this case, as in the noise-only case although the processing gain is lower in higher velocities (2 dB).

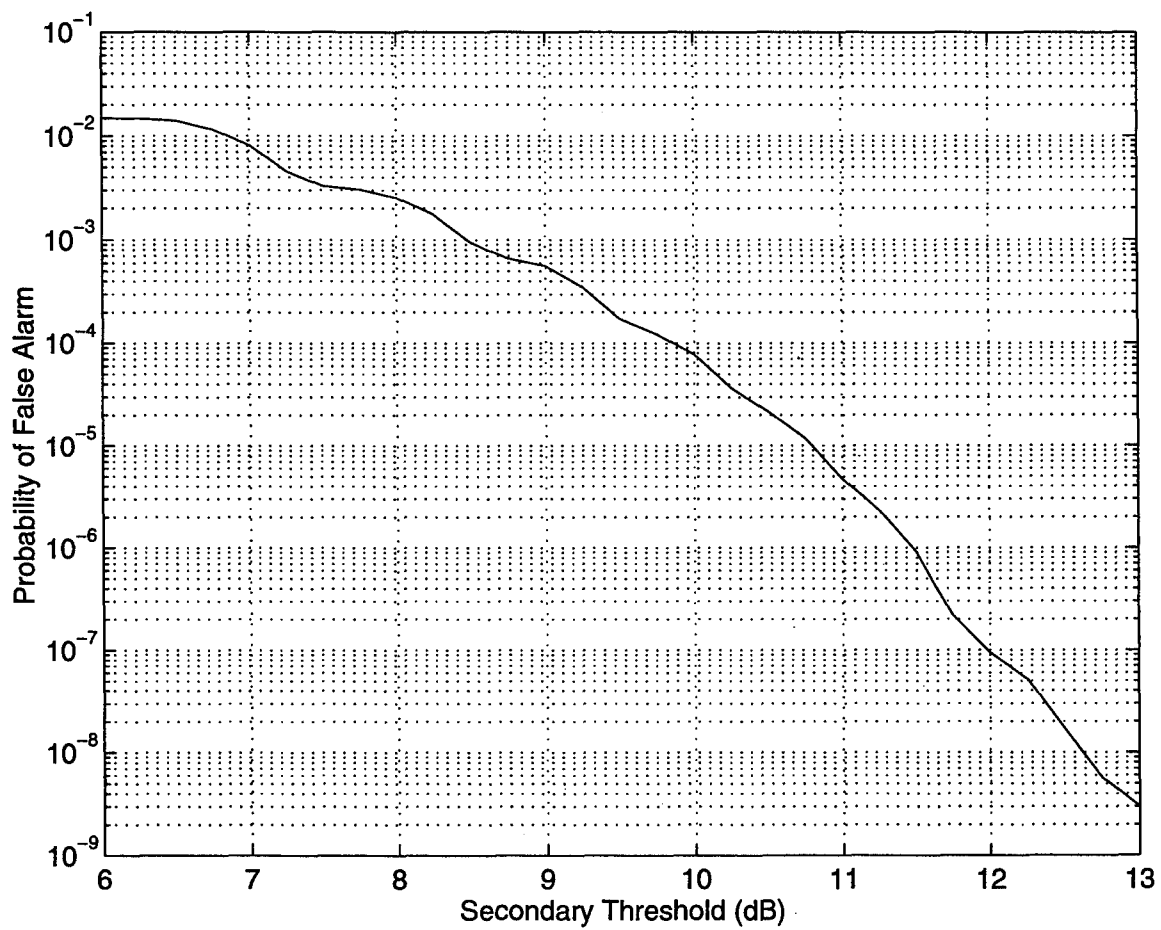


Figure 43. Hough Detector P_{fa} as a Function of Secondary Threshold.

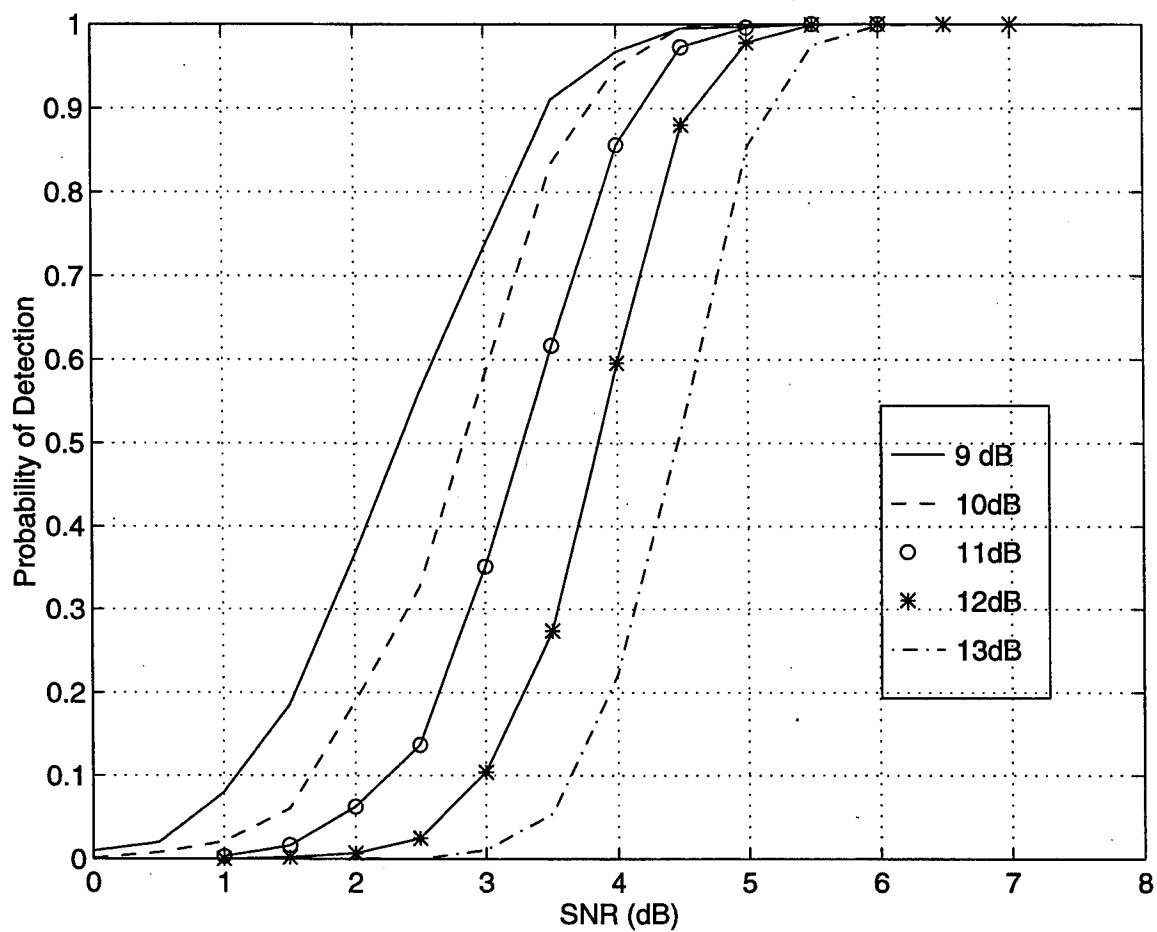


Figure 44. Hough Detector P_d as a Function of SNR for a Nonfluctuating Stationary Target with Additive Rayleigh Noise Scenario. Different Curves Denote Different secondary Threshold Settings.

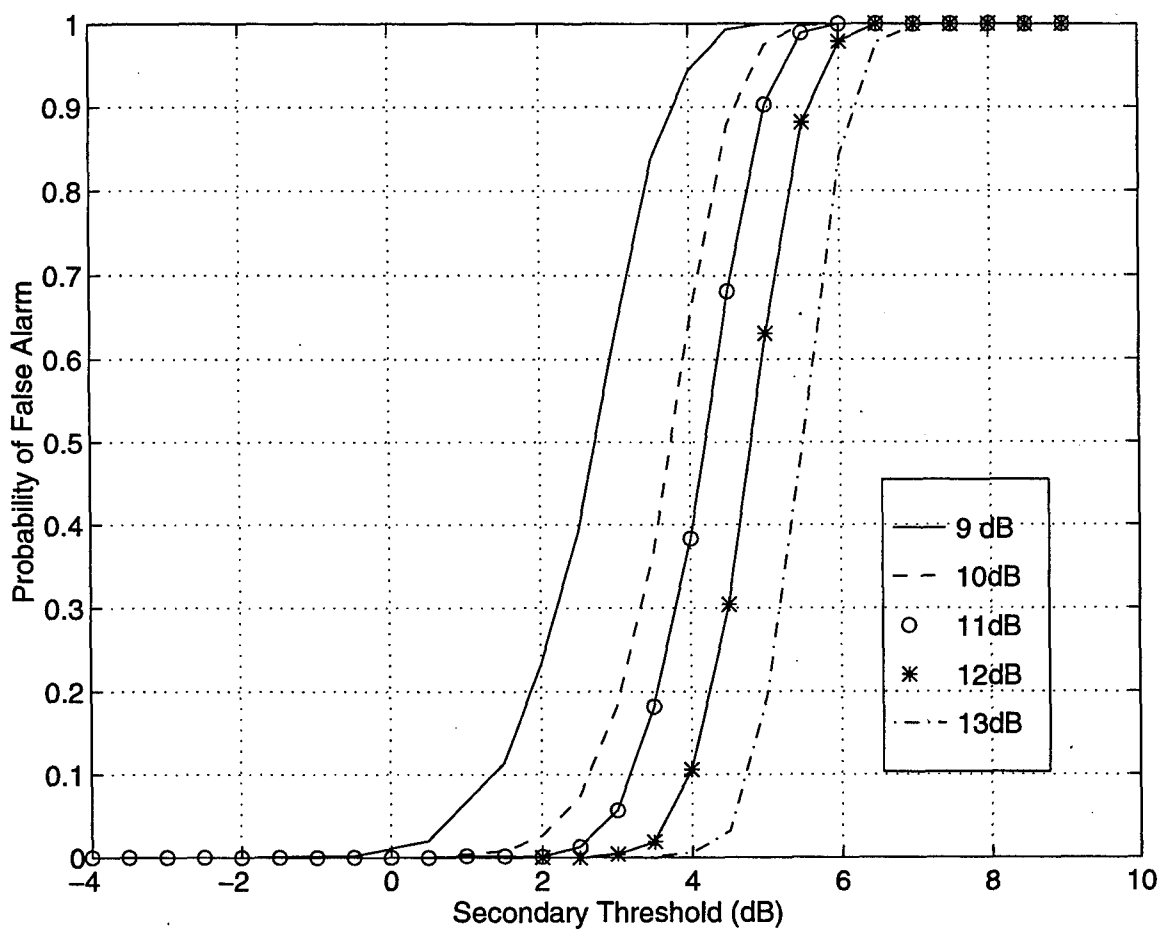


Figure 45. Hough Detector P_d as a Function of SNR for a Nonfluctuating 5 Knot Target with Additive Rayleigh Noise Scenario. Different Curves Denote Different secondary Threshold Settings.

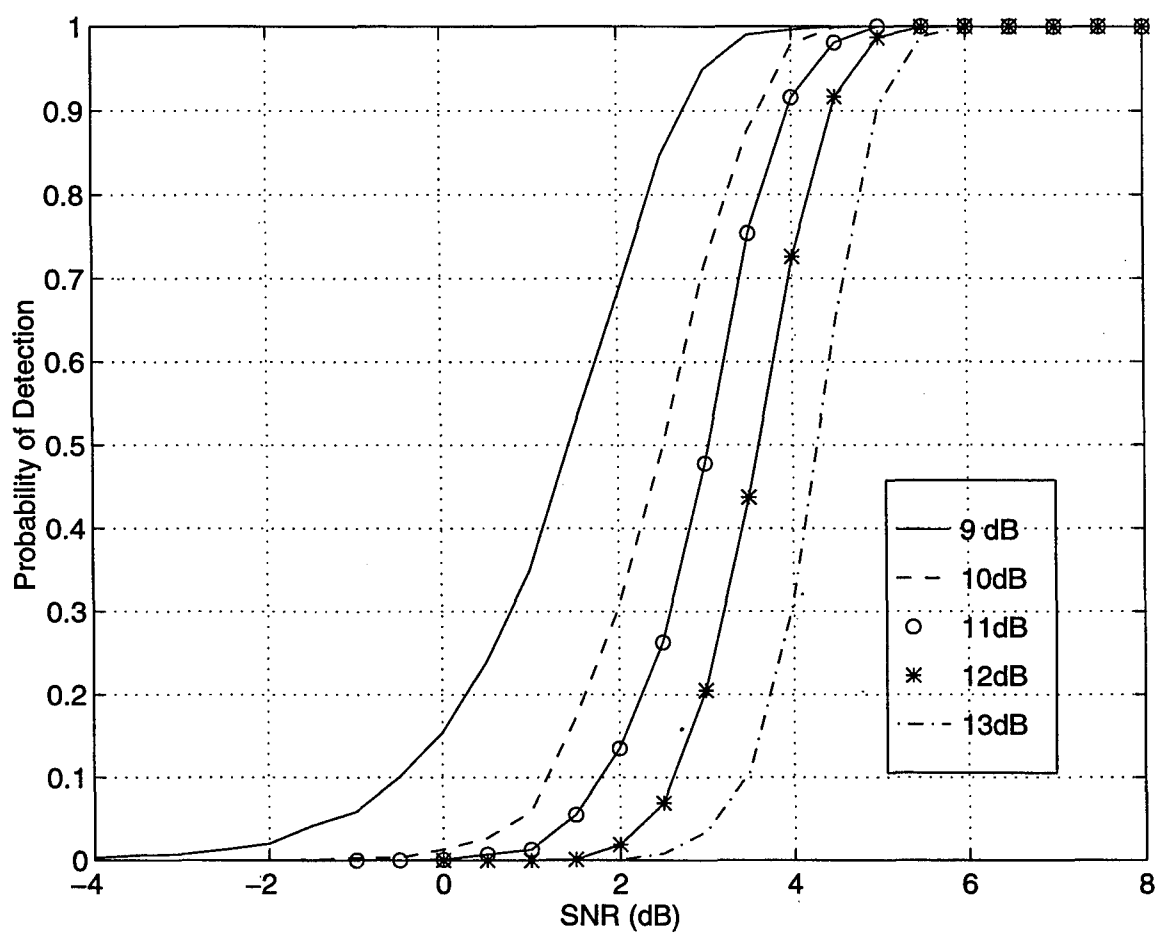


Figure 46. Hough Detector P_d as a Function of SNR for a Nonfluctuating 25 Knot Target with Additive Rayleigh Noise Scenario. Different Curves Denote Different secondary Threshold Settings.

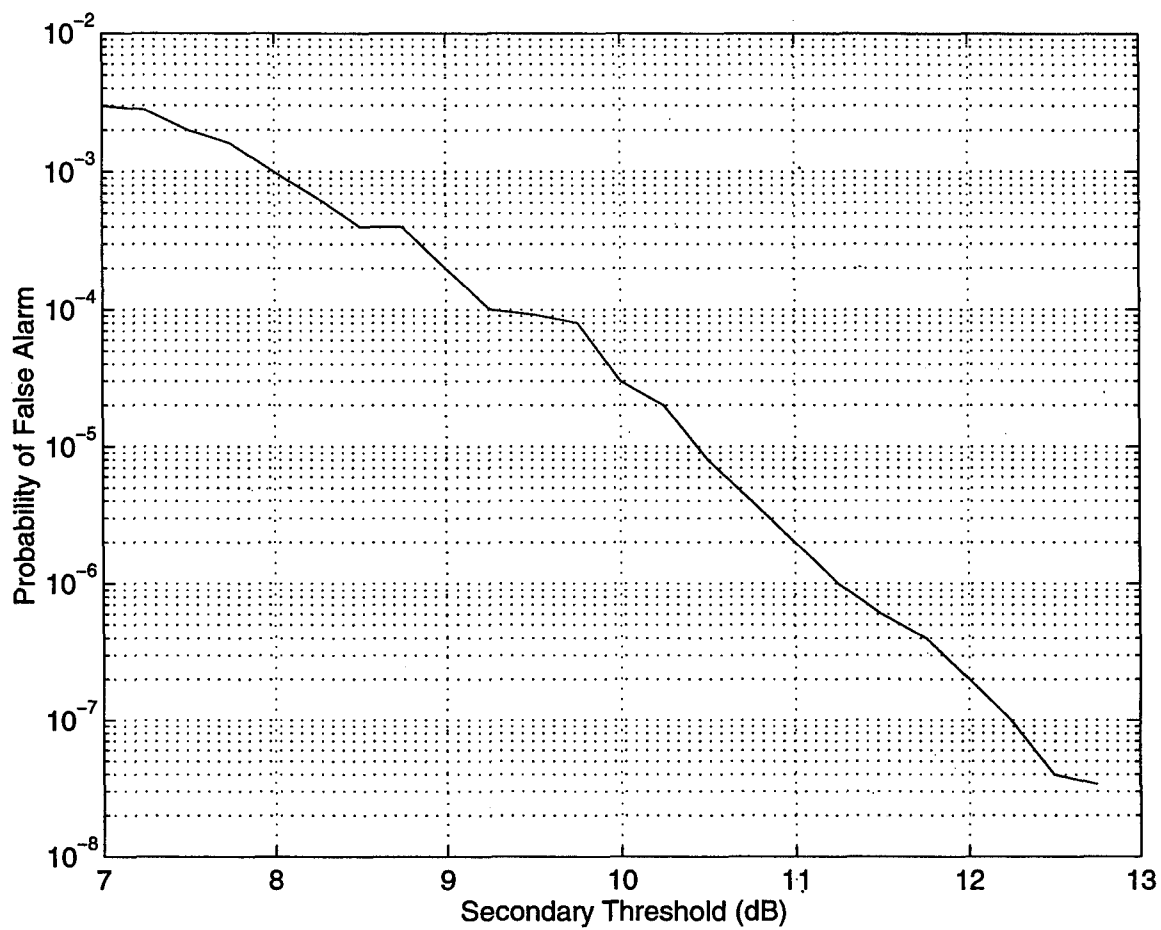


Figure 47. Binary Integration Hough Detector P_{fa} as a Function of Secondary Threshold.

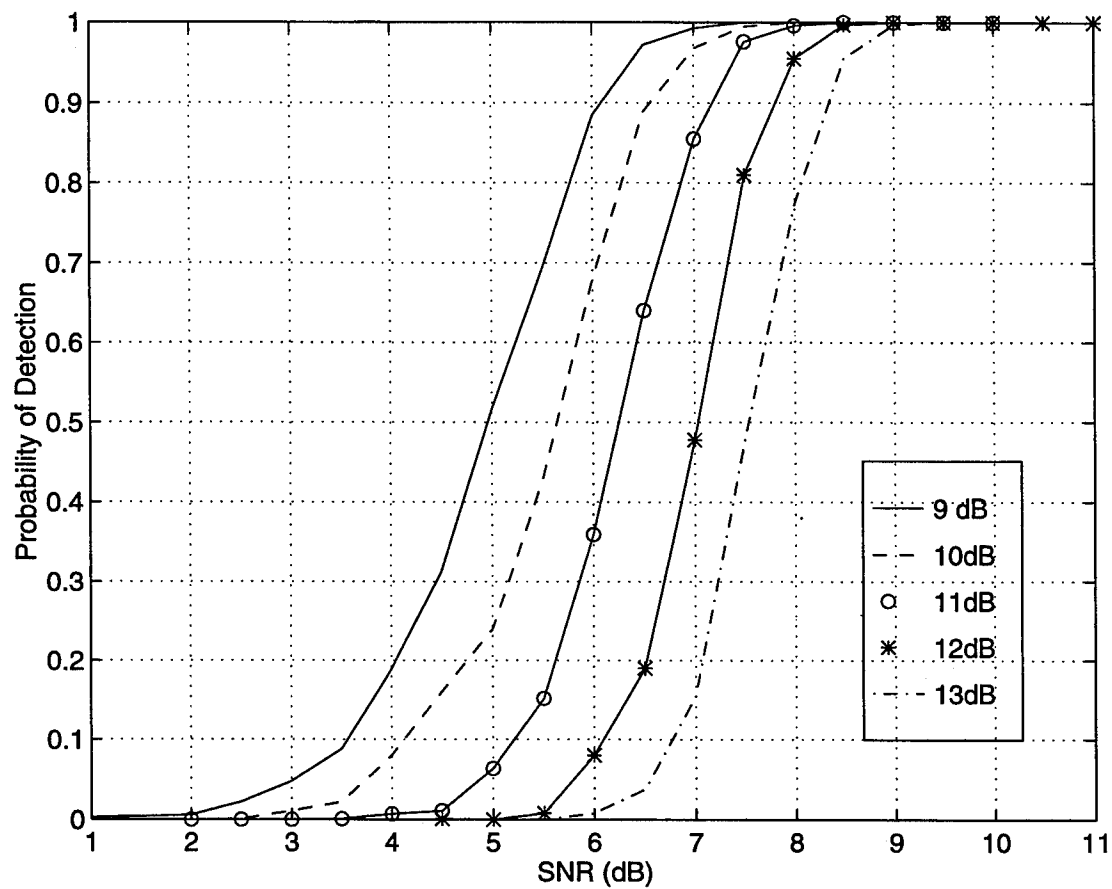


Figure 48. Binary Integration Hough Detector P_d as a Function of SNR for a Nonfluctuating Stationary Target with Additive Rayleigh Noise Scenario. Different Curves Denote Different secondary Threshold settings.

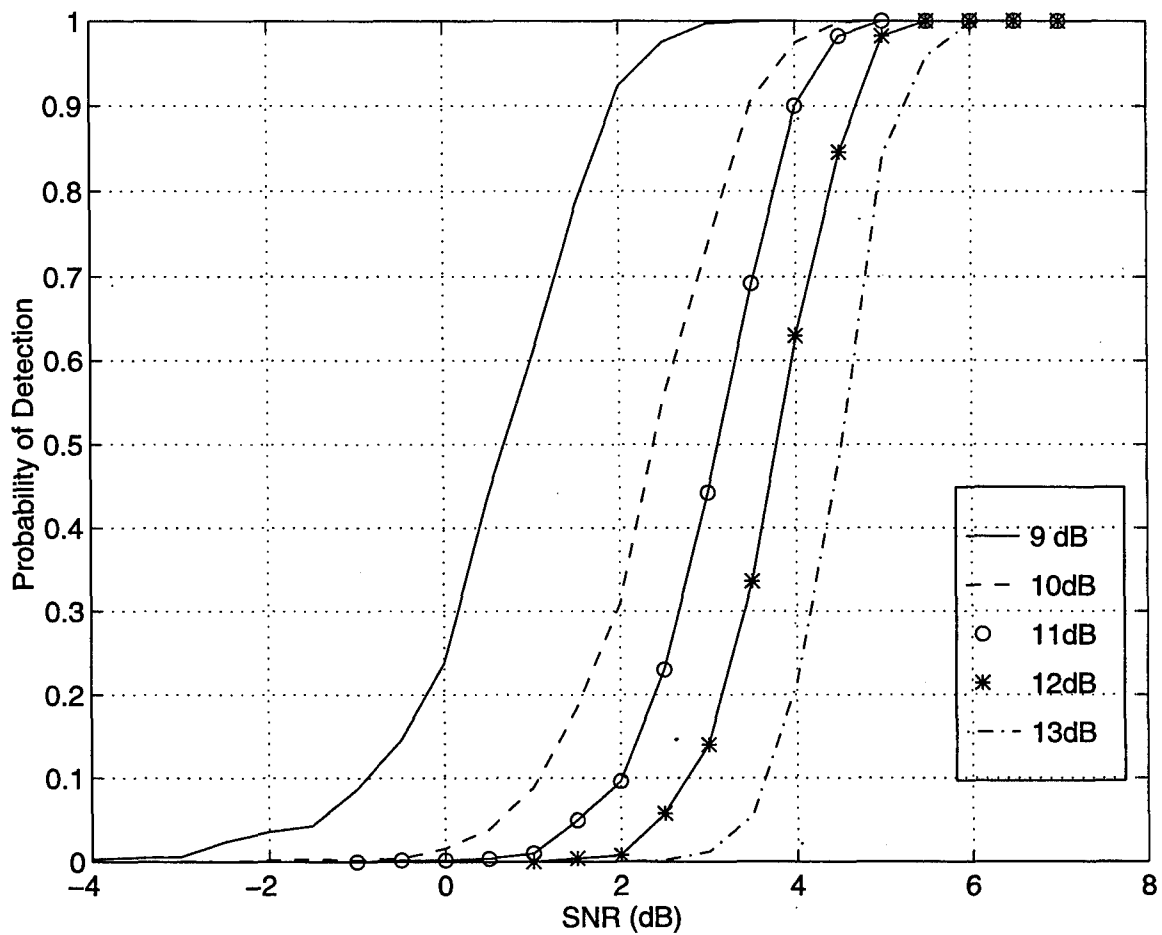


Figure 49. Binary integration Hough Detector P_d as a Function of SNR for a Nonfluctuating 15 knot Target with Additive Rayleigh Noise Scenario. Different Curves Denote Different secondary Threshold Settings.

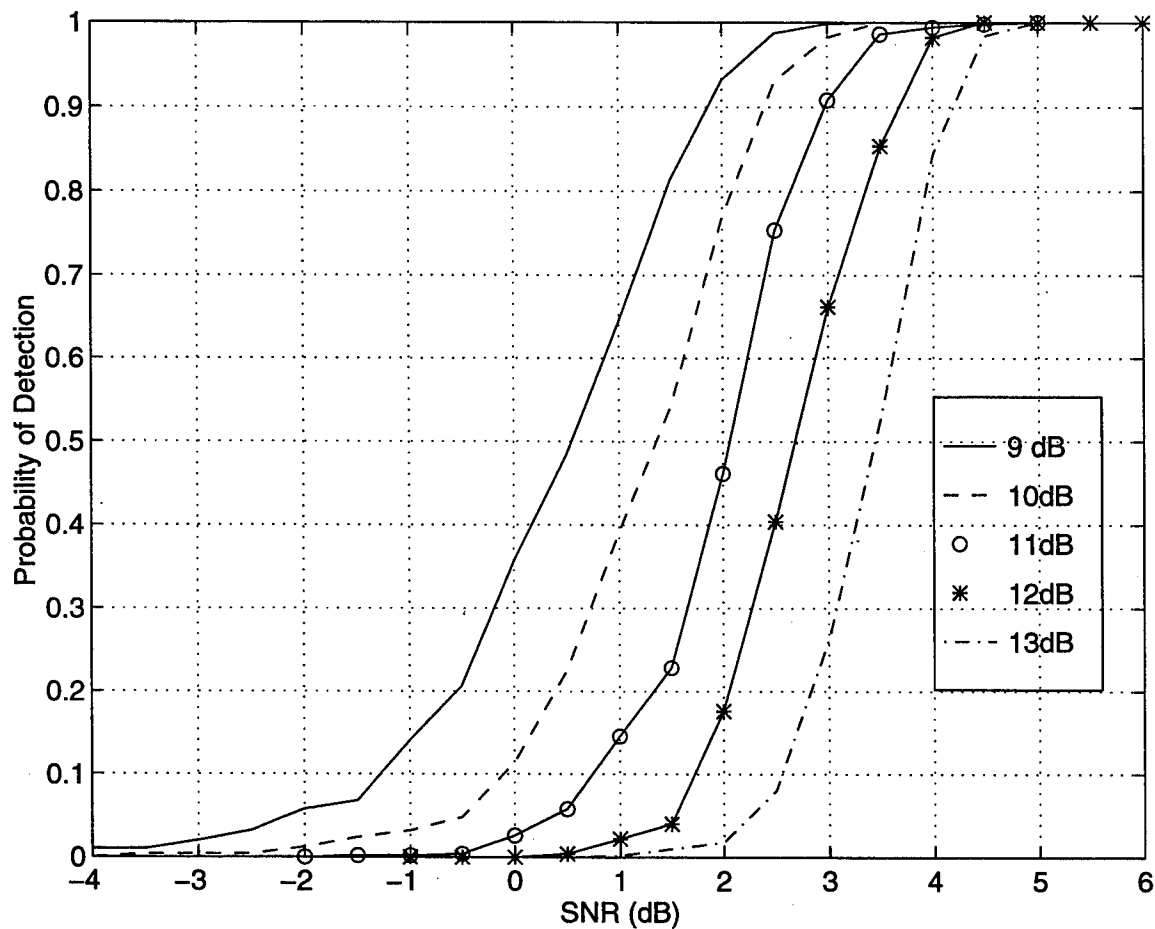


Figure 50. Binary integration Hough Detector P_d as a Function of SNR for a Nonfluctuating 25 knot Target with Additive Rayleigh Noise Scenario. Different Curves Denote Different secondary Threshold Settings.

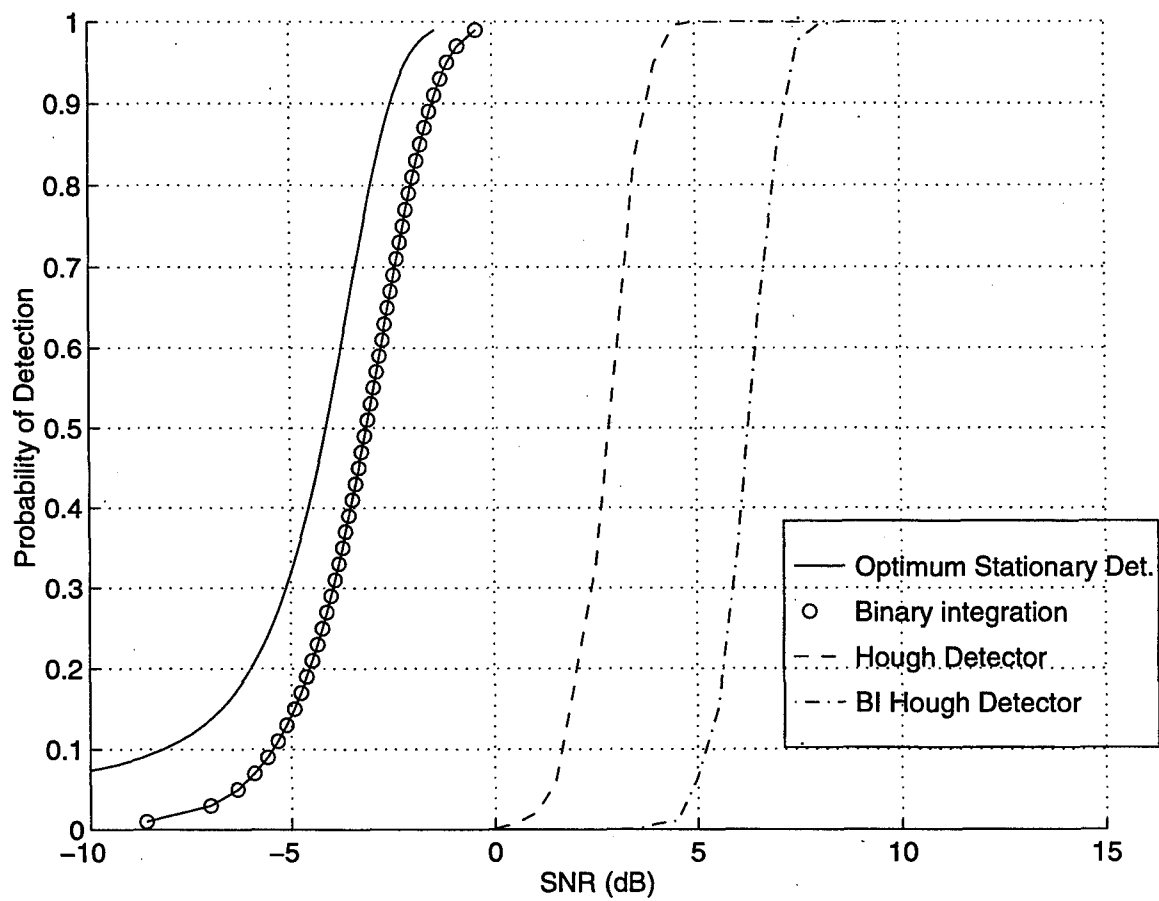
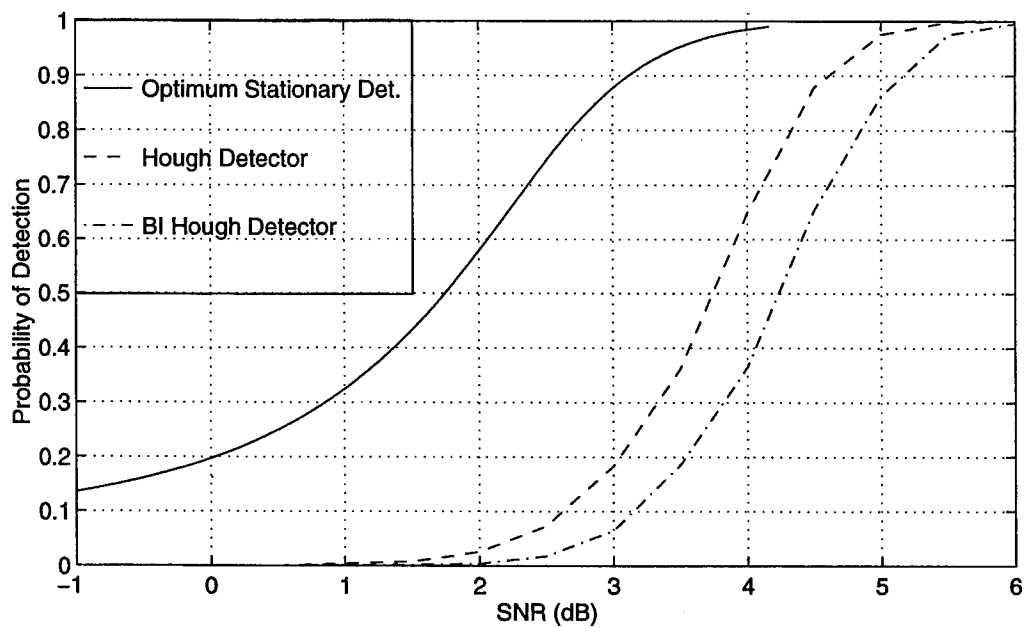
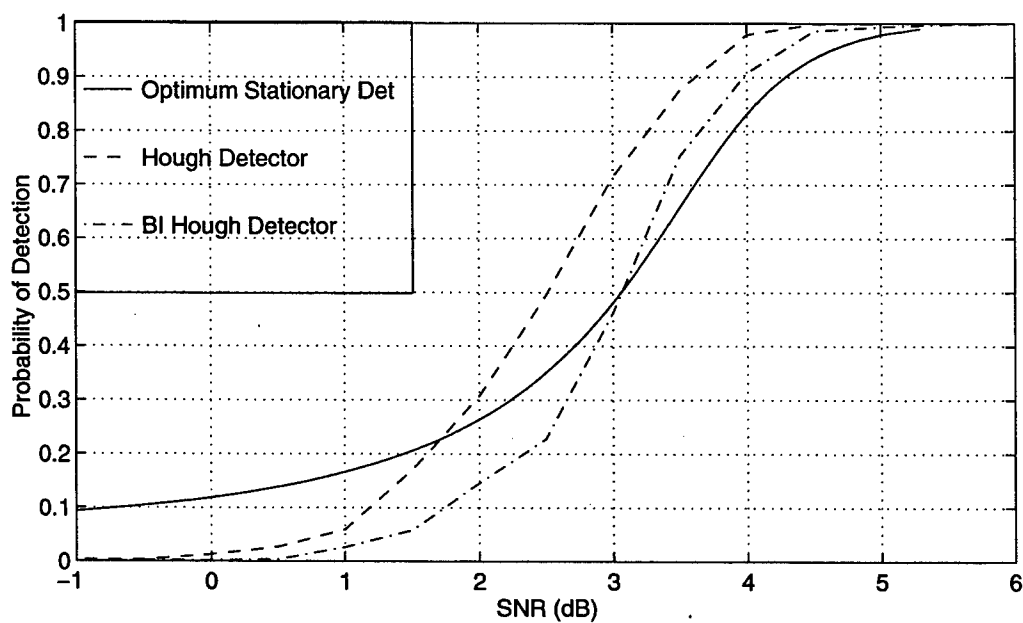


Figure 51. P_d as a Function of SNR for a Nonfluctuating stationary Target with Additive Rayleigh Noise scenario @ $P_{fa}=3 \cdot 10^{-4}$. Different curves denote different detection schemes.



(a)



(b)

Figure 52. P_d as a Function of SNR for a Nonfluctuating Target with Additive Rayleigh Noise scenario @ $P_{fa}=3 \cdot 10^{-4}$, Different curves denote different detection schemes.

(a) Target Speed 5 Knots.

(b) Target Speed 25 Knots.

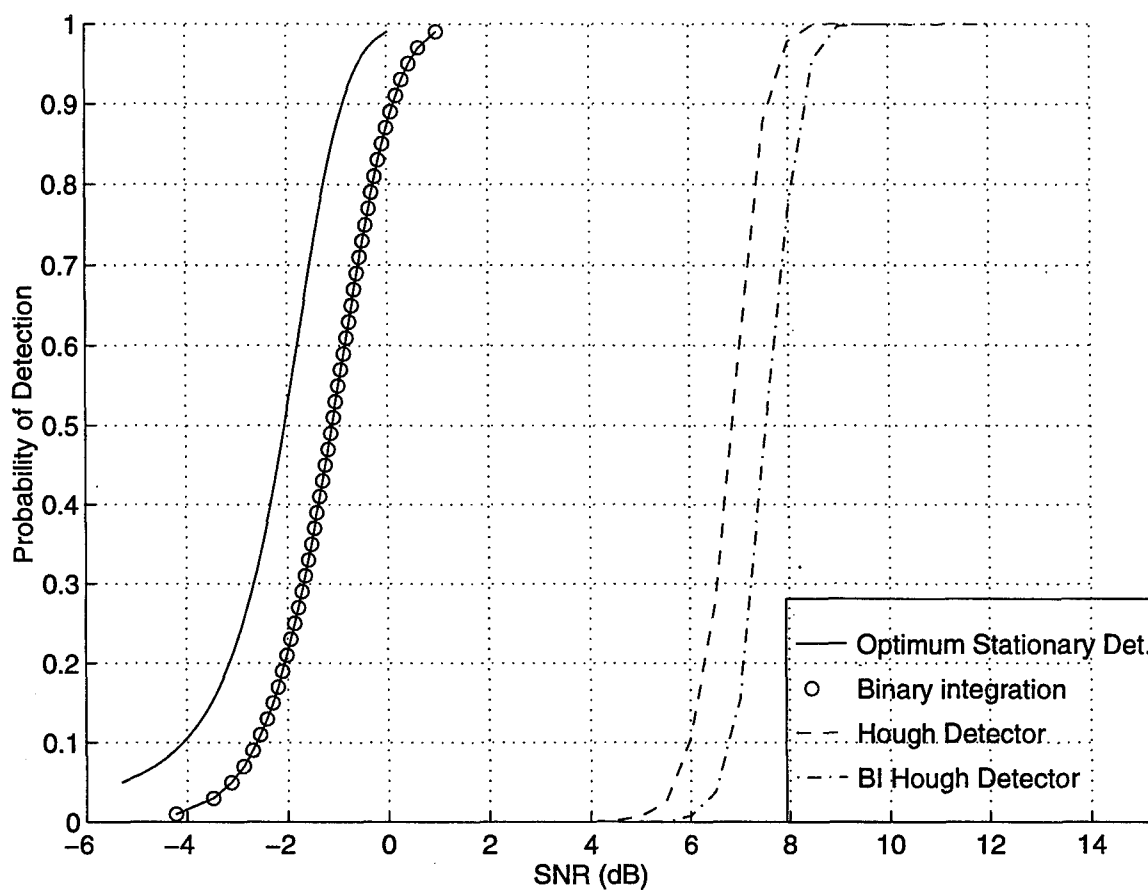
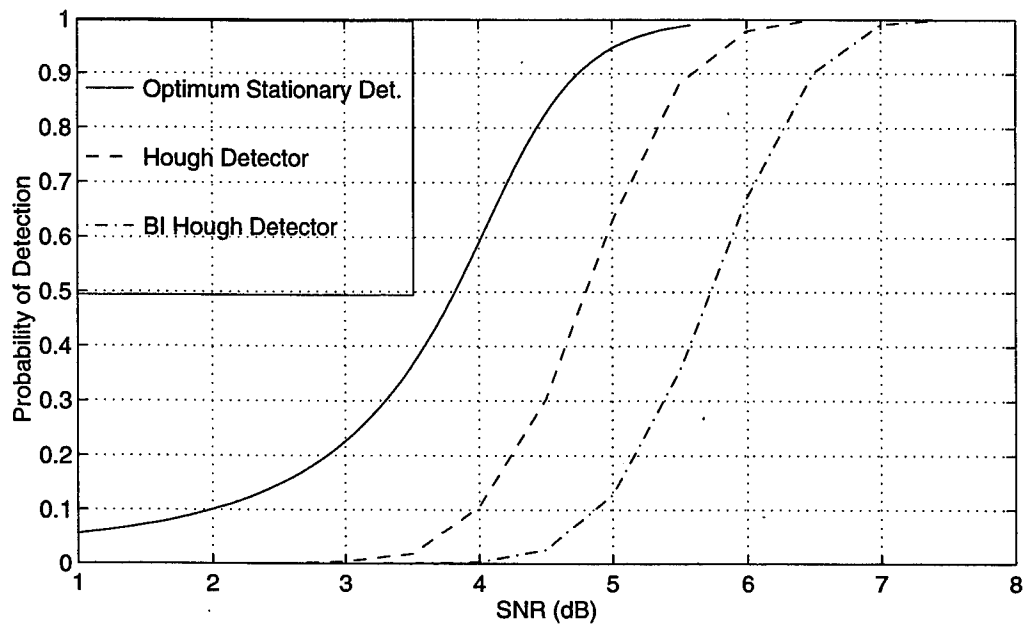
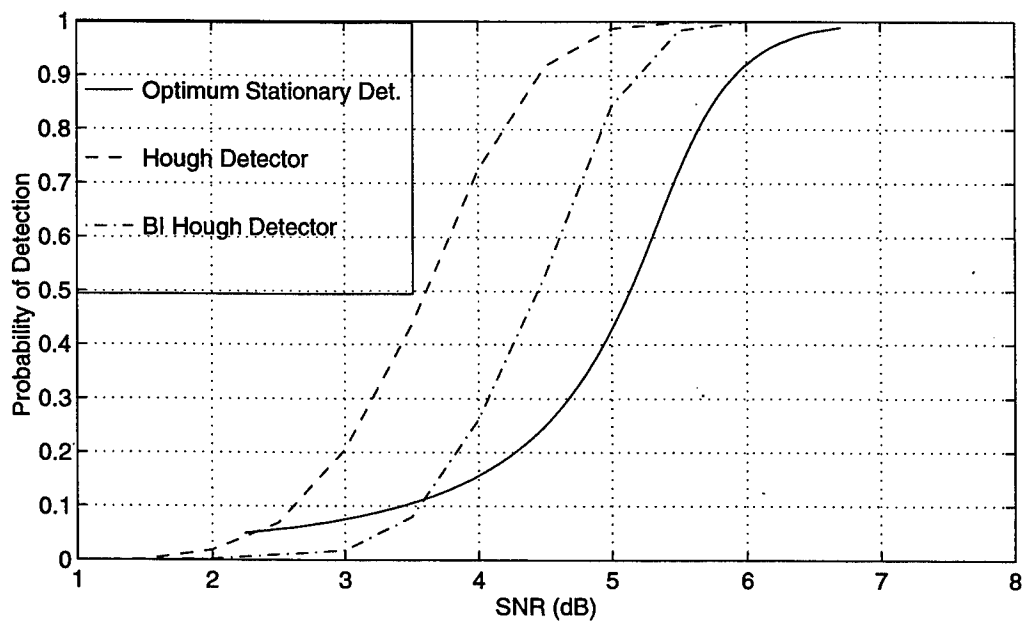


Figure 53. P_d as a Function of SNR for a Nonfluctuating stationary Target with Additive Rayleigh Noise scenario @ $P_{fa}=1 \cdot 10^{-7}$. Different curves denote different detection schemes.



(a)



(b)

Figure 54. P_d as a Function of SNR for a Nonfluctuating Target with Additive Rayleigh Noise scenario @ $P_{fa}=1 \cdot 10^{-7}$. Different curves denote different detection schemes.

(a) Target Speed 5 Knots.

(b) Target Speed 25 Knots.

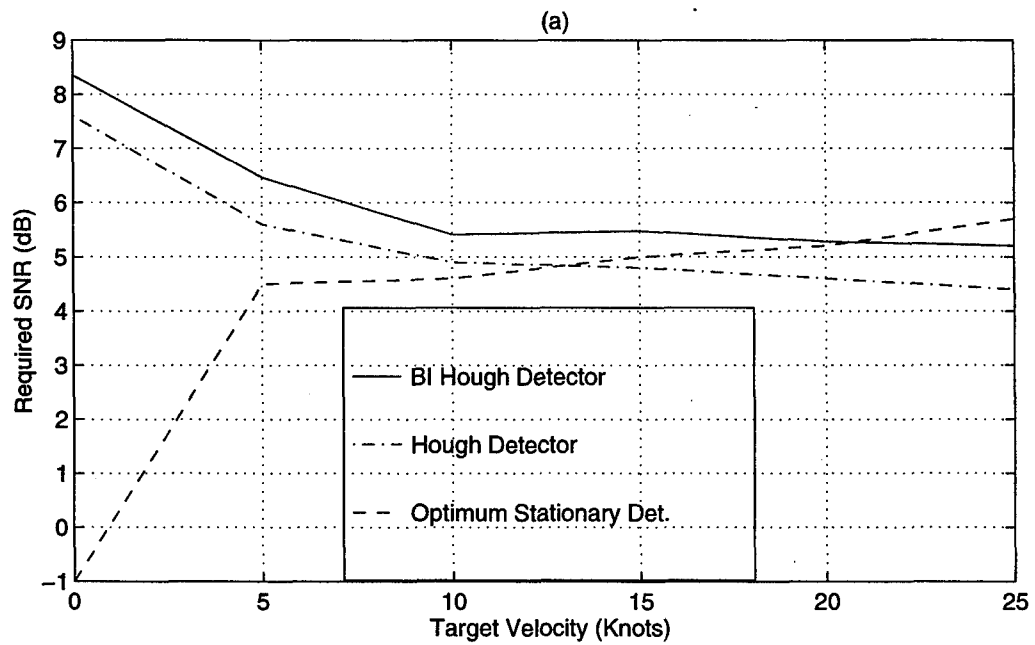
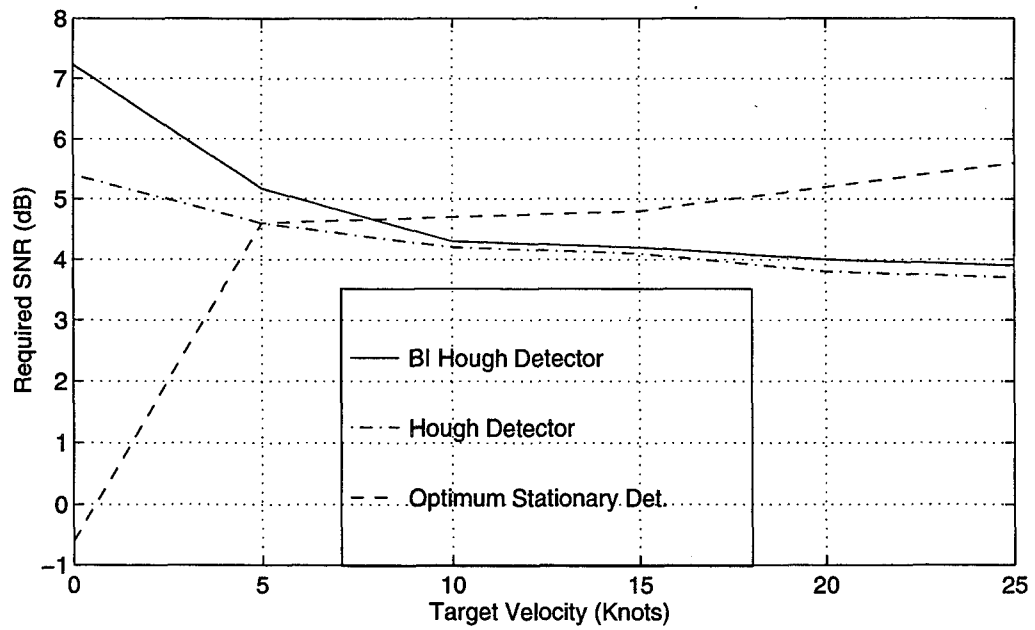


Figure 55. Required SNR to Achieve $P_d=0.9$ as a Function of Target Speed in Knots, for Optimum Detection Process and the Hough Detector.

(a) $P_{fa} = 3 \cdot 10^{-4}$.

(b) $P_{fa} = 1 \cdot 10^{-7}$.

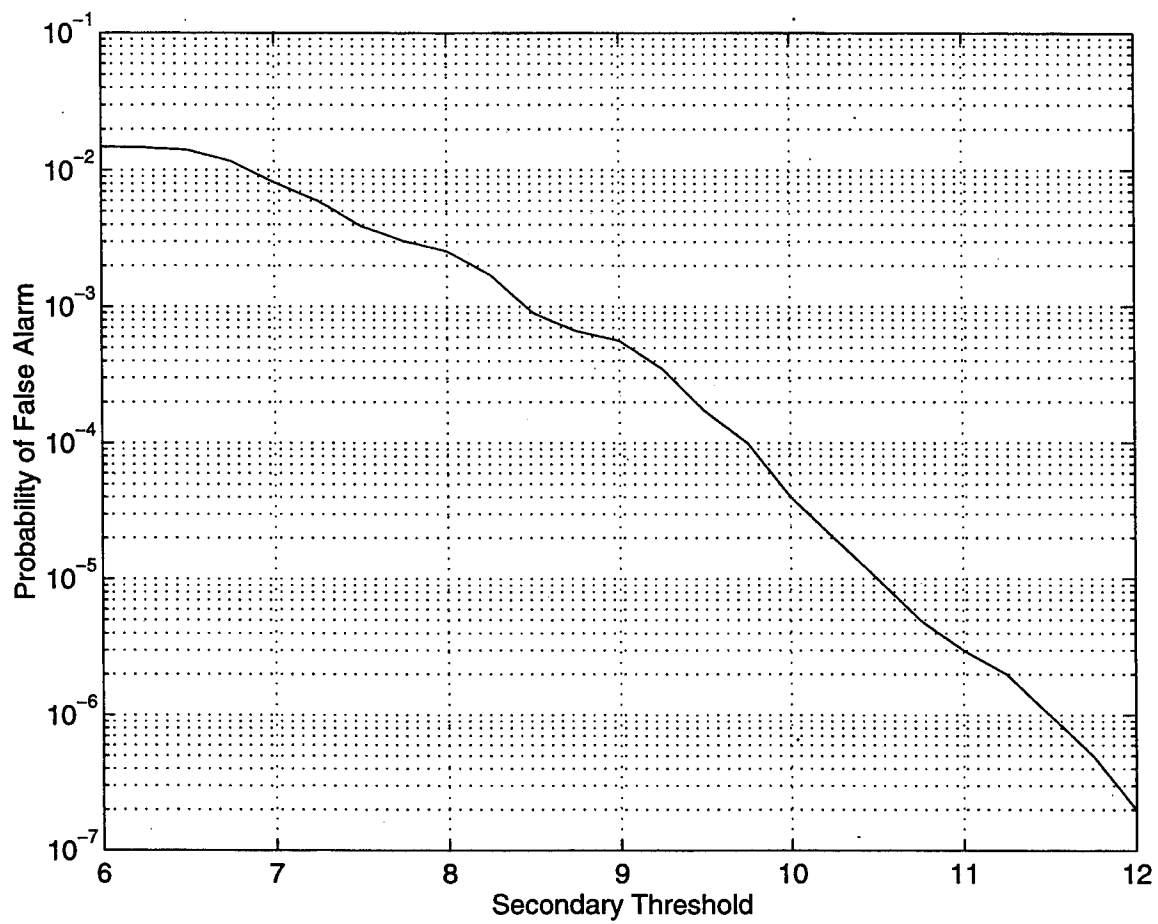


Figure 56. Hough Detector P_{fa} as a Function of Secondary Threshold for the Additive K-Distributed Clutter Case.

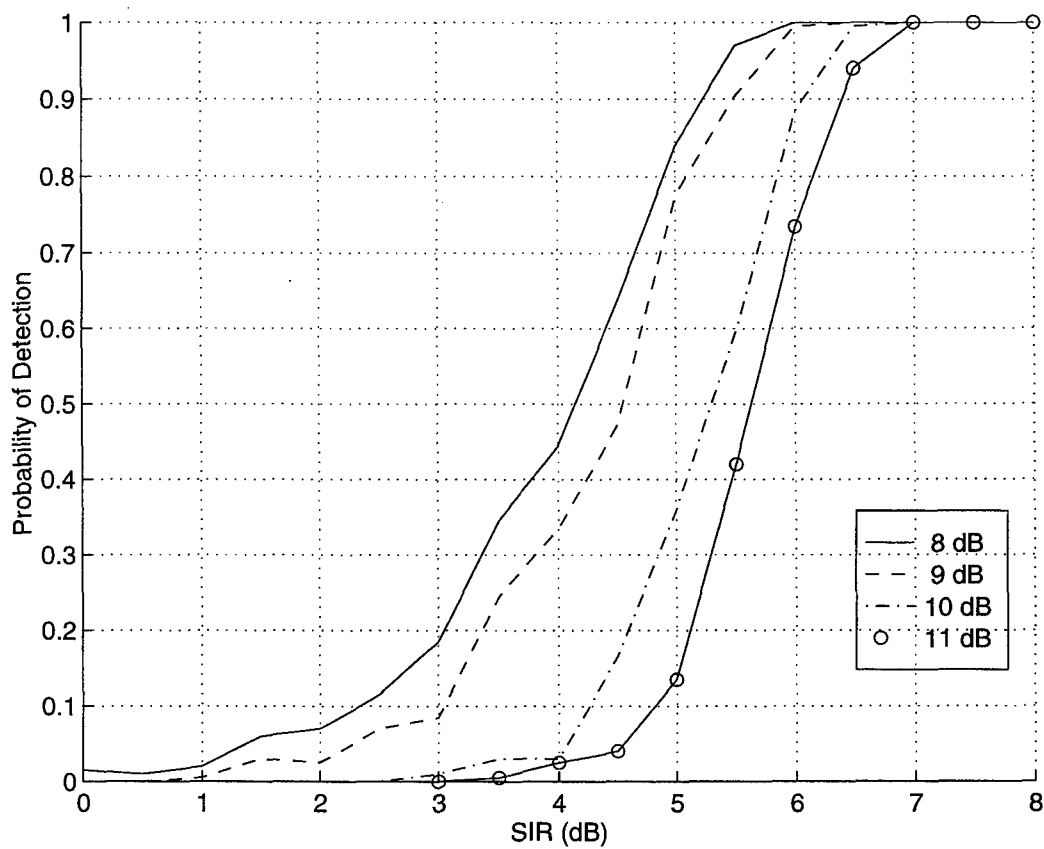


Figure 57. Hough Detector P_d as a Function of SNR for a Nonfluctuating Stationary Target with Additive K-Distributed Clutter Scenario. Different Curves Denote Different secondary Threshold Settings.

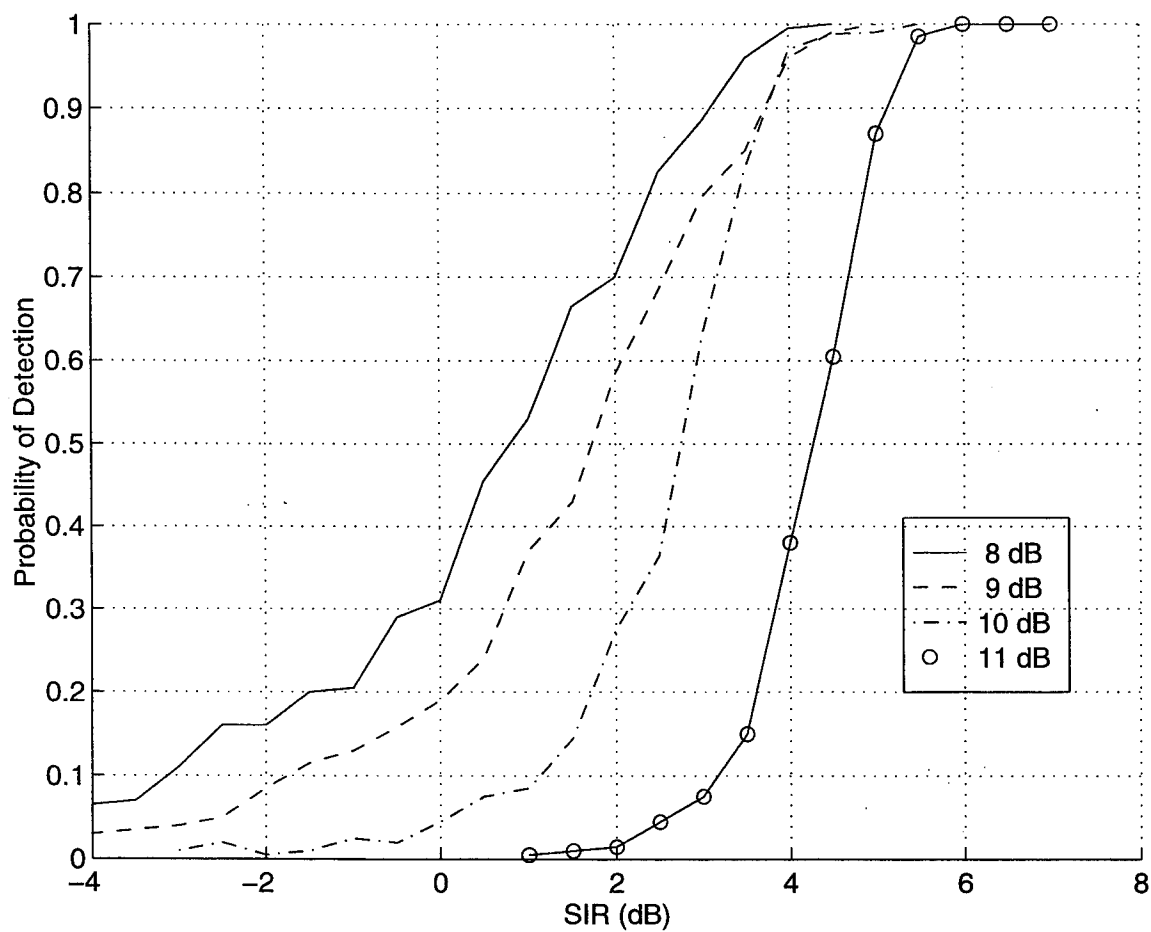


Figure 58. Hough Detector P_d as a Function of SNR for a Nonfluctuating 15 knot Target with Additive K-Distributed Clutter Scenario. Different Curves Denote Different secondary Threshold Settings.

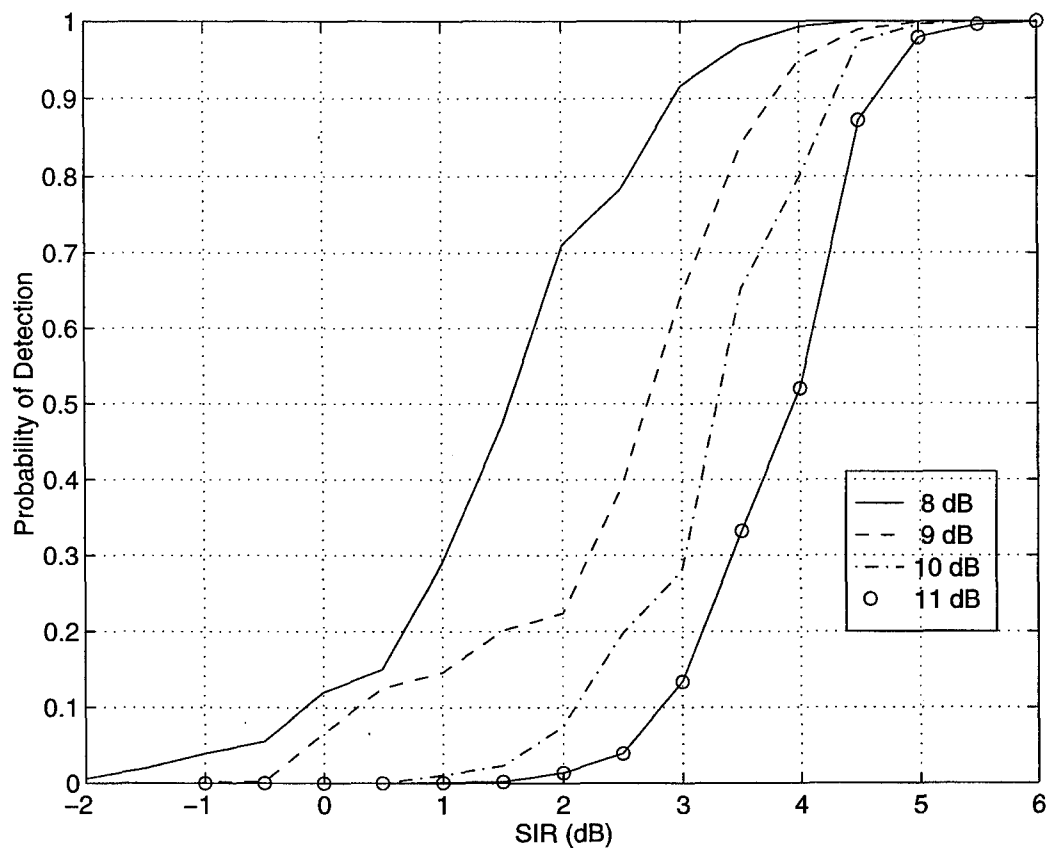
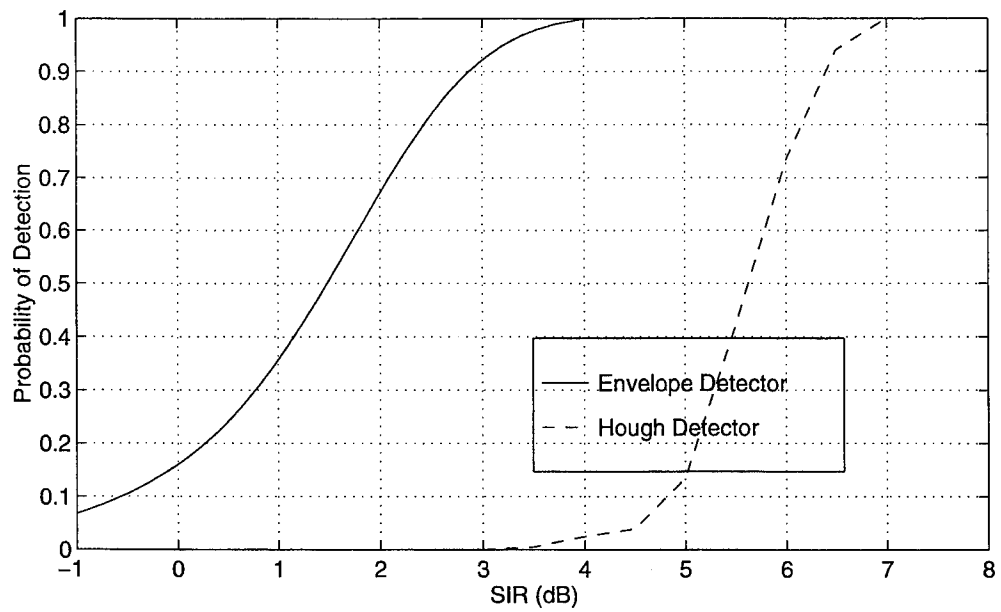
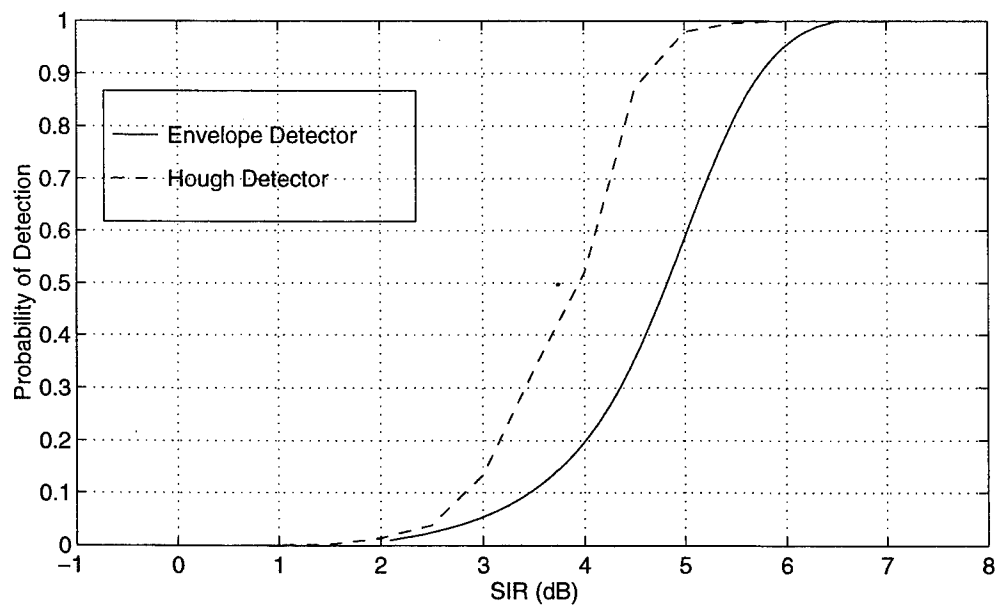


Figure 59. Hough Detector P_d as a Function of SNR for a Nonfluctuating 25 knot Target with Additive K-Distributed Clutter Scenario. Different Curves Denote Different secondary Threshold Settings.



(a)



(b)

Figure 60. P_d as a Function of SNR for a Nonfluctuating Target with Additive K-Distributed Clutter Scenario @ $P_{fa}=8 \cdot 10^{-5}$. Different curves denote different detection schemes.

- (a) Stationary Target.
- (b) Target Speed 25 Knots.

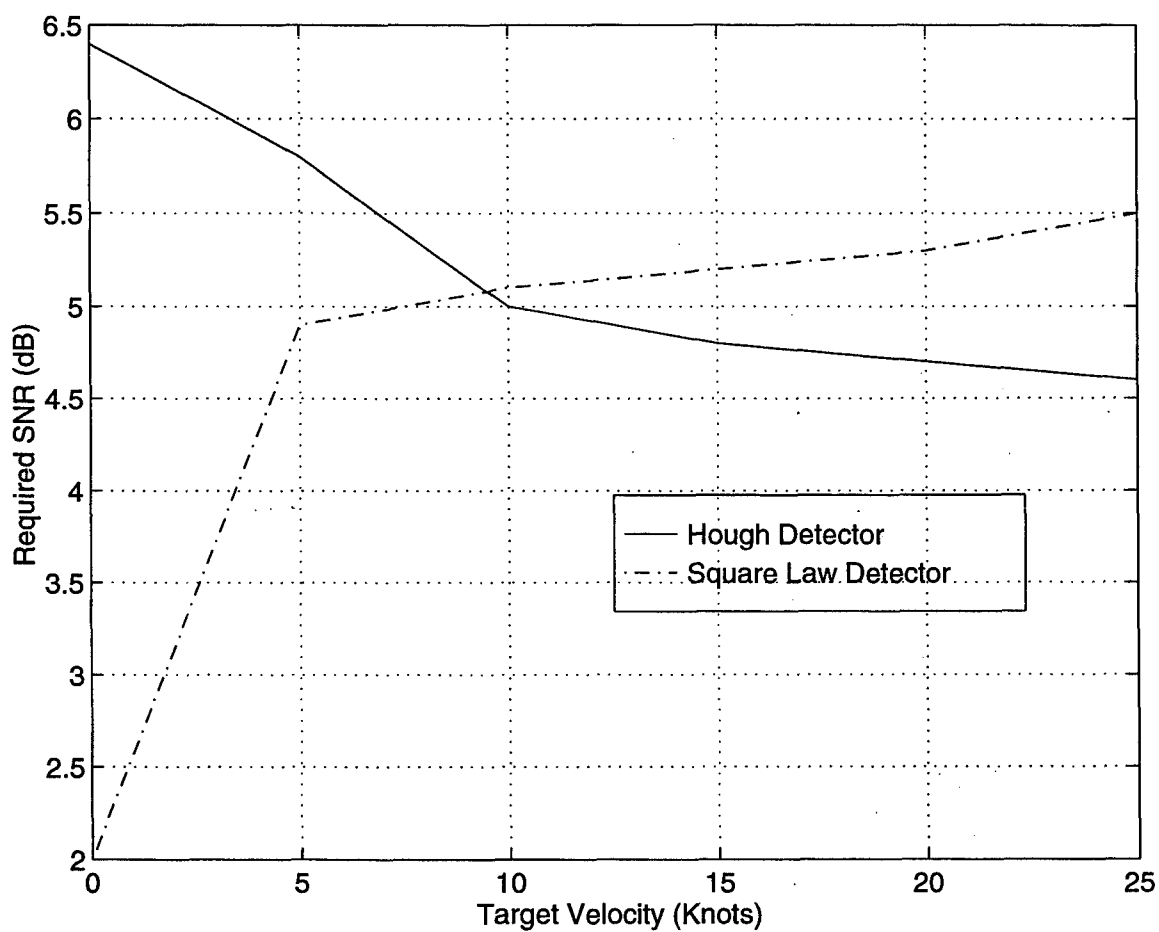


Figure 61. Required SNR to Achieve $P_d=0.9$ @ $P_{fa}=8 \cdot 10^{-5}$ as a Function of Target Speed in Knots, for Square Law Detection Process and the Hough Detector, (for the Additive K-Distributed Clutter Scenario).

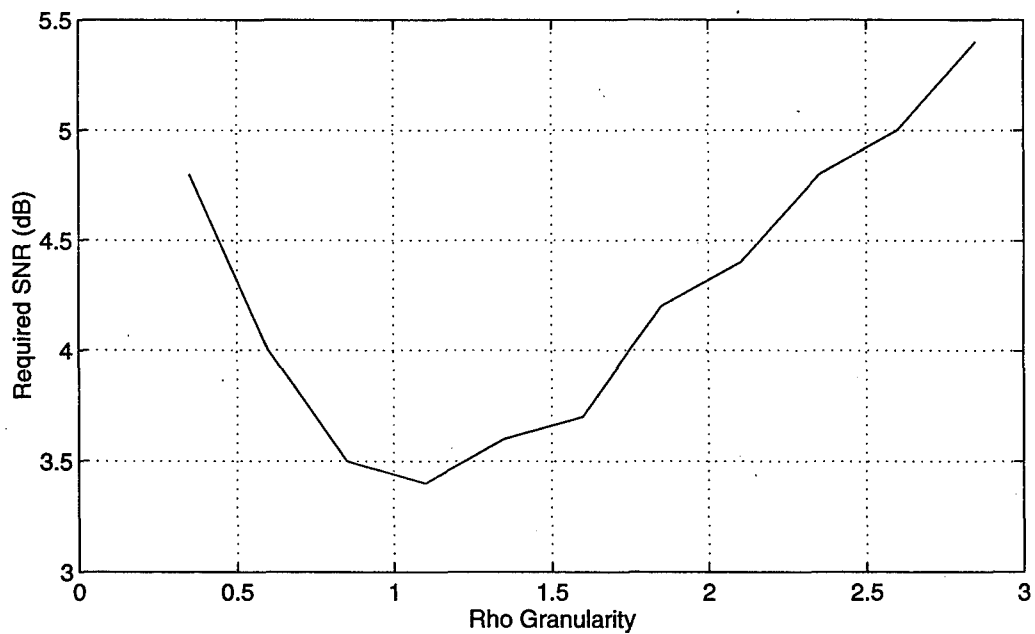
E. PARAMETERS SELECTION

1. Parameter Space

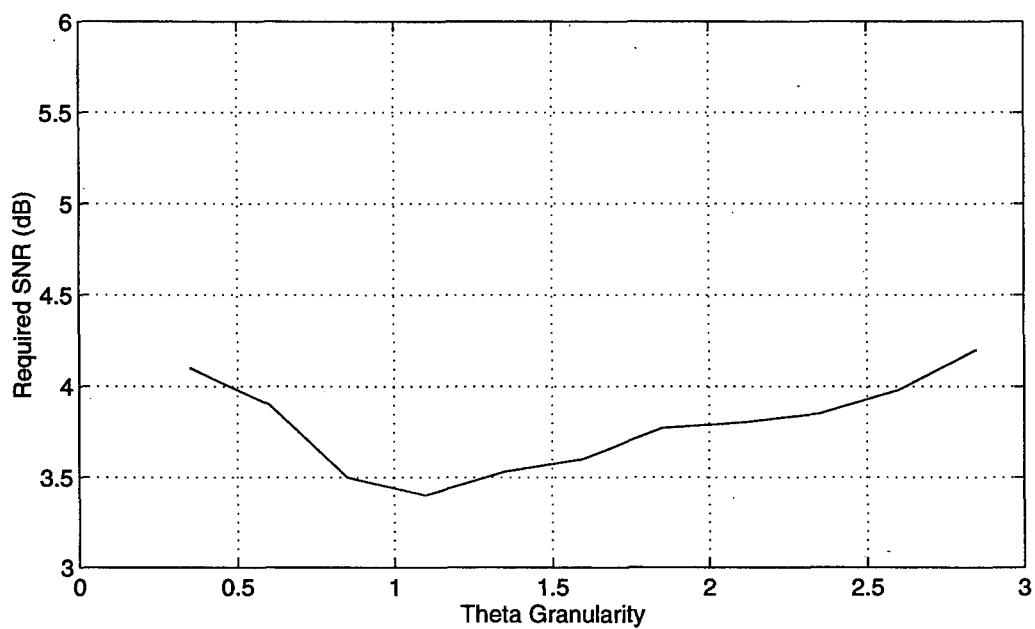
To determine the optimum granularity in the Hough space, we consider a nonfluctuating 25 Knot constant velocity target using the additive Rayleigh noise scenario. Using the procedure described in Section D we evaluate the detection performance, i.e., P_d as a function of required SNR, for the different granularity in the parameter space. Figure 62a shows the required SNR to achieve a P_d of 0.9, with secondary threshold of 12 dB (corresponding to P_{fa} of $1 \cdot 10^{-7}$). The θ granularity was fixed at $\Delta\theta=1^\circ$ and $\Delta\rho$ values were varied between 0.25° to 2.75° . Figure 62b presents the required SNR to achieve $P_d=0.9$ for the same scenario with fixed $\Delta\rho$ and $\Delta\theta$ ranging from 0.25° to 2.75° . The results obtained for the different granularity cases follow the general expected behavior. Selecting a very fine granularity results in splitting the target into several parameter cells, while a coarse granularity causes the noise to add up in fewer cells, forming false peaks in the parameter space, which dictates higher values of ξ to achieve the same P_d . The optimum choice is close to the granularity hat we used in the simulation, i.e., $\Delta\theta=1^\circ$ and $\Delta\rho=1$.

2. Primary and Secondary Thresholds

The second factor that affects the Hough detector performance is the primary and secondary threshold settings. As discussed in Chapter IV, the P_{fa} is determined by both the primary and secondary thresholds. To determine the optimal values for each, we evaluate the P_d as a function of required SNR for different values of primary threshold and apply secondary threshold s that yields constant P_{fa} . Figure 63 shows the results for the required SNR to achieve P_d of 0.9 and a P_{fa} of $1 \cdot 10^{-7}$, as a function of the ξ for the scenario of nonfluctuating 25 knot constant velocity target with additive Rayleigh noise. The primary threshold is varied from $\frac{1}{1000}$ to $\frac{1}{2}$. We observe that the optimum choice for the primary threshold is about $\frac{1}{30}$. The primary threshold used to evaluate the detection performance is $\frac{1}{200}$, which is a compromise between optimum detection performance and the required computing power when applying a low primary threshold.



(a)



(b)

Figure 62. Required SNR a Function of Parameter Space Granularity @ $P_d=0.9$, $\xi=12$ dB.

(a) $\Delta\theta=1$, ρ varies.

(b) $\Delta\rho=1$, θ varies.

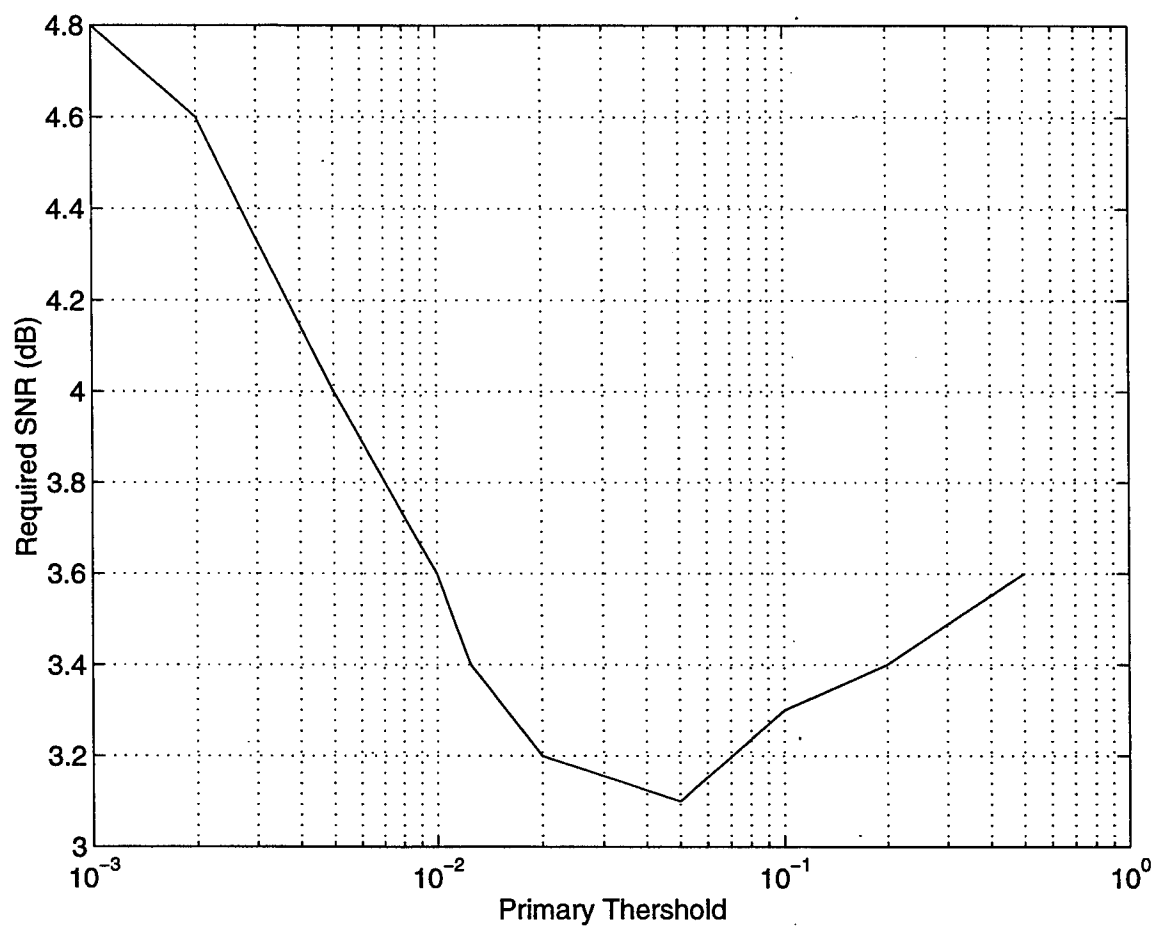


Figure 63. Required SNR as a Function of Primary Threshold @ $P_d=0.9$, $\xi=12$ dB.

VI. CONCLUSIONS

In this thesis, the track-before-detect processing method, using the Hough transform for target detection and tracking by a high resolution search radar, was examined. An efficient algorithm for Hough detector implementation offered by Carlson, Evans and Wilson [Ref. 1], was used, and a comprehensive simulation was built to test the algorithm for several scenarios. The system performance was evaluated and compared against traditional detection schemes. The detection capability of the detector for small targets in the presence of noise and sea clutter, was proven, as well as, the tracking feature obtained by the system as part of the detection process, which eliminates the need to revisit the target for tracking information.

The algorithm presents an improved detection performance, compared to conventional detection schemes, when the scenario is composed of moving targets embedded in Rayleigh noise or K-distributed sea clutter. This provides a solution to the range-walk problem, which occurs in traditional detection schemes where targets with inter-cell motion are not completely integrated. The problem is solved using this method, since the algorithm detects trajectories rather than single resolution cells. A scenario with a 25 knot constant velocity target in additive noise, shows a processing gain of about 3 dB, relative to the optimal stationary detector for this particular parameter selection. When considering a stationary target with additive Rayleigh noise, the detection performance is significantly degraded compared to the optimal detector, or to the binary integration detection process. The required SNR to achieve $P_d=0.9$ with a P_{fa} of 10^{-7} is about 5 dB for this case. This results mainly from the limited integration time that the detector uses and the resulting relatively short trajectories in the time-range domain. The detector employed was designed to detect straight trajectories in the time-range domain. However, the algorithm was able to find the tangent to the curves trajectory of an accelerating target, which indicates the feasibility of using this algorithm in more complex scenarios than a constant speed target. Evaluating the detector performance in the presence of K-distributed sea clutter, which is the main interest of maritime search radars, shows promising results and the processing gain for a 25 knots constant velocity

target was found to be 1.5 dB.

The main drawback of the method is its sensitivity to parameter selection, both in the time-range space and in the Hough space. The radar parameters must be well matched to the target's kinematics to enable satisfactory results. Using unmatched radar range resolution, or scan rates, causes the target to stay in the same resolution cell and reduces the detector performances dramatically, as no significant line in the time-range domain exists. The same performance degradation results from improper selection of parameter space granularity. Using coarse granularity leads to noise adding up to significant lines while fine granularity results in the target splitting into several parameter cells. Optimization evaluation for the Hough space granularity reveals that the optimum values for $\Delta\theta$ and $\Delta\rho$ should be determined in accordance with the time-range and Hough space parameter selection. Another trade off that should be considered when applying the algorithm is the one between primary and secondary threshold settings. The results obtained in this work show that an optimal choice between the two thresholds exists. However, choosing a low primary threshold level implies higher computational load; therefore, the threshold setting should be selected in accordance with the available computing power. This might dictate using higher than optimum primary threshold level to enable real time application of the algorithm. A possible detector problem occurs for multiple target scenarios when one target masks the other targets, or when small targets are masked by noise. One optional solution uses the binary integration Hough transform, which allows multiple target resolving; however, the detection performance in this case is degraded by about 1 dB. Other alternatives to solve this problem involve multiple threshold algorithms and were not investigated in this thesis.

APPENDIX A . MATLAB SOURCE CODE

The algorithms described in chapter IV were implemented using MATLAB software. The different functions are listed below.

A. HOUGH TRANSFORM

```
function [RT,Q,angnum]=ht(bi,type,dat)
% Filename : ht.m
% Title: Hough Transform
% Date of last Revision: 10 Mar 95
% Comments:
%     This m file computes the Hough transform using the classical H- Transform.
% Input variables:
%     bi- flag which indicates if we perform HT (0) or binary integration HT (1)
%     type- Defines the environment simulation noise(0) or noise plus clutter (1)
%     dat-File name contains the radar, target and space parameters
% Output variables:
%     RT- Matrix containing the Hough transform values of the radar echoes.
%     Q- Matrix contains the power of the accumulative Hough transform
%     angnum- Number of required angle bins in the Hough transform.
% Associated Matlab Functions:
%     rtmap.m (generates time-range map)
%     iht.m
% Associated Matlab files
%     rdata.m (radar parameters)
% Initialization
eval([dat]);
[tmap,pwr,mgres,pmap,echo,T,dt ] =rtmap(dat,type);
angnum=181/angres;
N=linspace(0,180,angnum);
t1=0:dt:T;
t=0:length(t1)-1;
if bi==1
    pwr=ones(size(pwr));
end
% Hough transform
H2=[sin(N*pi/180)];
H1=[cos(N*pi/180)];
dimen=size(trhit)
sumlen=0;
for p=1:dimen(2)
    len(p)=max(size(find(trhit(:,p))));
    for q =1:len(p)
        R(1:length(N),sumlen+q)=H1*trhit(q,p)+H2*t1(p);
    end
end
```

```

    sumlen=sumlen+len(p);
end
if sum(len)~=0
    offset=abs(min(R(:)));
end
RT=(round((R+offset.*ones(size(R)))./rhores))+1;
if ( max(RT(:))>rhonum
    RT=RT.*rhonum ./max(RT(:));
end
dimh=size(RT);
Q=zeros(angnum,max(RT(:)));
for l=1:dimh(2)
    for k=1:dimh(1)
        Q(k,RT(k,l))=Q(k,RT(k,l))+pwr(l);
    end
end
end

```

B. INVERSE HOUGH TRANSFORM

```

function [rho,tet,rng]=iht(Q,T,dt)
% Filename : iht.m
% Title: inverse Hough Transform
% Date of last Revision: 10 Mar 95
% Comments:
%     This m file computes the inverse Hough transform
% Input variables:
%     Q- Matrix contains the power of the accumulative Hough transform
%     T- Integration time in time-range domain
%     dt - Time interval between processed dwells
% Output variables:
%     rho- The rho value where the peak in the Hough domain was detected
%     tet- The theta value where the peak in the Hough domain was detected
%     rng- Range locations of the detected trajectory
% Associated Matlab Functions:
%     ht.m
%     trmap.m
% Associated Matlab files
%     rdata.m
t=0:dt:T;
snr2=max(Q(:))/0.913;
[tet,rho]=find(Q>snr2);
ntr=length(rho);
for test=1:50
    if ntr>3
        snr2=snr2*1.0233;
    end
end
for k=1:length(rho);
    rho1(z)=(rho(k)-1)*rhores-offset;
    r0(k)= rho1(k)/cos(tet(k)*pi/180);

```

```

a(k)=-tan((90-tet(k))*pi/180);
rng(k,:)=t./a(k)+r0(k);
end

```

C. RADAR DATA PARAMETERS

```

% Filename : rdata.m
% Title: radar parameters
% Date of last Revision: 10 Mar 1995
% comments:
%     m file that contains the simulated radar and target parameters
% Input variables:
%     None
% Output variables:
%     Radar and target parameters as defined in the program
% Associated Matlab Functions:
%     ht.m
%     iht.m
%     trmap.m
% Associated Matlab files
%     None
% Radar and environment parameters
rpm=240;           % antenna speed
sigm1=10;          % target1 cross section (m^2)
sigm2=10;          % target2 cross section (m^2)
pt=1e6;            % radar peak power (w)
gt=1e4;            % radar antenna gain
lambda=0.1;        % radar wavelength
scan=100;          % # of antenna scans used
pw=0.02;           % radar pulse width
thetag=0.5;        % Grazing angle
rc=100;            % cross range resolution
s1=1/3;            % swell direction
k1=1.7;            % polarization factor
% Targets parameters
teta1=0;           % target1 heading ( relative to the radar)
teta2=0;           % target2 heading ( relative to the radar)
r01=10;            % target1 initial range
r02=10.005;        % target2 initial range
v01=20;            % target1 speed
v02=25;            % target2 speed
snrdb=20           % SNR in dB
num=1;             % number of targets to be simulated
% Time-range and Hough space parameters
rngnum=128;        % number of range cells to be integration in the time-range space
rhores=1;          % defines the granularity for rho in the Hough domain
angres=1;          % defines the granularity for theta in the Hough domain
rhonum=256;        % defines number of the cells in the transform
pfa=1/100;         % defines the requires primary  $P_{fa}$  in the time-range domain
bi=1;              % flag indicates if we perform HT (0) or binary integration HT (1)

```

```
type=1;          % Defines environment simulation noise(0) or noise plus clutter (1)
```

D. TIME-RANGE MAP GENERATION

```
function [trmap,pwr,rngres,pmap,echo,T,dt] =rtmap(dat,type)
% File name: rtmap.m
% Title: Time-Range Map Generation
% Date of last revision: 10 Mar 1995
% Comments :
%     This m file creates simulated time range map composed of target noise and clutter
% Input variables:
%     dat- File name contains the radar and target parameters
%     type- Defines the environment simulation noise(0) or noise plus clutter (1)
% Output variables:
%     T - Total time length in which the radar echoes are processed
%     dt - Time interval between processed dwells
%     pwr -Vector containing the power of the received radar echoes.
%     trmap - Matrix containing the hits crossing primary threshold (2 by length(t))
%     rngres - The radar range resolution ( in ft)
%     pmap- Vector contains the time-range hits power
% Associated matlab functions
%     ht.m
%     iht.m
% Associates matlab functions
%     rdata.m
eval([dat]);
dt=60/rpm;
T=scan*dt;
t=0:dt:T;
rngres= pw*150*3.281;
snr=(10)^(snrdb/10);
[r1,r2,P1,P2]=tgt(t,dat);
P=(P1+P2)/2;
means=mean(P);
sigmn= sqrt(means/(2*snr));
thers=-sigmn*log(pfa);
pmap=zeros(scan,rngnum);
for i=1:scan+1
    pmap(i,r(i)+1)= pmap(i,r1(i)+1)+(P1(i));
    pmap(i,r1(i)+1)= pmap(i,r2(i)+1)+(P2(i));
end
vmap=sqrt(pmap);
rtot=zeros(length(t),rngbin);
if type==0
    for i=1:min(size((vmap)))
        [noise]=rayn(rngbin);
        noisei= (sigmn.*noise(:,1));
        noiseq= (sigmn.*noise(:,2));
        echo=sqrt((vmap(i,:)-noiseq).^2+noisei.^2);
        loc=find((echo(i,:))>thers);
```

```

        pwr(i,:)=zeros(size(temp3));
        pwr(i,loc)=echo(i,loc);
        rtot(i,:)=(loc,zeros(1,ngbin-length(loc)));
    end
elseif type==1
    pwr=[];
    for i=1:min(size(vmap))
        inrf=kcltr(means,ngbin,dat);
        echo=sqrt((M(i,:)-inrf(:,2)).^2+(inrf(:,1)).^2);
        loc=find((echo(i,:))>thers);
        pwr=[pwr echo(loc)];
        rtot(i,:)=(loc,zeros(1,ngbin-length(loc)));
    end
end
trhit=[rtot'];

```

E. TARGET SIMULATION

```

function [r1,r2,P1,P2]=tgt(T,dt,dat)
% File name: tgt.m
% Title: target simulation
% Date of last revision: 10 Mar 1995
% Comments :
%     This m file creates simulated targets in accordance with the radar equation
% Input variables:
%     dat - File name contains the radar and targets parameters
%     T - Total time length in which the radar echoes are processed
%     dt - Time interval between processed dwells
% Output variables:
%     r1,2- Target range
%     P1,2- Target received power
% Associated matlab functions
%     trmap.m
% Associated matlab files
%     rdata.m
eval[dat]
t=0:dt:T;
r1=r01*6076-(v01*6076/3600)*t*cos(teta1);
r2=r02*6076-(v02*6076/3600)*t*cos(teta2);
r1=floor((r1./rngres))+0.5);
r2=floor((r2./rngres))+0.5);
P1=((pt*gt^2*labdda^2*sigm)/((4*pi)^3.*r1/3.218).^4));
P2=((pt*gt^2*labdda^2*sigm)/((4*pi)^3.*r2/3.218).^4));
if num==1
    P1=[];r1=[];
end

```

F. RAYLEIGH NOISE SIMULATION

```

function [ray]= rayn(N)

```

```

% File name: rayn.m
% Title: Rayleigh noise Simulation
% Date of last revision: Mar 10 1995
% Comments :
%     This m file simulates Rayleigh noise
% Input variables:
%     N- Number of noise points to be simulated
% Output variables:
%     ray- Matrix containing the I and Q components of the noise (2xN)
% Associated Matlab functions:
%     trmap.m
% Associated Matlab Files:
%     None
n=1:N;
rnd1=randn(size(n));
rnd2=randn(size(n));
rnd=sqrt(rnd1.^2+rnd2.^2);
rndang=2*pi.*rand(size(n));
ray=[rnd'.*sin(rndang)',rnd'.*cos(rndang)'];

```

G. K-DISTRIBUTION CLUTTER SIMULATION

```

function [cltr]=noise1(sig,N,dat)
% Filename : kcltr.m
% Title: k distributed clutter simulation
% Date of last Revision: 10 Mar. 1995
% comments
%     This m file simulates distributed clutter
% Input variables:
%     sig-Signal power
% Output variables:
%     cltr-Matrix containing the I and Q components of the interference (2xN)
% Associated Matlab functions
%     trmap.m
% Associated matlab files
%     rdata.m
eval(dat);
sf=10^(0.67*log10(thetag)+0.625*log10(pw*1e3*rc/30)+s1-k1);
pc=sig*(10^(cnr/10))/(1+10^(cnr/10));
pn=sig^2/(1+(10^(cnr/10)));
f=floor(sf); a=sf-f; l=0;
p=exp(1)/(a+exp(1));
c=(a+exp(1))/(exp(1)*gamma(a+1));
cnt=floor(2*c*s);
b=sqrt(2*sf/pc);
ran=rand(N,f);
for i=1:N
    x(i)=-log(prod(ran(i,:)));
    g(i)=x(i);
end

```

```

if a~=0
    for i=1:cnt
        u=rand; v=rand;
        if u<p
            y=v^(1/a); q=exp(-y);
        else
            y=1-log(v); q=y^(a-1);
        end
        if rand<=q
            l=l+1; g(l)=x(l)+y;
        end
        if l==N
            break
        end
    end
end
i=1:N;
chi(i)=(sqrt(g(i)))./b;
inrf(i)=(sqrt((chi(i).)^2+0.5*pn)).*sqrt(-2*log(rand(size(i)))));
rndang=2*pi.*rand(size(inrf));
cltr=[(inrf1.*sin(rndang))',(inrf.*cos(rndang))];

```

H. HOUGH DETECTOR PROBABILITY OF DETECTION

```

function [pd ]=prdet (p1,p2,s1,s2 ,simlen,bi,type,dat)
% Filename :prdet.m
% Title: probability of detection of the Hough detector
% Date of last Revision: 10 Mar 1995
% Comments:
%     This m file computes probability of detection ( $P_d$ ) of the Hough detector as a
%     function of the secondary threshold , for different primary threshold settings
%     ( in steps of 0.25 dB)
% Input variables:
%     p1,p2- Primary threshold boundaries (in dB)
%     s1,s2- Secondary threshold boundaries (in dB)
%     bi- Flag which indicates if we perform HT (0) or binary integration HT (1)
%     simlen- Number of repetitions in each SNR point ( primary and secondary )
%     type- Defines the environment simulation noise(0) or noise plus clutter (1)
%     pfa- Defines the requires primary  $P_{fa}$  in the time-range domain
% Output variables:
%     pd- Matrix containing the pd
%     val - Matrix containing the primary and secondary threshold used for pd
% Associated Matlab functions:
%     ht.m
%     iht.m
% Associated Matlab files:
%     none
m=0,n=0;
for snr2db =s1:0.25:s2
    m=m+1;
    snr2=10^(snr2db/10);

```

```

for snrdb= p1:0.25:p2
    n=n+1;
    hit1=0
    for count=1:simlen
        [RT,Q,angnum]=ht(bi,type,dat);
        [rho,tet,ring]=iht(Q,t);
        for i=1:length(tet)
            if tet(i)<=reftet(tgt)+1 & tet(i)>=reftet(tgt)-1
                if rho(i)-offset<=refrho(tgt) +1& rho(i)-offset>=refrho(tgt)-1
                    hit(i)=1;
                end
            end
        end
        if sum (hit)>0
            hit1=hit1+1;
            hit=0;
        end
    end
    pd(m,n)=hit1./simlen;
    hit1=0;
end
end
val=[s1:s2;p1:p2];

```

I. HOUGH DETECTOR PROBABILITY OF FALSE ALARM

```

function [pfa ]=prfa (s1,s2,simlen,bi,type,dat)
% Filename : prfa.m
% Title: probability of false alarm of the Hough detector
% Date of last Revision: 10 Mar 1995
% Comments:
%     This m file computes probability of detection ( $P_{fa}$ ) of the Hough detector as a
%     function of the secondary threshold (in steps of 0.25 dB)
% Input variables:
%     s1,s2-Secondary threshold boundaries (in dB)
%     simlen-Number of repetitions in each SNR point ( primary and secondary )
%     dat-File name contains the radar and target parameters
% Output variables:
%     pfa-Matrix containing the probability of false alarm
%     val-Vector containing the secondary threshold used for the  $p_{fa}$ 
% Associated Matlab functions:
%     ht.m
%     iht.m
% Associated Matlab files:
%     none
m=0 ;
for snr2db =s1:0.25:s2
    m=m+1;
    snr2=10^(snr2db/10);
    for count=1:simlen

```



```

[RT,Q,angnum]=ht(bi,type,dat);
[rho,tet,rg]=iht(Q,t);
hit(count)=length(rho);
end
pfa(m)=sum(hit)/simlen;
end
val=s1:s2 ;

```

J. ALBERSHEIM METHOD

```

function [snr,pd]=alber(M,N,DC,pfa)
% File name: alber.m
% Title: albersheim metod
% Date of last revision: Mar 10 1995
% Comments :
%   This m files implement the albersheim equation-required snr to
%   obtain a given pd and pfa including collapsing loss
% input variables:
%   M-Overall number of Signal cells
%   N-Number of overall cells
%   pfa-Required probability of false alarm
%   DC- Detectablity factor for a coherent process ( vector size 1x99)
% Output variables:
%   snr-Required snr to obtain a given pd and pfa
%   pd- pd corresponds to the snr
% Associated Matlab Functions:
%   None
% Associated Matlab Files:
%   None

pd=0.01:0.01:0.99;
A=log(0.62/pfa);
B=log(pd./(1-pd));
snr1=-5*log10(N)+(6.2+4.54/(sqrt(N+0.44))).*log10(A+0.12.*A.*B+1.7.*B);
rho=N/M;
dc=10.^(DC./10);
l= 10*log10((1+sqrt(1+9.2*rho*M./dc))./(1+sqrt(1+9.2*M./dc)));
snr=snr1+l;

```

K. BINARY INTEGRATION THRESHOLD

```

function [q]=binther(N,M,PFA)
% File name:binther.m
% Title: binary integration threshold
% Date of last revision: Mar 10 1995
% Comments :
%   This m file computes the required threshold level needed to obtain overall PFA
% input variables:
%   M- Overall number of Signal cells
%   N-Number of overall cells

```

```

%      PFA- Overall  $P_{FA}$  required for the binary integration process
%      Output variables:
%      pfa-Single pulse probability of false alarm
%      Associated Matlab Functions:
%      binsnr.m
%      Associated Matlab Files:
%      None
steps=-0.1;
test=100;
x=1e-9;
k=M:N;
delt=1e-6*PFA;
for kk=M:N
    noverk(kk-M+1)=prod(1:N)/(prod(1:N-kk)*(gamma(kk+1)));
end
for loop=1:500
    p=x.^k;
    q=(1-x).^(N-k);
    r=sum(noverk.*p.*q);
    if abs(r-PFA)<=delt
        break
    else
        if sign(test)~=sign(r-PFA)
            steps=-0.5*steps;
        end
    end
end
x=x+steps;
test= r-PFA;
end
if loop==500
    input('no convergence in Pfa','s')
    break
end
q =-log(x);

```

L. BINARY INTEGRATION PROBABILITY OF DETECTION

```

function[pd]=binpd(N,M,PD)
% Title: binary integration probability of detection
% Date of last revision: Mar 10 1995
% Comments :
%      This m file computes the requires single pulse  $p_d$  needed to obtain overall  $P_D$ 
%      input variables:
%      M-Overall number of Signal cells
%      N-Number of overall cells
%      PD-Overall  $P_D$  required for the binary integration process
%      Output variables:
%      pfa-Single pulse probability of detection
%      Associated Matlab functions:
%      binsnr.m

```

```

% Associated Matlab Files:
%      None
for l=1:length(PD)
    test=100;
    x=1e-4;
    steps=-0.1;
    k=M:N;
    delt=1e-6;
    for i=M:N
        noverk(kk-M +1)=prod(i+1:N)/ prod(1:(N-i));
    end
    for loop=1:500
        p=x.^k;
        q=(1-x).^(N-k);
        r=sum(noverk.*p.*q);
        if abs(test-PD(l) )<=delt
            break
        else
            if sign(test)~=sign(r-PD(pp) )
                steps=-0.5*steps;
            end
            x=x+steps;
        end
        clear p q
        test= r-PD(pp) ;
    end
    if loop==500
        input ('no convergence in PD','s')
        break
    end
    pd(r)=x;
    clear r k i noverk
end

```

M. BINARY INTEGRATION DETECTION PERFORMANCE

```

function[SNR]=binpdnr(N,PD,PFA)
% File name: binsnr.m
% Title: binary integrationprobability of detection
% Date of last revision: Mar 10 1995
% Comments :
%      This m files computes the required snr to obtain a given pd and pfa
%      using binary integration processing
% input varaibles:
%      M- Overall number of Signal cells
%      N-Number of overall cells
%      PD- Overall  $P_D$  required for the binary integration process
% Output variables:
%      snr- Required SNR to achieve to defined  $P_D$ 
% Associated Matlab functions:

```

```

%      binther.m
%      binpd.m
% Associated Matlab Files:
%      None
M=0.4*N;
test=100;
delt=0.0001;
steps=-.1;
snr=1e-2;
[q]=binther(N,M,PFA);
[pd]=binpd(N,M,PD);
for count=1:length(pd)
    for loop=1:1000
        h(1)=exp(-snr);
        f(1)=q *exp(-q );
        d(1)=h(1);
        for k=2:50
            f(k)=q *f(k-1)/k;
            d(k)=snr*d(k-1)/(k-1);
            h(k)=h(k-1)+d(k);
        end
        Q(count)=1-sum(f.*h);
        if abs(Q(count)-pd(count))<=delt
            break
        else
            if sign(test)~=sign(Q(count)-pd(count) )
                steps=-0.5*steps;
            end
            snr=snr+steps;
        end
        if loop==500
            input('no convergence','s')
            break
        end
        test= Q(count)-pd(count);
    end
    SNR(count)=snr;
    clear d h f Q
end

```

N. GRAPHICS UTILITY

```

% Filename : graplot.m
% Title: plotting utility
% Date of last Revision: 10 Mar 1995
% Comments:
%      This m file plots the time-range space and the Hough space parameters
%      Several plotting options are available to choose from.
% input variables:

```

```

%      None
% Output variables:
%      None
% Associated Matlab functions:
%      ht.m
%      iht.m
%      alber.m
%      binsnr.m
% Associated Matlab files:
%      rdata.m
close all
k=menu('Select Required Plot','Raw Data Mesh Plot','Raw data Time-Power Plot','Range -Time Plot','Hough
X-form Mesh Plot','Hough X-form Rho-Theta Plot');
if k==1
    figure(1)
    y1=t1-T;
    x1=0:angnum;
    subplot(211),surf(x1',y1,10*log10(echo))
    ylabel('Time (sec)')
    xlabel('Range')
    zlabel('Power (db)')
elseif k==2
    stairs(t1-T,10*log10(pmap)), grid
    axis([-T 0 (min(10*log10(pmap)))-10 (max(10*log10(pmap)))+10 ])
    xlabel('time')
    ylabel('power (db)')
elseif k==3
    hold on
    plot(R1,t1-T,'r')
    plot(R2,t1-T,'r')
    for i=1:length(rho1)
        plot(rng(i,:),t1-T,'b')
    end
    xlabel('Range'),ylabel('Time'),grid
    title(['Target echos range res =', num2str(rangres),'ft'])
elseif k==4
    x1=0:angnum-1;
    y1=min(R(:)):rhoes:max(R(:));
    surf(x1',y1,Q'),grid
    xlabel('Theta')
    ylabel('Rho')
    zlabel('Power')
    title(' Hough space parameters')
elseif k==5
    N=linspace(0,180,angnum);
    plot (N,R,'r'),grid
    xlabel('theta')
    ylabel('Rho')
    title(' Hough space parameters')
elseif k==6

```

```

plot(10*log10(SNR),PD,'b'),grid

hold on
plot(10*log10(snr),pd,'r')
xlabel('SNR (dB)'),ylabel('Pd'),title('Binary Integration Detection Performance')
text(1,1,'Pfa',num2str(pfa))
legend('Optimal detector','binary integration')
end

```

0. MAIN PROGRAM

```

% File name:main.m
% Title:main program
% Date of last revision: Mar 10 1995
% Comments :
%     This m file activates the different programs
% input variables:
%     simpar- File name contains the simulation parameters for the performance comparison
% Output variables:
%     None
% Associated Matlab functions:
%     ht.m
%     iht.m
%     alber.m
%     binsnr.m
%     graplot.m
% Associated Matlab Files:
%     rdata.m
dat=input('Enter data file Name');
k=menu('Select Required program','Hough detector','Hough detector Pd','Hough detector pfa','performance comparison');
if k==1
    [RT,Q,angnum]=ht(bi,type,dat)
    [rho,tet,rng]=iht(Q,T,dt);
elseif k==2
    load simpar;
    [pd ]=prdet (p1,p2,s1,s2 ,simlen,bi,type,dat);
elseif k==3
    load simpar;
    [pfa ]=prfa (s1,s2,simlen,bi,type,dat);
elseif k==4
    load comerpar;
    [snr,pd]=alber(M,N,DC,pfa);
    [SNR]=binpdnr(N,PD,PFA);
end
graplot

```

LIST OF REFERENCES

1. B.D. Carlson, E. Evans, S. Wilson, "Search Radar Detection and Track with the Hough Transform," *IEEE Transactions on Aerospace and Electronic Systems*, Vol. AES-30, No. 1, January, 1994.
2. J. Smith, R. Logan, "AN/APS-116 Periscope Detection Radar," *IEEE Transactions on Aerospace and Electronic Systems*, Vol. AES-16, No. 1, January, 1980.
3. S. Reed, M. Gagilardo, M. Shao, "Application of Three Dimensional Filtering to Moving Target Detection," *IEEE Transactions on Aerospace and Electronic Systems*, Vol. AES-19, No. 6, November, 1983.
4. Y. Barniv, "Dynamic Programming Solution for Detection Dim Moving Target," *IEEE Transactions on Aerospace and Electronic Systems*, Vol. AES-21, No. 1, January, 1985.
5. D.C. Schleher, "Periscope Detection Radar", To Be Presented in International Radar Convention, Washington D.C. May, 1995.
6. J.D. Kramer, W.S. Reid, "Track Before Detect Processing for a Range Ambiguous Radar," *IEEE National Radar Conference*, New York, NY, April, 1993.
7. J.L. Harmon, "Track Before Detect Performance for High PRF Search Mode," *IEEE National Radar Conference*, New York, NY, April, 1991.
8. J. Illingworth, J. Kittler, "A Survey of the Hough Transform," *Computer Vision, Graphics and Image Processing*, Vol. 44, No. 1, October, 1988.
9. W. Albersheim, "A Closed Form Approximation to Robertson's Detection Characteristics," *Proceedings of the IEEE (Letters)*, Vol. 69, July, 1981.
10. D.K. Barton, "Simple Procedures for Radar Detection Calculations," *IEEE Transactions on Aerospace and Electronic Systems*, Vol. AES-5, September, 1969.
11. J. Marcum, P. Swerling, "Studies of Target Detection by Pulse Radar," *IRE Transactions on Information Theory*, Vol. IT-6, No. 3, April, 1960.
12. S. Watts, "Radar Detection Prediction in K- Distributed Sea Clutter and Thermal Noise," *IEEE Transactions on Aerospace and Electronic Systems*, Vol. AES-23, No. 1, January, 1987.

13. K. Ward, "Compound Representation of High Resolution Clutter," *Electronic Letters*, Vol. 17, 1981.
14. K. Ward, "Maritime Surveillance Radar, Part 1: Radar Scattering from the Ocean Surface," *IEE Proceedings*, Vol. 137, Pt. f, April, 1990.
15. X. Hou, N. Morinaga, T. Namekawa, "Direct Evaluation of Radar Detection Probabilities," *IEEE Transactions on Aerospace and Electronic Systems*, Vol. 23, No. 4, July, 1985.
16. X. Hou, N. Morinaga, "Detection Performance in K- Distributed and Correlated Rayleigh Clutter," *IEEE Transactions on Aerospace and Electronic Systems*, Vol. 25, No. 5, September, 1989.
17. D.C. Schleher, "Simulation of K Distributed Clutter," *Aerospace and Electronics Magazine*, April, 1995.
18. D.C. Schleher, *Automatic Detection and Radar Data Processing*, Artech House, Dedham, MA, 1980.
19. D.C. Schleher, *Introduction to Electronic Warfare*, Artech House, Dedham, MA, 1986.
20. W.F. McGee, "Another Recursive Method of Computing the Q Function," *IEEE Transaction on Information Theory*, Vol. IT-16, No. 4, July, 1970.
21. F. Nathanson, *Radar Design Principles*, 2nd edition, McGraw-Hill, New York, NY, 1990.
22. W.H. Press, S.A. Teukolsky, W.T. Vetterling, P.B. Flannery, *Numerical Recipes in FORTRAN*, 2nd edition, Cambridge Press, New York, NY, 1992.
23. R. Prengaman, R. Thurber, W.Bath, "A Retrospective Detection Algorithm For Extraction Of Weak Targets In Clutter And Interference Environments," *IEEE International Radar Conference*, London, October, 1982.

INITIAL DISTRIBUTION LIST

		No. of Copies
1.	Defense Technical Information Center 8725 John J. Kingman Rd., STE 0944 Ft. Belvoir, VA 22060-6218	2
2.	Dudley Knox Library Naval Postgraduate School 411 Dyer Rd. Monterey, CA 93943-5101	2
3.	Chairman, Code EC Department of Electrical and Computer Engineering Naval Postgraduate School Monterey, California 93943-5121	1
4.	Professor D. Curtis Schleher, Code EW/Sc Department of Electronic Warfare Naval Postgraduate School Monterey, California 93943-5126	1
5.	Professor Robert G. Hutchins, Code EC/Hu Department of Electrical and Computer Engineering Naval Postgraduate School Monterey, California 93943-5121	1
6.	Professor G. Gil, Code EC/Gi Department of Electrical and Computer Engineering Naval Postgraduate School Monterey, California 93943-5121	1
7.	Israeli Navy Headquarters Library Military Mail 01068 Hakirya, Tel-Aviv Israel	1

- | | | |
|-----|---|---|
| 8. | Naval Attache
Embassy of Israel
3514 International Dr
Washington D.C. 20008 | 1 |
| 9. | Head of Electronics Department
Israeli Navy Headquarters
Military Mail 01068
Hakirya, Tel-Aviv
Israel | 1 |
| 10. | LCDR Moshe Elazar
6 Eilat St. 32298
Haifa
Israel | 1 |